Long-Term Coastal Dynamics along the Lagos State Coastline in the Context of Climate Change

Master Thesis

Tijn Schell

Faculty of Civil Engineering and Geosciences

TU Delft

CDR

CDR International B.V.

Long-Term Coastal Dynamics along the Lagos State Coastline in the Context of Climate Change

by

Tijn Schell

to obtain the degree of Master of Science
at the Delft University of Technology,
to be defended publicly on Tuesday June 3, 2025 at 13:45 AM.

Student number: 4899083
Project duration: October 1, 2024 – June 4, 2025
Thesis committee: Dr. Ir. J. A. A. Antolínez, Delft University of Technology
Dr. Ir. J. A. Arriaga Garcia, Delft University of Technology
Ir. B. J. van der Spek, CDR International BV

Cover: provided by Dirk Heijboer of CDR International BV.

An electronic version of this thesis is available at http://repository.tudelft.nl/.

TU Delft

CDR International B.V.

Abstract

The Lagos State coastline is increasingly vulnerable to erosion, driven by both a dominant eastward longshore sediment transport and ongoing human interventions. Climate change, through rising sea levels and a changing wave climate, is expected to further influence shoreline dynamics in the coming decades. Understanding how these factors interact is crucial for supporting long-term coastal management along this coastline of major economic and social significance.

This study investigates the impact of climate change on shoreline evolution over a 50-year timescale, focusing on sea level rise, changes in significant wave height, and changes in wave direction. The one-dimensional shoreline evolution model ShorelineS was applied and calibrated using satellite derived historical shoreline data. Simulations were performed for a range of climate scenarios, allowing for a separate evaluation of the individual contributions of sea level rise, changing wave height, and changing wave direction to coastal erosion and accretion patterns.

Longshore sediment transport is projected to increase by up to 20% by 2075 under extreme RCP8.5 scenarios. This intensification directly drives changes in shoreline dynamics, leading to amplified erosion in some areas and enhanced accretion in others. Projected shoreline retreat can reach up to 700 meters locally under baseline conditions (i.e., without climate change) by 2075. Climate change can further amplify these patterns, with shoreline retreat increasing by up to 10% in erosion-prone areas near coastal structures. In contrast, accretive zones show a more moderated response due to counteracting effects between sea level rise and wave-driven accretion.

Wave direction changes were found to have the strongest localized impact on shoreline retreat near coastal structures, while the influence of wave height changes was less consistent and more variable along the coast. Sea level rise causes relatively uniform retreat along the entire coastline.

The results provide spatially explicit projections of shoreline retreat and accretion, offering insights into areas most at risk. These findings support the development of targeted, adaptive coastal management strategies for Lagos State in the face of a changing climate.

Preface

This master thesis is the product of research executed in collaboration with CDR International BV and the Delft University of Technology. With it, I conclude my degree of Master of Science in Hydraulic Engineering.

One dimensional shoreline models can provide valuable insights in shoreline dynamics particularly because they can be applied over large spatial and temporal scales. This research aims to explore the applicability of such a model to assess the long term effects of climate change on shoreline evolution along the Lagos State coastline.

Doing research on the influence of climate change on the shoreline dynamics is something that has interested me throughout every step of this master thesis, from the literature study to finalizing the report. Working with different unfamiliar numerical models was challenging, but also rewarding when expected coastal dynamics emerged from the simulations.

I would like to sincerely thank my supervisors, José Antolinez, Jaime Garcia and Bart-Jan van der Spek for their invaluable guidance, constructive feedback, and continuous support throughout this research project. Your positivity and enthusiasm made this a truly rewarding experience. A special thanks as well to Stijn Dijsselbloem and David Heineke from CDR International BV for their continuous support throughout this process, both in setting up the models and in proofreading my report. I would also like to thank all the people of CDR for making me me feel a part of the team. Taking me and Quinten on a two day trip to Friesland while only just having started was truly amazing. The weekly drinks and company activities also made the entire process much more enjoyable.

I would like to thank my parents, brother, grandparents and cousins for always showing genuine interest in my project. I am also grateful to my grandpa for nurturing my interest in science and engineering. A big thank you as well to the amazing people who I have met throughout my time as a student and have made this time unforgettable. Finally, I would like to dedicate this work to Maarten.

Tijn Schell
Rotterdam, May 2025

Contents

1

Introduction

1.1. Research context and problem

This study focuses on the coast of Lagos State, home to the city Lagos, Nigeria's largest urban centre with a population nearing 16 million. Lagos is currently the second most populous city on the African continent and continues to grow rapidly with an annual population increase of 6–8%, more than double the national average of 2.6% [1, 2]. Between 2000 and 2015, Nigeria's economy expanded significantly, with a GDP growth rate of 7% annually [3]. Given its economic importance and dense population, the coastal area of Lagos State plays a crucial role in the country's future development.

The wave climate at the Lagos State coast is characterized by high-energetic south-south-west swell waves. Due to the predominance of waves approaching from the south-southwest, a large eastward-directed longshore current is induced, which has been estimated to be around $650.000m^3 - 1.000.000m^3$ per year [4]. These conditions make the Nigerian coast highly vulnerable to coastal erosion, with local rates reaching up to 11 metres per year [5]. According to research by Croitoru et al. [6] on behalf of the West African Coastal Areas Management Program (WACA), The World Bank and The Global Program Of Sustainability (GPS), erosion alone has cost 1.65 billion US dollars in the year 2018 for just Lagos State, representing 1.7% of the state's GDP [6].

Climate change significantly influences the Nigerian coast through both rising sea levels and changes in wave climate, creating challenges for future coastal management. Recent research has linked global climate change to rising sea levels, higher ambient temperatures, and intensified weather events, largely attributed to human activities [7, 8, 9, 10]. Projections indicate that sea levels along the Lagos State coast could rise by up to 80 cm by 2100 [11]. Additionally, according to Hemer et al. [12], wave climate projections suggest an increase in significant wave height for the region by 2070–2100 compared to 1979–2009 and a westward shift in wave direction [12].

In order to combat this coastal erosion, several hard engineering solutions, such as groynes [13], have been implemented. While these structures have provided localized relief, they have also caused sediment deficits downstream (to the east), intensifying erosion in those areas. These groynes also trap the sediment resulting in a sediment deficit downstream (to the east) of these ports. Despite these measures, and in some locations because of them, Lagos is still struggeling with the protection of it's coastline and according to the State Commissioner for Waterfront Infrastructure Development, Yacoob Alebiosu, it is a priority to protect the coastal villages [14].

1.2. Research objective

This research project aims to assess the long-term impact of climate change on shoreline evolution along the Lagos State coastline. Specifically, the study investigates how sea level rise and changes in wave height and wave direction influence patterns of erosion and accretion over a 50-year period. By applying the one-dimensional shoreline evolution model ShorelineS, the project provides a spatially detailed analysis of expected coastal change and identifies areas most at risk of future erosion.

1.3. Research scope

The Nigerian coast is approximately 700 km long, this study will focus mainly on the western part of the coast of Nigeria defined by the Lagos state coast. This area is defined from the border with Benin up to the border between Ogun and Ondo. This area comprises approximately 200 km and includes Lagos city and important economical areas like the Lekki port.

To incorporate the influence of climate change and to analyse the response of the beach on a long-term time scale, a time scale of 50 years will be used in this research project. Sea level rise, the significant wave height and wave direction will be the climate change related variables used to assess their impact on coastal erosion along the Lagos State coast.

There are multiple models possible that can be used to model the morphological response of a shoreline. In this research project the model ShorelineS will be used as it has proven to be a good model for making long-term evaluations and impact assessments of coastal structures [15]. It is a free-form coastline model that is open source and was initiated by stichting Deltares and IHE-Delft [16].

1.4. Research question

The main research question for this thesis project will be: *How will sea level rise and changing wave climate affect long-term shoreline dynamics along the Lagos State coastline?*

- Sub-question 1: What are the projected changes in wave climate and sea level over 50 years at the Lagos State coast?
- Sub-question 2: What engineering workflows are available to simulate long-term coastal morphological evolution in the context of climate change?
- Sub-question 3: How can historical data be used to calibrate the engineering workflows?
- Sub-question 4: What are the expected patterns of erosion and accretion along the Lagos State coastline under future climate scenarios?
- Sub-question 5: What are the relative contributions of different climate change variables (e.g. sea level rise, wave height, wave direction) to projected shoreline change?

2

Literature Review

This literature review establishes the theoretical foundation for the thesis project by examining relevant scholarly works and research. The literature review begins by discussing the coastal dynamics at the Lagos State Coast. Secondly, this section explores the available models and provides a comprehensive explanation of the ShorelineS model.

2.1. The Lagos State coast

This section introduces the relevant coastal dynamics at the Lagos State Coast. First, the present day structures and the Lagos Lagoon will be outlined after which the wave climate and climate change influence will be introduced. Following this, existing modeling studies of the region will be reviewed. The Lagos State Coast is approximately 200 km long at stretches from the border between Benin and Nigeria to the border between the state of Lagos and the state of Ogun.

Lagos state coast is located in the Bight of Benin, which is also part of the Gulf of Guinea. The areas can be seen in figure 2.1

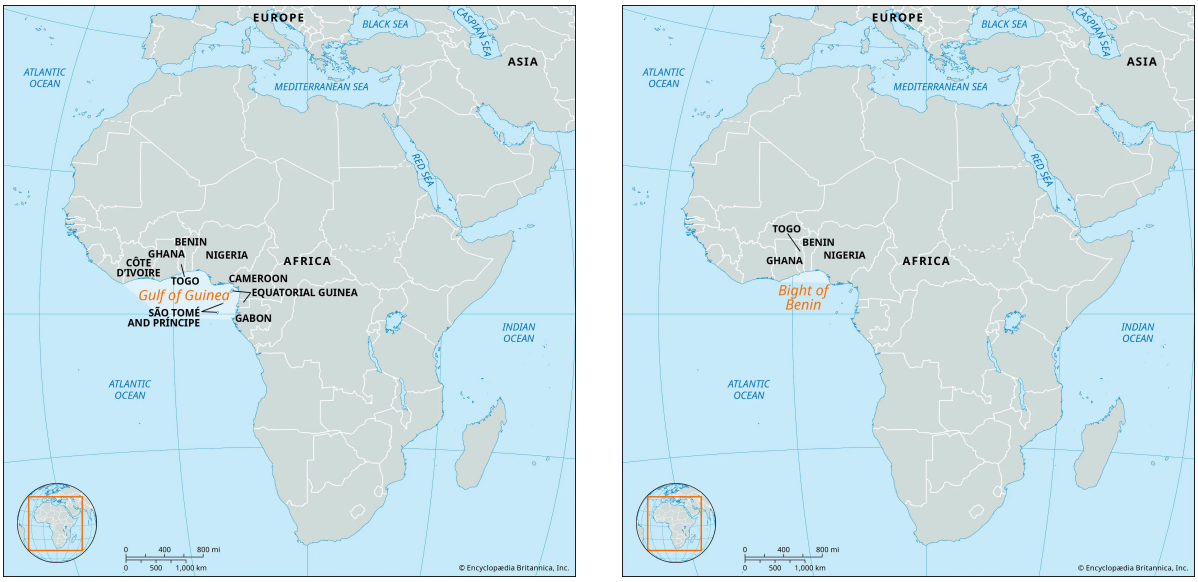

(a) Gulf of Guinea map.

(b) Bight of Benin map.

Figure 2.1: Maps showing the Gulf of Guinea (left) and the Bight of Benin (right). Sources: [17] and [18].

2.1.1. Structures

Along the Lagos State coastline there are various different structures that will be introduced in this section. First of all, when moving along the coastline from west to east, the Commodore Channel is found, which functions as the harbor channel connecting the harbors of Lagos to the oceans and as the tidal inlet for the Lagos Lagoon. The channel is fixed by a mole on the west site and Eko Atlantic on the east side. Right after Eko Atlantic a groyne scheme is implemented. Further to the east two harbors are found, Dangote Quays Lekki and Lekki Port.

Eko Atlantic

Eko Atlantic is a newly created reclaimed area at the coast of Lagos City. The project, initiated in 2008, is a public-private partnership project between the Lagos State government and South Energyx Nigeria Limited (SENL). It's aim is to increase housing stock, attract investors and to increase coastal resilience [19]. It will eventually span an area of 9 Km^2, protected by revetments. In 2012, vanBentum [20] conducted research on the long-term morphological impact of Eko Atlantic and found that, while the total erosion volumes remain unaffected, the erosion is shifted further downstream in an eastward direction [20]. A recent satellite image can be seen in figure 2.4.

Groyne Scheme

Just eastward of Eko Atlantic, a groyne scheme consisting of 19 groynes has been implemented to locally preserve the coastline. The system has provided local relief, but on the east side of the groynes, significant erosion is occurring as can be seen in figure 2.2, which shows the groyne scheme east of EKO Atlantic.

Figure 2.2: Satellite image showing the groyne scheme east of EKO Atlantic [21].

Lekki Deep Sea Port

Approximately 50 km to the east from the groyne scheme, the Lekki Deep Sea Port is found. This port can accommodate ships of 16.5 meters depth. Construction of this port started around 2018 and has caused erosion on the western side and accretion on the eastern side since.

Dangote Quays Lekki

Furthermore, approximately 10 km east of the Lekki Deep Sea Port, Dangote Quays Lekki is located. The design, which was performed by CDR International BV, uses the eastern longshore transport to its advantage by making use of a Sandbar Breakwater. A paper was published by Spek et al. [22] on its design. Figure 2.3 shows both Lekki Deep Sea Port and Dangote Quays Lekki with the Sandbar Breakwater.

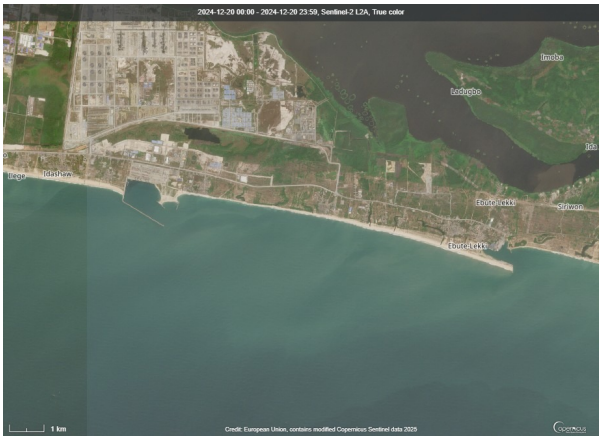

Figure 2.3: Satellite image showing Lekki Deep Sea Port (left) and Dangote Quays Lekki with the Sandbar Breakwater (right) Sentinel-2 Image, True Color [21].

Figure 2.4: EKO Atlantic and the Commodore Channel Sentinel-2 Image, True Color [21].

2.1.2. Lagos Lagoon

The Lagos Lagoon is one of the biggest lagoons of the West African coast with an area of approximately $200km^2$. [20]. The Lagos Lagoon is primarily connected to the sea by the Commodore Channel, which is a tidal inlet that functions as the entrance of the Lagos Harbour. It is situated on the west side of EKO Atlantic as can be seen in figure 2.4. According to Bentum the Lagos Lagoon acts as a sediment sink depending on sea level rise where a 5 mm/year rise will result in a sediment import of 75,000 m^3 per year and 10 mm/year will result in a sediment import of 150,000 m^3 per year.

Tidal inlets are characterized by the reversal of flow during the transition of the tide into ebb or flood. During flood the water flows from the sea into the Lagos Lagoon via the channel, during ebb the water flows out into the sea again. However, because this study looks at the long term development of the Lagos State coast, the short term tidal implications will not be taken into consideration.

2.1.3. Wave Climate

The wave climate is analyzed by the usage of ERA5 Hindcast data at location 6° N, 3.5° E, which is approximately 48 km off the coast of Lagos State.

In figure 2.5 the wave rose that was deducted from this data has been plotted. As can be noticed, the wave direction is south-south-west and has a narrow directional bandwidth.

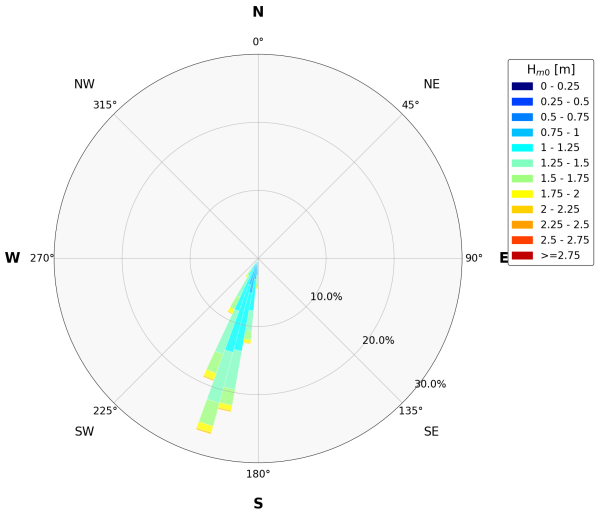

Figure 2.5: Wave rose based on offshore hindcast wave data from the ERA5 Hindcast and Reanalysis Archives for location 6° N, 3.5° E (approximately 48 km off the coast) for the period 1959–2021 [23]

The wave climate at location 6° N, 3.5° E is also characterized by seasonal patterns as can be seen in figure 2.6. The significant wave height shows some seasonal fluctuation with a peak during the wet season (June-September) and low values not going lower than 0.75 m. The peak wave period remains uniform throughout the year with values between 10 - 16 s.

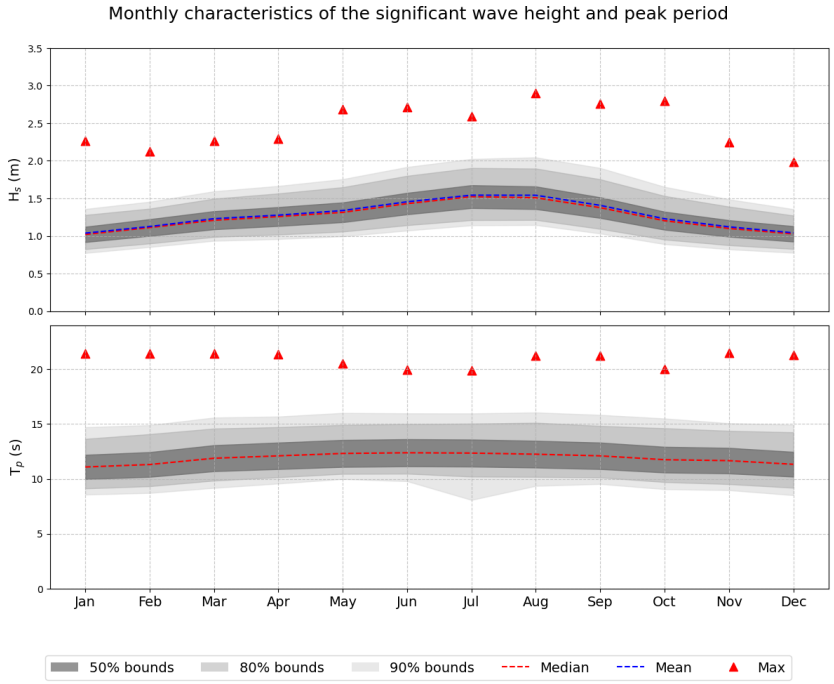

Figure 2.6: Seasonal characteristics for the significant wave height and the peak period, based on offshore hindcast wave data from the ERA5 Hindcast and Reanalysis Archives for location 6° N, 3.5° E (approximately 48 km off the coast) for the period 1959–2021 [23]

Furthermore, an analysis of the past 110 years of waves and coastline evolution to climate variability at the Niger Delta (located east of the Lagos State Coast) with a dataset obtained from the ECMWF ERA-20C atmospheric reanalysis showed that the significant wave height has increased by 0.264 m presently (1980-2010) compared to 80 years before (1900-1930). Also for the mean wave period an

increase was visible of 0.32 s in the same time span, along with a 2-degree shift in wave direction (θm), indicating a westward trend [24].

2.1.4. Future projections wave climate

This section introduces the future projections for the wave climate at the Lagos State coast. Projecting future values for the wave climate is challenging and involves considerable uncertainty as it depends on climate scenarios and choices made in the future.

Worldwide projections of the wave direction, significant wave height and wave period are available through the Coordinated Ocean Wave Climate Project (COWCLIP) phase 2, where the first coordinated multivariate ensemble of 21th century global (wind-)wave was made available based on ten CMIP-5-based state-of-the-art wave climate studies [25]. In this thesis project, 20 of these globel wave climate projections were used to assess the projected wave climate at 6° N, 3° E for two different RCP scenarios (RCP4.5 and RCP8.5). The results can be seen in figure 2.7.

These wave climate projections are derived using a combination of global climate models (GCMs) and spectral wave models. First, future atmospheric conditions such as wind speed and direction are simulated using GCMs developed under the Coupled Model Intercomparison Project Phase 5 (CMIP5), based on different greenhouse gas emission scenarios (RCP4.5 and RCP8.5). These wind fields are then used to force global wave models, which compute how waves evolve over time and space in response to wind forcing. By harmonizing the outputs of multiple such model pairings, the COWCLIP Phase 2 ensemble provides physically consistent and spatially comprehensive projections of future changes in significant wave height, mean wave direction, and wave period. This coordinated modeling approach also allows for quantification of inter-model uncertainty.

The significant wave height is projected to increase under both scenarios for the majority of the global wave climate projections. Under RCP4.5 the median of the projections for the significant wave height lies at +1.31 % with a maximum of + 3.5% and a minimum of -1.3 %. Under RCP8.5, both the median and extremes indicate a more pronounced increase with a median of +3.3 % and a maximum of +6.5% and a minimum of -0.4 %.

The wave direction is also projected to change. Under both scenarios, the inter quartile range, which represents the middle 50% of the model projections, lies largely or entirely above the 0 line, indicating that wave directions will shift further westward. Under RCP4.5, the median increase is +0.3° with a maximum of +0.8° and a minimum of -0.5°. For RCP8.5, the median is +0.3° and the maximum is +1.7° and the minimum -0.6°.

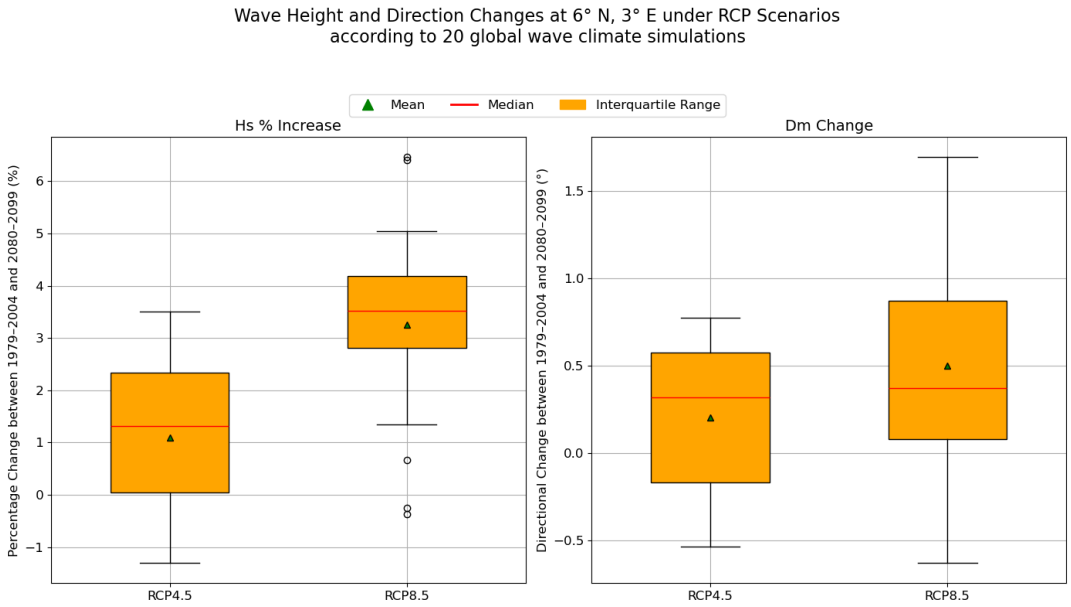

Figure 2.7: Projections for changes in significant wave height and wave direction between 1979-2004 and 2080-2099 for different scenarios (RCP4.5 and RCP8.5) based on COWCLIP phase 2 [25]

2.1.5. Sea Level Rise

Throughout Earth's history, sea levels have experienced significant fluctuations over time. However, recent observations linking global climate change to rising sea levels in certain regions have been largely attributed to human activities. Increasingly, scientists concur that climate change has contributed to a global rise in sea levels, higher ambient temperatures, intensified precipitation, and other extreme weather events [7, 8, 9, 10]. According to the IPCC AR6 Shared Socioeconomic Pathways (SSP), the sea level rise in front off the coast of Lagos State is expected to increase up to 1.4 meters. The different projections for the different SSP's are shown in table 2.1 [26].

Climate scenario	SLR range
SSP1-2.6	0.18 m to 0.887 m
SSP2-4.5	0.295 m to 1.073 m
SSP3-7.0	0.417 m to 1.234 m
SSP5-8.5	0.502 m to 1.401 m

Table 2.1: Sea level rise offshore Lagos State Coastline (at the 6° N, 3° E)[26] for four different Shared Socioeconomic Pathways (SSP's).

2.1.6. Longshore Sediment Transport

The longshore sediment transport is the net movement of sediment particles through a fixed vertical plane perpendicular to the shoreline [27]. Accurately quantifying longshore sediment transport presents significant challenges due to the complexities involved in its direct measurement. The longshore sediment transport at Lagos State coast has been estimated in earlier studies. Van Bentum [20] found a yearly mean eastward longshore sediment transport of roughly $600.000\ m^3/year$ to $700.000\ m^3/year$ around EKO Atlantic. Around the same location, at Lagos Harbor, Allersma and Tilmans [28] found a mean eastward longshore sediment transport of $500,000\ m^3/year$ to $1,000,000\ m^3/year$. Van der Spek et al. [22] calculated the longshore transport at Lekki Quays by using the CERC formula and found an average value between $650,000\ m^3/year$ to $1,000,000\ m^3/year$, with yearly fluctuations of +-20%. At this Lekki coast, Wang, Shen, and Zhao [4] found a net eastward sediment transport between $584,000\ m^3/year$ to $962,000\ m^3/year$.

2.1.7. Previous Modeling Studies in the Gulf of Guinea

Numerous studies have examined the historical, current, and projected changes along the Gulf of Guinea coastline. This section provides an overview of the current state of knowledge on modeling and characterizing the Gulf of Guinea's coastal dynamics.

Giardino et al. [29] have modeled the West African coastline (Ivory Coast - Benin) with the Unibest model in order to come up with a large-scale sediment budget accounting for human interventions and climate change. In this systematic approach, the climate change impacts were investigated for the time period 2075-2100. Based on their finding, they have proposed a suggestion for setting up a regional sediment management plan. Furthermore, they found that the influence of sea level rise on the sediment budget is less compared to the influence of the changing wave climate. Especially the shift in the direction of the waves will induce an alternation of erosive and accretive patterns [30].

Abessolo Ondoa et al. [31] and Abessolo et al. [32] have also researched the coastal dynamics off (the bight of) Benin. First of all, in 2017 a study was conducted in which the storm-impact and seasonal cycles at the coast of Grand Popo, Benin were researched. The research was based on video monitoring from 2013-2016 accompanied by field data and Wavewatch III IOWAGA wave hindcast data. They found that the alongshore average shoreline position was determined more by the seasonal wave height pattern than the storm intensity [31].

Additionally, a research was conducted in which the CASCADE coastal evolution model was used to assess the coastline of the Bight of Benin in the period from 2000-2015 taking into consideration anthropogenic influences (such as coastal structures) excluding climate change. The results were used to estimate the needed amount of sediment to combat the coastal erosion in the area [32].

Furthermore, Landsat images from 1990 - 2015 were used to assess the shoreline change in the Bight of Benin [33]. This article complements the research by Almar et al. [34], which examined the origins and temporal dynamics of the wave climate impacting this coastline. It includes calculations of sand volumes transported alongshore by wave action and provides estimates of how climate change might affect the wave regime and longshore sediment transport [34].

The influence of the Lekki Port has been studied over a timespan of almost 20 years by Wang, Shen, and Zhao with the use of shoreline evolution model Litdrift. It was found that under natural conditions the shoreline near to the Lekki Deep Sea port is relatively stable. The shoreline to the west will shift to the tip of the breakwater in the next 20 years. However, sand bypassing will start earlier [4]. The shoreline to the East of Lekki Deep Sea Port will shift a maximum of 260 meters in the next 200 years.

Finally, the MIKE 21/3 model was used in two studies: one by Daramola et al. (2022) assessing the impact of sea level rise on coastal retreat along Nigeria's Mahin mud coast and another by Badru et al. (2022) modeling sediment transport along the southwestern coast of Nigeria. Both studies were conducted over relatively short time scales: two days in September 2020 and three months in 2011, respectively. For the Mahin mud coast it was found that the eastern part is most vulnerable to sea level rise and for the southwester coast of Nigeria it was found that reactive, site-specific hard-engineering coastal management approaches will give counter-productive results and a long-term, regional wide coastal management is needed.

2.2. Available models

Various models are available for (long-term) coastal modeling. They all vary in complexity, computational demands and stability. Every model has its own advantages/disadvantages, simplification and assumptions. This section will give an overview of the available models and explain the model that will be used in this thesis project.

There have been numerous (review) papers that give a very clear overview of the available models. In 2020 Montaño et al. [37] published a paper in which both shoreline evolution models and machine learning techniques were tested on the Tairua beach in New Zealand with a calibration period from 1999-2014 and a forecast period from 2014-2017 [37]. Furthermore, a review paper by Mutagi, Yadav, and Hiremath [38] was published in 2022, which gives an overview of different available models used for alongshore, cross-shores, sandy coasts and estuaries for both long-term and short-terms periods [38]. Additionally, another review paper was published by Hoagland et al. [39] in 2023, which focuses

more on the application of models on Coastal Barriers, such as those found along parts of the Lagos State coastline [39].

Finally, a paper by Hunt et al. [40] from 2023 present an overview of shoreline modeling techniques differing in complexity [40]. The paper categorizes these models into four main groups: Data Driven models, Semi-Empirical models, Reduced-Complexity models and Process-Based models. A summary of the different models is presented in table 2.2 and a morphodynamic modeling complexity spectrum with simplified model examples is given in figure 2.8. The next chapter gives an overview of these four categories.

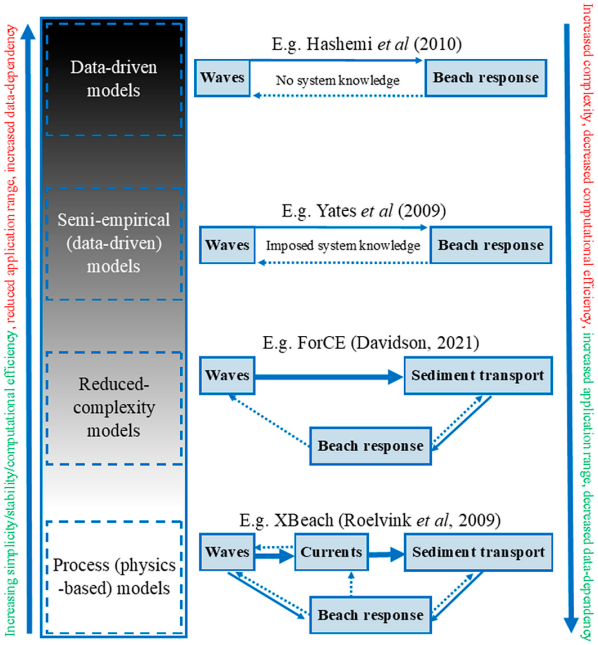

Figure 2.8: The morphodynamic modelling complexity spectrum (left), with corresponding simplified model examples on the right. Advantages/disadvantages are shown in green/red, respectively. [40].

2.2.1. Data Driven models

Data-driven models predict future or previously unseen coastal states by identifying empirical relationships between the forcing and the response time-series, without requiring prior understanding of the physical processes at play. The main advantage of this approach is that it overcomes gaps in system knowledge by allowing the algorithm to learn patterns directly from the data. Data-driven models include two types of models: statistical models and machine learning models. In Machine Learning models, there are no underlying assumptions of the structure of the relationship in the data and the model is trained to find such a structure. Statistical models rely on predefined assumptions about the relationships between variables [41, 40].

Examples of statistical models include: 1) Empirical Orthogonal Function (EOF) analysis, which is used to decompose the temporal evolution of different modes of morphology, where the modes can represent key beach processes [42, 43, 44, 45]; 2) Canonical Correlation Analysis (CCA), which identifies linear combinations of variables in one set (e.g., wave forcing) that are most strongly correlated with linear combinations of variables in another set (e.g., beach profile changes) [46, 47, 48, 49]; and 3) Bayesian Networks (BN), which are probabilistic models that represent conditional dependencies that link variables [50, 51, 52, 53].

In Machine Learning models, algorithms enable computers to learn from datasets. Examples of Machine Learning models are Artificial Neural Networks (ANNs) and Recurrent Neural Networks (RNNs). In ANNs, the relationship between the input (e.g., wave parameters) and output (e.g., beach response) is established through multiple hidden layers, where the connections are quantified and adjusted during the model's training process [54, 55, 56, 57]. RNNs differ from ANNs by incorporating 'memory,' which allows them to account for dependencies on previous data points [58] [41].

During the recent 'Shoreshop' by Montaño et al. [37] it was shown that data-driven models performed comparable to semi-empirical models. However, a lack of generality was observed when applying the data-driven models to new sites or when forcing conditions outside the training datasets were used.

2.2.2. Semi-Empirical models

In Semi-Empirical models, the wave parameters (e.g. wave height, period and direction) are directly linked to coastal response. These models are generally quite simplistic as they skip the intermediate steps of computing for example sediment transport or wave shoaling and dissipation. Some well-known Semi-Empirical models are the shoreline position model by Miller and Dean [59] (2004), the equilibrium profile model by Davidson and Turner [60] (2009) and the ShoreFor model by Davidson, Splinter, and Turner [61] (2013) . The shoreline position model by Miller and Dean was one of the first to develop a semi-empirical model to forecast shoreline change. Davidson and Turner proposed an equilibrium profile model that incorporates a forcing term proportional to the squared dimensionless fall velocity, along with a constant (static) equilibrium term, which is set equal to the mean dimensionless fall velocity. The ShoreFor model by Davidson builds on this previous model and includes a dynamic equilibrium term . Numerous other semi-empirical models exist [62, 63, 64, 65, 66, 67, 68, 69, 70]; however, for the sake of providing a concise overview, they have been excluded from the table [40].

2.2.3. Process-Based models

Process-Based models, also called physics-driven or bottom-up models, demonstrate a significant degree of variation, including area and coastal profile models and depth-averaged (1D/2D) and depth-resolving models (2D/3D). Generally these kind of models are computationally expensive, meaning that longer timescales might take more effort to compute. One of the best known Process-Based models is the Delft3D model, developed by Deltares, which investigates hydrodynamics, simulates wave propagation, sediment transport, currents, morphology, estuarine, and coastal environments [71]. XBEACH is another model where Deltares was one of the developers alongside with UNESCO-IHE, Delft University of Technology and the University of Miami. This is a two-dimensional model for wave propagation, long waves and mean flow, sediment transport and morphological changes of the nearshore area, beaches, dunes and backbarrier during storms [72]. Mike21 is another established model that is used for simulating hydrodynamics and hydraulic phenomena in estuaries, coastal waters, seas, short waves, sediment transport, wave dynamics, and harbors [73]. Telemac is another model that stands out for its efficient and flexible use of finite element methods, which sets it apart from other models [74]. Furthermore, FINEL (FINite ELements) is an inhouse hydrodynamic flow model from Svasek Hydraulics that can be applied in 1D, 2DH, 2DV, and 3D scenarios. This model is designed to map complex phenomena such as sediment transport, morphological seabed developments, and the interaction between waves, currents, water levels, and varying seabed topography [75].

2.2.4. Reduced-Complexity models

Reduced-Complexity models cover a wide range of different models with different dimensionalities and complexities. Generally speaking, they include key processes, focusing only on specific aspects that are crucial to the representation of that process [76]. Overall, they perform better with more complex coastal environments than data-driven or semi-empirical models.

Reduced-complexity models can be categorized into three types based on their primary focus: models that primarily simulate cross-shore evolution, models that focus on longshore evolution, and models that integrate both cross-shore and longshore processes. SBEACH is a cross-shore evolution model that was developed in 1989 by Larson and Kraus and it models wave shoaling, dissipation and setup across the beach profile [77]. A model that follows a similar method to that of SBEACH is ForCE. The ForCe model is computationally efficient and stable, accommodating changes in water levels caused by tides, storm surges, and long-term sea-level rise (dynamic equalibrium) [78].

One of the most well-known 1D long-shore shorline models is GENESIS (GENEralized model for SImulating Shoreline change). The model, grounded in one-line shoreline change theory, assumes a consistent beach profile shape, simplifying shoreline evolution to the movement of a single reference point, such as the Mean High Water shoreline. It accounts for sediment transport driven by oblique wave approaches and longshore wave height gradients, making it one of the most widely used tools for predicting shoreline evolution on longshore transport-dominated beaches over timeframes of 1–100

months and spatial scales of 1–100 kilometers [79]. Similar to GENESIS, varies other one-line models were developed such as ONELINE [80], LITPACK [81], UNIBEST-CL+ [82], LONGMOOR [83] and most recently ShorelineS [16].

Lastly, there are also Reduced-Complexity models that incorporate both cross and long-shore processes. CoSMoS-COAST is such a hybrid one-line model that incorporates shoreline displacement due to cross-shore transport processes, it was developed by Vitousek et al. [64] in 2017 . The LX-Shore model [84] integrates the Kamphuis [80] longshore transport model with the ShoreFor model [61] which results in a model capable of modeling complex morphologies such as sand spits. Antolínez et al. [85] (2019) developed the COCOONED (CrOss-shOre, loNg-shorE and foreDune evolution model) which incorporates the CERC longshore transport model within a one-line equation, including a hybrid transformation of waves and dune erosion, while also accounting for cross-shore processes. The CEM (Coastal Evolution Model) simulates the evolution of sandy, wave-dominated coastlines under varying wave climates. This one-line model is specifically designed to explore how large-scale shoreline patterns emerge from changes in wave direction and climate. CEM2D, which is inspired by CEM, additionally simulates mesoscale morphodynamic evolution, depositional features, and sediment transport driven by changes in water levels [86, 87, 88].

Another model that simulates the long-term evolution of shoreline and long shore and cross shore sediment transport is the CASCADE model, developed by Larson, Kraus, and Hanson [89] in 2002. Build upon the CASCADE model is the GenCade mode, which is also build upon the GENESIS model. It is a shoreline change and sand transport model which was build by the US Army Corps of Engineers in 2012 [90]. Furthermore, the Q2D-Morfo model, which was made by Arriaga et al. [91] is a model that is based on the wave-driven alongshore sediment transport, including cross-shore transport in a simplified way and neglecting tides [91].

Model Category	Model Name	Description	Reference	Year
Data Driven Models - Statistical	Empirical Orthogonal Function (EOF)	Decomposes morphological changes into modes for analysis and prediction.	[42, 43, 44, 45]	NA
	Canonical Correlation Analysis (CCA)	Identifies linear combinations of variables in one set (e.g., wave forcing) that are most strongly correlated with linear combinations of variables in another set (e.g., beach profile changes).	[46, 47, 48, 49]	NA
	Bayesian Networks (BN)	Probabilistic model that represents conditional dependencies between variables.	[50, 51, 52, 53]	
Data Driven Models - Machine Learning	Artificial Neural Networks (ANNs)	Relationship between output (e.g., beach response) and input (e.g., wave forcing) is learned during training.	[54, 55, 56, 57]	NA
	Recurrent Neural Networks (RNNs)	Able to incorporate 'memory,' which allows them to account for dependencies on previous data points.	[58]	2021
Semi-Empirical Models	Shoreline Change Model	Forecasts shoreline change.	[59]	2004
	Equilibrium Profile Model	Incorporates dimensionless fall velocity for shoreline evolution.	[60]	2009
	ShoreFor Model	Includes a dynamic equilibrium term; applies to global cross-shore transport-dominated coasts.	[61]	2013
Reduced-Complexity Models	SBEACH	Cross-shore evolution model modeling wave shoaling, dissipation, and setup across the beach profile.	[77]	1989
	ForCe	Computationally efficient and stable, accommodating changes in water levels caused by tides, storm surges, and long-term sea-level rise (dynamic equilibrium).	[78]	2021
	GENESIS	One-line model for shoreline evolution driven by sediment transport and wave gradients.	[79]	1989
	ONELINE	A simplified one-line model focused on shoreline change due to sediment transport and wave dynamics.	[80]	1993
	LITPACK	A software package that includes a one-line shoreline change model as part of its suite for simulating coastal sediment transport and morphodynamics.	[81]	2016
	UNIBEST-CL+	A numerical model that uses one-line theory for simulating long-term shoreline evolution and sediment transport along coasts.	[82]	2011
	LONGMOOR	A one-line numerical shoreline evolution model.	[83]	2018
	ShorelineS	A modern one-line model designed for efficient shoreline evolution predictions over large spatial and temporal scales.	[16]	2020
	CoSMoS-COAST	Hybrid model combining cross-shore and longshore processes for shoreline displacement.	[64]	2017
	LX-Shore model	Combines longshore and cross-shore sediment transport for complex morphologies.	[84]	2018
	COCOONED	Models cross-shore and longshore sediment transport along with foredune evolution.	[85]	2019
	CEM	Predicts mesoscale morphodynamic coastline evolution and sediment transport.	[86, 87]	2001
	GenCade	A shoreline change and sand transport model combining CASCADE and GENESIS.	[90]	2012
	CASCADE	Long-term shoreline and sediment transport model.	[89]	2002
Process-Based Models	Delft3D	Simulates complex wave, sediment, and morphological dynamics.	[71]	2004
	XBeach	Focused on storm impact on coastal morphology, including dune erosion.	[72]	2009
	MIKE21	A comprehensive modelling system for the simulation of hydraulics and hydraulic-related phenomena in estuaries, coastal waters and seas.	[73]	1992
	TELEMAC	Simulates 2D/3D hydrodynamics and sediment transport processes.	[74]	2013
	FINEL	Svasek Hydraulics's inhouse hydrodynamic flow model that can be applied in 1D, 2DH, 2DV, and 3D scenarios.	[75]	NA

Table 2.2: Overview of available models, their descriptions, references, and years.

2.2.5. Model Selection

Based on the comparison of available model types, ShorelineS was selected for this study due to its suitability for large-scale, long-term shoreline evolution modeling. While process-based models like Delft3D offer detailed representations of physical processes, they are computationally expensive and require extensive site specific input data, often unavailable for the Lagos State coastline. On the other hand, reduced-complexity one-line models such as ShorelineS strike a balance between physical realism and computational efficiency, making them well suited for simulating decadal scale coastal changes under multiple climate scenarios.

2.3. ShorelineS

This paragraph explains the functioning of ShorelineS. ShorelineS, being a one-dimensional (1D) coastline model, is particularly well-suited for studying the long-term evolution of coastlines. The model focuses on broad temporal and spatial scales, making it useful for studying the coastal dynamics of Lagos State's 200 km-wide coastline over a timescale of several decades. ShorelineS is recently developed by J.A. Roelvink (Deltares/Unesco-IHE/TU Delft) and B.J.A. Huisman (Deltares/TU Delft).

In the model, the coastline is represented as a series of grid points that dynamically expand or contract based on changes in sediment volume. Figure 2.9 provides a visualization of this concept. These grid points simulate the movement of the active coastal profile, capturing the evolution of the coastline contour. The conservation equation used in ShorelineS to update the coastline is:

$$\frac{\delta n}{\delta t} = -\frac{1}{D_s}\frac{\delta Q_s}{\delta s} - \frac{RSLR}{\tan(\beta)} + \frac{1}{D_s}\sum q_i \tag{2.1}$$

Where:

- n is the cross-shore coordinate
- s is the longshore coordinate
- t is time
- D_s is the active profile height
- Q_s is the longshore sediment transport
- $\tan(\beta)$ is the average profile slope
- $RSLR$ is Relative Sea Level Rise
- q_i are other source or sink terms

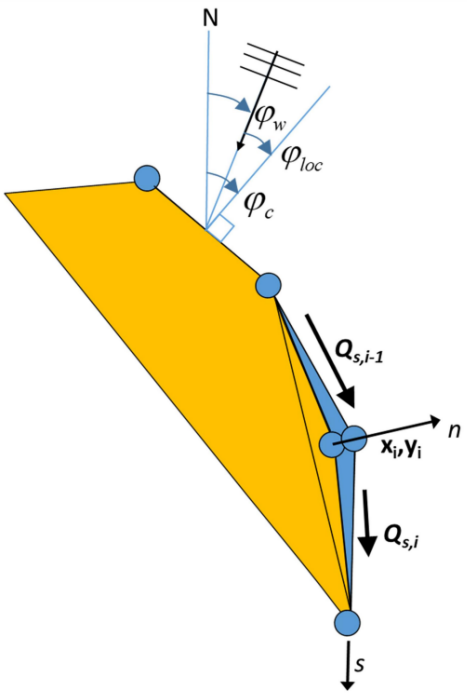

Figure 2.9: Coastline schematization used in ShorelineS, from [16].

In line with other 1D coastline models, ShorelineS assumes that the cross-shore profile remains in equilibrium. This assumption justifies the exclusion of cross-shore sediment transport processes. Consequently, coastline changes are primarily driven by wave-induced longshore sediment transport. The longshore transport equations available in ShorelineS are listed in Table 2.3.

Longshore Transport Equation	Formula
CERC1	$Q_s = bq_{scal}H_{s,off}^{5/2}2\sin(\phi_{\text{off}})$
CERC2	$Q_s = K_1 q_{scal} t_{sc} H_s^{12/5} T^{1/5} \cos^{6/5}(\phi_{\text{off}}) \sin(\phi_{\text{off}})$
CERC3	$Q_s = K_2 q_{scal} t_{sc} b H_{s,br}^{5/2} \sin(2\phi_{\text{br}})$
Kamphuis	$Q_s = 2.33 q_{scal} t_{sc} K_3 H_{s,br}^2 T_p^{1.5} \tan_\beta^{0.75} D_{50}^{-0.25} \sin^{0.6}(2\phi_{br})$
Mil-Homens	$Q_s = 0.15 q_{scal} t_{sc} K_3 H_{s,br}^{2.75} T_p^{0.89} \tan_\beta^{0.86} D_{50}^{-0.69} \sin^{0.5}(2\phi_{br})$
Van Rijn 2014	$Q_s = 0.0006 \cdot q_{scal} t_{sc} K_4 K_{swell} \rho_s \tan_\beta^{0.4} D_{50}^{-0.6} H_{s,br}^{2.6} v_{total}$

Table 2.3: ShorelineS longshore transport equations.

CERC1 and CERC2
While most transport equation make use of the wave angle at breaking, which are indicated by a subscript *br*, CERC1 and CERC2 use the offshore significant wave height ($H_{s,off}$) and wave direction (ϕ_{off}). CERC1 is the simplest formula and has as main function to illustrate the principles of behaviour of the coastline model. CERC2 is based on CERC1 and includes refraction and shoaling in the formula.

Two coefficients for CERC1 and CERC2 are introduced, b and K_1. These are computed as:

$$b = \frac{k\rho\sqrt{g/k}}{16(\rho_s - \rho)(1-p)} \tag{2.2}$$

$$K_1 = \left(\frac{g\gamma}{2\pi}\right)^{1/5} K_0, \quad K_0 \approx 0.4 \tag{2.3}$$

Where:

- k is the wave number
- g is the gravitational acceleration
- ρ_s is the density of sediment
- γ is the breaking index
- K_1 is the default calibration coefficient according to the Shore Protection Manual [92].

CERC3
CERC3 is widely used in models such as GENESIS, it is derived from CERC1, but applied after wave transformation has taken place. $H_{s,br}$ and ϕ_{br} are therefor the significant wave height and wave direction at the breaking. In CERC3 scaling parameter K_2 is defined as followed:

$$K_2 = \frac{K_o}{16(1-p)(\rho_s - \rho_w)/\rho_w}\sqrt{\frac{g}{\gamma}} \tag{2.4}$$

Kamphuis & Mil-Homens
The Kamphuis and Mil-Homens equation are similar to CERC3, but introduce extra input parameters such as beach slope (β) and grain size (D_{50}) to achieve more precise outcomes with reduced calibration effort. Also the wave period (T_p) is incorporated in this formula. Mil-Homens differs from Kamphuis as it has re-calibrated the parameters. The K_3 parameter is defined as followed:

$$K_3 = \frac{1}{(1-p)(\rho_s - \rho_w)} \tag{2.5}$$

Van Rijn 2014
The van Rijn equation from 2014 is similar to the Mil-Homens and Kamphuis equations, but require also a swell-parameter (K_{swell}), which depends on the occurrence of swell waves and a parameter to account for additional currents (v_{total}), which is defined as:

$$v_{total} = v_{wave} + v_{current} \tag{2.6}$$

$$v_{wave} = 0.3(gH_{s,br})^{0.5} sin(2\phi_{br}) \tag{2.7}$$

It must be noted that in the current version of ShorelineS $v_{current}$ is set to zero. K_4 is defined as:

$$K_4 = \frac{1}{\rho_s(1-\rho)} \tag{2.8}$$

And K_{swell} is defined as:

$$K_{swell} = 0.015P_{swell} + (1 - 0.01P_{swell}) \tag{2.9}$$

2.3.1. Numerical implementation

This subparagraph aims to explain the numerical implementation of ShorelineS. ShorelineS uses two column vectors, x_cm and y_cm, which may be in a cartesian (metric) system. Each set of coordinates defines a single point. These points collectively represent the dynamic evolution of the coastline.

In ShorelineS, the offshore wave climate can be specified using one of three methods [16]:

1. By means of wave direction and a spreading sector. A uniform distribution is assumed between the mean wave direction and plus or minus half the spreading sector. For time step a random wave direction will be chosen from this sector.
2. By means of a wave climate considering a number of wave conditions. A condition will be chosen randomly for every timestep.
3. By means of a time series of wave conditions, for which the model will interpolate in time.

ShorelineS applies Snell's law for refraction and depth-induced breaking (based on the breaking index (γ). Shoaling is based on the change in wave-celerity and group velocity at the considered depths. The transformation of deep-water waves to the toe of the dynamic profile assumes parallel offshore depth contours.

Boundary Conditions
Four options are available for the definition of the boundary conditions in ShorelineS. A closed boundary where there is no sediment transport at the boundary. A fixed coastline position, which ensures that the transport at the boundary is the same as the transport in the adjacent transport point of the coastline which results in a zero transport gradient. A third option is a fixed coastline orientation, in this case the initial orientation of the coastline is kept constant. The last option is a periodic boundary where the computed transport rates at the start and end grid points will be averaged throughout the simulation [16].

2.3.2. Coastline evolution

In this section, the approach of ShorelineS to simulate coastline evolution is discussed. As illustrated in Figure 2.9, the local orientation of the coastline is determined by the positions of adjacent points. For each coastline point, the longshore sediment transport is computed. If there is a transport gradient between two points, the coastline will either erode or accrete accordingly. The mass-conservation equation, previously introduced as Equation 2.1, is solved using a staggered forward time-central space explicit scheme.

$$\Delta n_i^j = -\frac{1}{D_c}\frac{2(Q_{s,i}^j - Q_{s,i-1}^j)}{L_i}\Delta t \tag{2.10}$$

Here, j is the time step index, Δt is the time step size, i indicates the point index, and L_i is the length of the corresponding grid element, calculated as: $L_i = \sqrt{(x_{i+1} - x_i)^2 + (y_{i+1} - y_i)^2}$. Where x and y are Cartesian coordinates. For normal displacement, the changes in coastline position are given by:

$$\Delta x_i^j = -n_i^j \frac{(y_{i+1} - y_{i-1})}{L_i} \tag{2.11}$$

$$\Delta y_i^j = n_i^j \frac{(x_{i+1} - x_{i-1})}{L_i} \tag{2.12}$$

$$x_i^{j+1} = x_i^j + \Delta x_i^j \tag{2.13}$$

$$y_i^{j+1} = y_i^j + \Delta y_i^j \tag{2.14}$$

A variable timestep is used by default in ShorelineS, which ensures computational stability. Since an explicit scheme is used, the time step is constrained for stability, ensuring the following criterion: $\frac{\epsilon \Delta t}{\Delta s^2} < \frac{1}{\epsilon}$. Here, ϵ is the diffusivity, related to the maximum gradient of sediment transport concerning the wave angle relative to the coast. The diffusivity can be approximated as: $\epsilon_{\text{max}} = \frac{2Q_{\text{max}}}{D_c}$, where Q_{max} is the maximum transport rate in the model. This imposes the following limit for the time step:

$$\Delta t < \frac{D_c \Delta s^2}{4Q_{\text{max}}} \tag{2.15}$$

2.3.3. Nourishments

Nourishments can be implemented in ShorelineS by defining a nourishment rate, area and timespan. The model then calculates the shoreline accretion rate by distributing the total volume across the specified coastline length and time period, accounting for the profile height D_c. Nourishments can also be used to prescribe a sediment sink by making the nourishment rate negative [16].

2.3.4. Spatially varying grids

ShorelineS allows for the use of a spatially varying grid, enabling finer resolution in areas of interest and coarser resolution elsewhere. This approach improves computational efficiency while preserving detail where it matters most.

2.3.5. Groyne handling

There are numerous coastal structures that can be defined in ShorelineS. This section will give an introduction to the way groynes are handled. Groynes can be inputted as x and y coordinates and will (partially) block or bypass alongshore sediment transport. Figure 2.10 shows how a groyne is handled in ShorelineS.

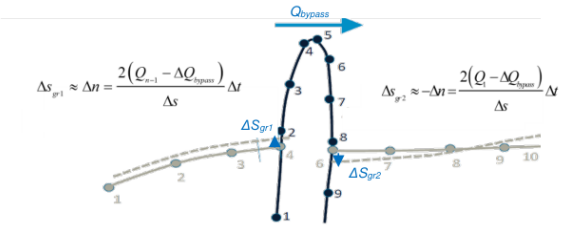

Figure 2.10: Handling of a groyne [16].

The bypassing of the groyne happens when the depth at the tip of the groyne (D_{LT}) is smaller than the active depth of the longshore transport (D_s).

$$QS_{bypass} = \begin{cases} \left(Fc - \frac{D_s}{D_{LT}}\right) QS_{updrift} & \text{if } D_s \leq D_{LT} \\ 0 & \text{if } D_s > D_{LT} \end{cases} \tag{2.16}$$

Where F_c is typically 1 based on the equilibrium profile shape of Dean. D_s is defined as followed:

$$D_s = A_p y_{str}^{2/3} \tag{2.17}$$

Where y_{str} is the distance from the structure's head to the nearest point of the coastline and A_p the sediment scale parameter depending on D_{50} and defined as $A_p = (1.04 + 0.086 * log(D_{50}))^2$. The active longshore transport (D_{LT}) is calculated as followed:

$$D_{LT} = \frac{A_w}{y}(H_{1/3})_b \tag{2.18}$$

Where A_w=1.27, a factor that converts the highest 1/10 waves to the significant wave height and y is the breaker index and $(H_{1/3})_b$ is the significant wave height at the breaker line. The bypassed sediment is distributed uniformly along the downdrift side of the groyne until reaching the location where the bypassed transport volume becomes smaller than the unshadowed transport.

Wave Diffraction

In addition to their impact on sediment transport, coastal structures also influence wave patterns. Structures such as groynes can create sheltered zones where wave diffraction plays a key role in shaping the coastline. In these areas, the incoming wave energy is reduced due to the reorientation of wave angles around the structure. This diffraction effect is modeled as a reduction in wave height, which depends on the angle and direction of the diffracted wave originating from a diffraction point, for example the tip of the structure.

3

Methodology

This chapter outlines the methodological approach used to address the research objective and sub-questions of this thesis. It begins with an overview of the overall methodology, followed by a detailed description of the wave transformation process. Subsequently, the application of the ShorelineS model is discussed. The chapter then addresses sources of uncertainty and concludes with a description of the conducted ShorelineS simulation runs.

3.1. Overall Methodology

To obtain predictions for the shoreline dynamics up to the year 2075 in ShorelineS, numerous steps have to be taken. First of all, the initial coastline and structures need to be schematized in the model. Secondly, the nearshore wave conditions need to determined. This is done by using 400 MDA selected offshore hindcast wave conditions for both sea and swell waves and transforming these to nearshore wave conditions with a SWAN model for the area of interest to be used as an input for a gaussian process model to transform the full offshore dataset to nearshore conditions. Calibration of the ShorelineS model will be done based on historical shoreline positions retrieved from satellite data. A schematization of the overall methodology can be seen in figure 3.1. This chapter provides a more detailed explanation of these steps. It first introduces the SWAN model and its associated components, followed by the set-up of the ShorelineS model. Finally, the chapter discusses the uncertainty in the modeling approach and presents the final ShorelineS simulations.

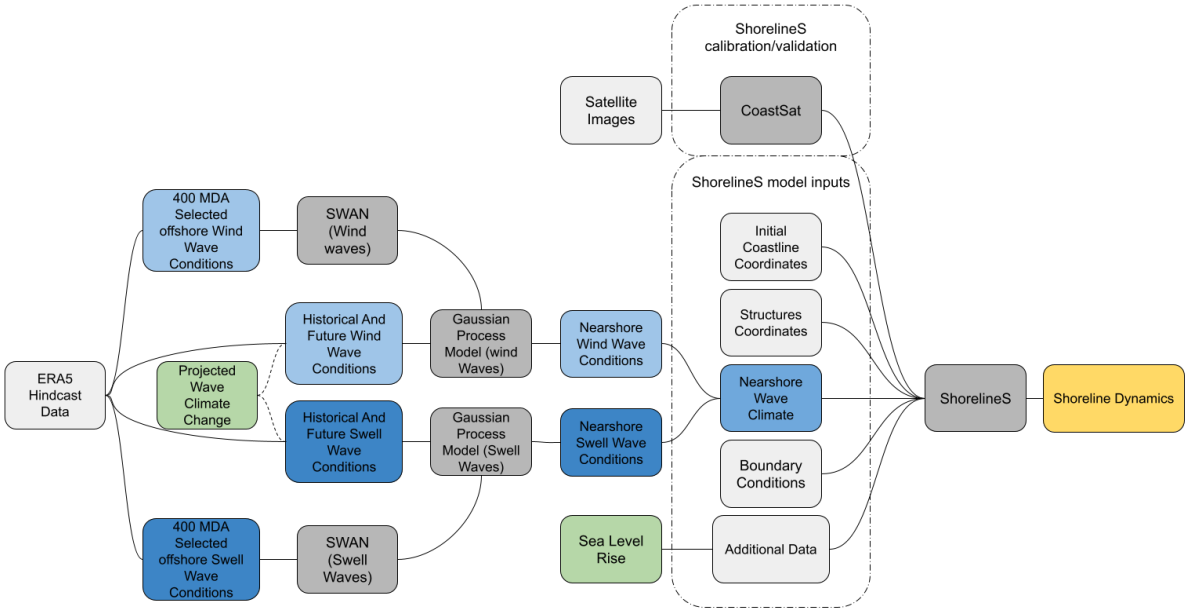

Figure 3.1: Schematic overview of the methodology applied in this thesis project. Light grey boxes indicate input data, while dark grey boxes represent the tools used.Light blue boxes relate to wind wave processes, and dark blue boxes to swell wave processes. Green boxes represent climate change-related components, and the yellow box indicates the final shoreline dynamics output.

3.2. Wave Transformation

This section provides the wave transformation process. First, an overview of the model set up of SWAN is given after which an overview of the model set-up is provided, followed by three assessments conducted to evaluate the computational grid. Subsequently, the Gaussian Process model used for nearshore wave transformation is introduced. Finally, the approach for incorporating climate change projections into the wave climate is described.

SWAN (Simulating WAves Nearshore) is a numerical wave model designed for simulating wave propagation in coastal and nearshore environments [93]. It is widely used in coastal engineering to model wave transformations, including refraction, diffraction, and breaking, under various conditions. It is capable of transforming offshore wave conditions into nearshore wave parameters.

3.2.1. Model set-up

In SWAN, there are multiple inputs that need to be defined: The Grid, the bathymetry, the offshore wave climate, wave breaking parameter and the model parameters.

Grid

This study employed a triangular grid where a coarser mesh density was applied in offshore regions, while a finer mesh density was implemented in nearshore areas to improve detail and accuracy in areas where coastal processes are more active. In the definition of the grid, boundaries need to allocated at which the wave climate is enforced. Three distinct offshore boundaries were established to simulate spatially varying wave conditions at the model's offshore limit. Figure 3.3 shows the grid's coarser and finer density as the shore is approached.

Bathymetry

The bathymetry used in the SWAN simulations is derived from publicly available GEBCO data. However, the accuracy of this dataset becomes worse in nearshore areas. To address this limitation, more precise Navionics data was utilized for nearshore regions and the grid was adjusted accordingly. The bathymetry is in line with the bathymetry used in earlier projects by CDR International BV in the same area and it can be seen in figure 3.2.

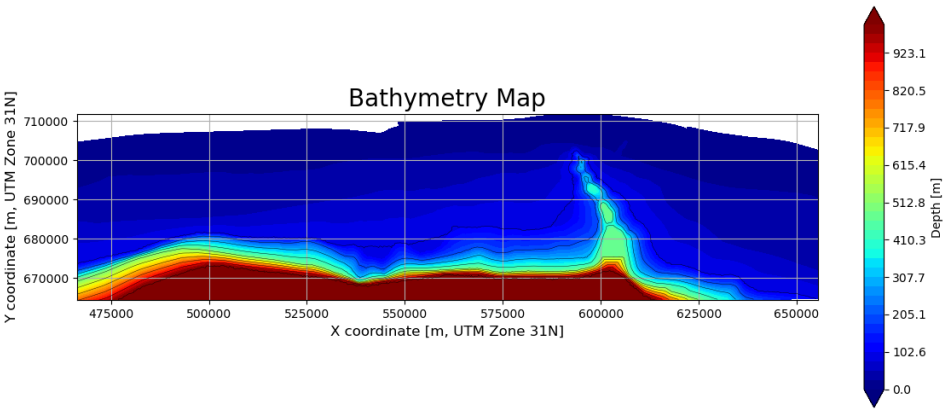

Figure 3.2: The bathymetry used as input in the SWAN model.

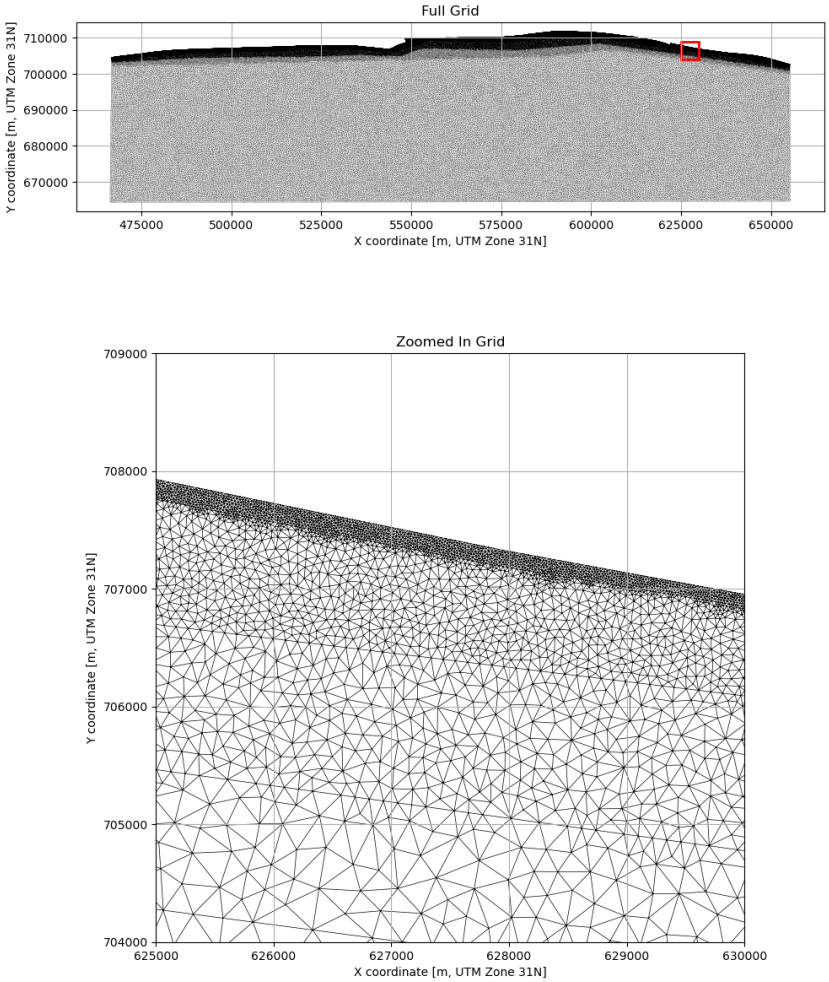

Figure 3.3: The original full grid and a zoomed in part of the grid to show to finer density near the shore.

Wave breaking index

In SWAN, the default of the breaking index is set to 0.73. However, for the SWAN runs related to swell the breaker index was set to 0.8. Swell waves are generally longer than wind waves and carry more energy. Swell waves have a higher breaker index compared to wind waves because they will act more as plunging breakers (gamma between 0.8 and 1.2) rather than spilling breakers (gamma between 0.6

and 0.8) [27]. For the SWAN runs related to wind a breaking index of 0.73 was used.

Model parameters
There are multiple parameters that need to be defined in SWAN. Parameters that differ from the default settings are listed below.

- TRIADS were turned on to include wave-wave interaction.
- WCAP was turned on to include the influence of white capping.
- Numerical parameters where SWAN stops the process if the relative change in H_s from one iteration to the next is less than [drel] and the curvature of the iteration curve of H_s normalized with H_s is less than [curvat] or the absolute change in H_s from one iteration to the next is less than [dabs]. Both conditions need to be fulfilled in [npnts] percentage of all wet points.
  - Dabs = 0.012
  - Drel = 0.012
  - Curvat = 0.012
  - Npnts = 99

Offshore Wave Climate
The offshore wave climate needs to be defined in SWAN in the form of H_s (signifcant waveheight), T_p (peak wave period), θ_w (wave direction) and θ_{dspr} (directional spreading) at the boundary of the grid. For both wind and swell waves, this data can be obtained from the ERA5 hindcast dataset [23], which provides global coverage at a 0.5° latitude/longitude resolution and spans a time series from 1959 to 2021. In chapter 3.2.3 a more elaborate explanation will be given on how this wave data was obtained. A directional spreading of 10° was used for swell waves, and 30° for wind waves.

3.2.2. Grid Assessment

During the set up of the SWAN model, the grid and bathymetry were used as shown in figures 3.2 and 3.3. Three assessments were conducted in order to assess the validity of this implemented grid and bathymetry. The tests are summarized in table 3.1 and a more extended explanation is given later in this chapter.

Assessment	Difference from original	Summary
Grid extent	Vertically expanded computational grid	Because the offshore waves propagate to the nearshore at an angle, a shadow zone arises. This assessment quantifies the extent of this shadow region.
Depth at boundary	Forcing boundary at 1000 m depth	It is assumed that the depth of the boundary forcing points is at 1000 m depth, however this is not everywhere the case in the original grid. This assessment utilizes boundary forcing points at 1000 m depth.
Depth ERA 5	Input wave conditions of 1000 m depth	It is assumed that the depth at which the input wave conditions were computed in the ERA5 dataset is also 1000 m. This was not the case and more offshore conditions were used that were computed at 1000 m depth.

Table 3.1: Grid assessments

Grid extent

The total width of the grid is about 200 km, which is the same width as the area of interest. However, because of offshore waves propagating towards the shore at differencing angles, a shadow zone arises where the nearshore waves representative of the actual wave conditions not representative of the

actual nearshore wave climate. The wave direction distributions are shown in table 3.2. As can be seen, most of the waves (>99%) are in the range of 180-220 degrees. Because of this unidirectional wave climate a large part of the nearshore waves will be accurate calculations of the actual nearshore wave climate. However, this unidirectional wave climate also has as a result that a part at the west side of the calculated nearshore wave conditions are not representable for the actual wave conditions. To determine which nearshore output points wave climate in the SWAN runs with the original grid are representable for the actual nearshore wave climate a horizontally expended grid was constructed

In order to test this, a larger grid was used to test various wave conditions from the previously defined direction bands. This grid can be seen in figure 3.4. As can be seen in figure 3.5b, for a wave direction between 200-210 degrees (which represent 25.61% of the waves) the first 25 points are not accurate. For wave direction 180 - 190 (figure 3.5a, representing 19.17% of the waves) it can be seen that the last 10 points are also not accurate. That is why the area of interest was refined by excluding the first 25 points and the last 10 points, effectively reducing the study domain by approximately 35 km. The results for all the different wave directions can be found in appendix A.

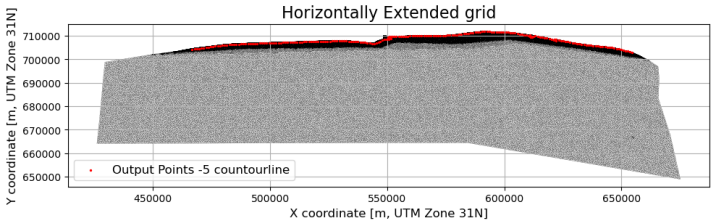

Figure 3.4: Horizontally extended grid with the output locations highlighted in red.

Wave Direction Range (degrees)	Percentage (%)
< 180	0.70
$180 - 190$	19.17
$190 - 200$	51.12
$200 - 210$	25.61
$210 - 220$	3.24
> 220	0.17

Table 3.2: Wave Direction Distribution from ERA5 Hindcast Data (1956–2020) at 6°N, 3°E

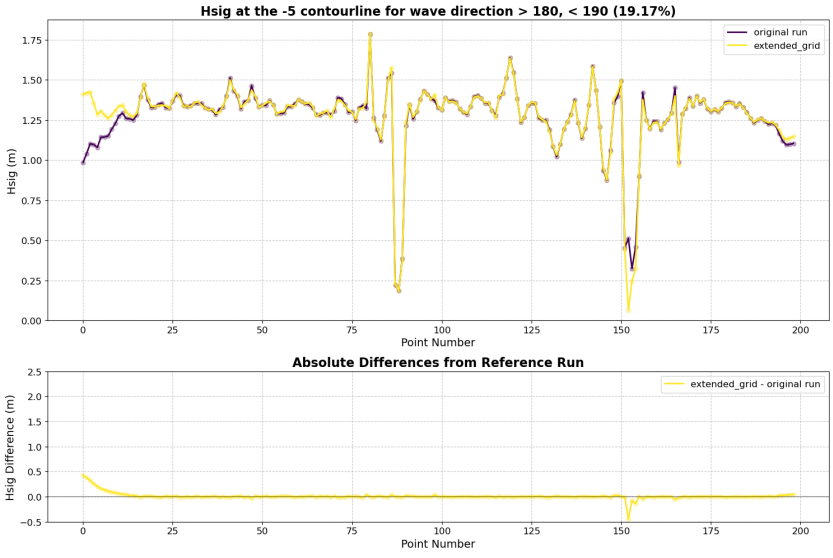

(a) Hsig for wave direction 180–190 (19.17%)

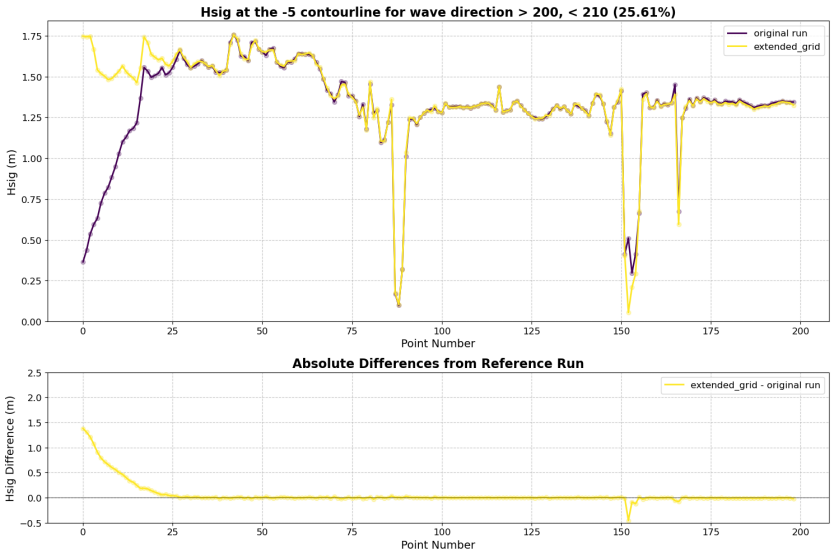

(b) Hsig for wave direction 200–210 (25.61%)

Figure 3.5: Top graph: Hsig at the output points at the -5m contourline for different wave directions. The yellow line represents the horizontally expended grid and the purple line represents the original smaller grid. Lower graph: absolute difference between waveheights at the -5m contourline modeled in the horizontally expended grid and the original grid.

Depth at boundary

The wave conditions are enforced on the southern boundary in figure 3.3. As can be seen in figure 3.3 and 3.2, the bathymetry at this southern boundary is not homogeneous. In the model, it is assumed that this depth is approximately 1000 meters, for a large part of the southern boundary this is the case, but for the eastern part depths go as low as 100 meters. This creates a potential source of error in the model's wave predictions. This has been tested by changing location of the forcing boundary in such a way that it falls in the 1000 m depth zone. This new grid can be seen in figure 3.6.

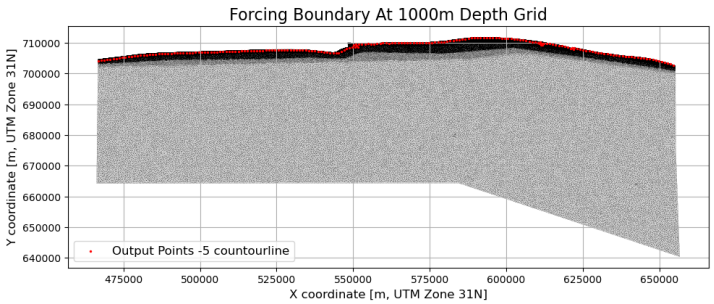

Figure 3.6: Forcing boundary at 1000 m depth grid with the output locations highlighted in red.

Again six different representative wave directions were simulated to investigate the influence of the difference in depth at the forcing boundary. The two most important results can be seen in figure 3.7 which shows the significant wave height at the -5 m output points for wave direction 180-190 and wave direction 190-200. The first shows a small discrepancy between the test run and the original run at the eastern boundary, which supports the conclusion of excluding the 10 most eastern points. The second plot shows the most frequent wave direction, for which no relevant discrepancies are noticed. All six representative wave directions can be seen in appendix A.

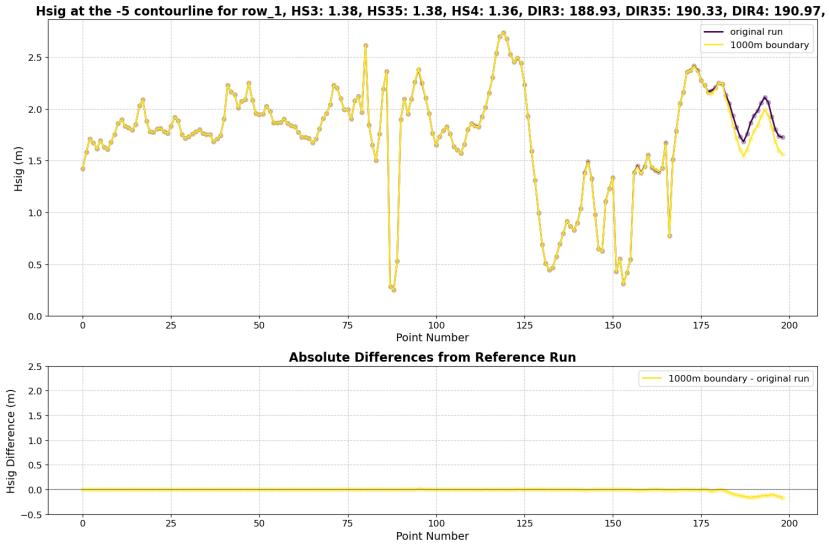

(a) Hsig at -5 m output locations for wave direction 180–190 (19.17%)

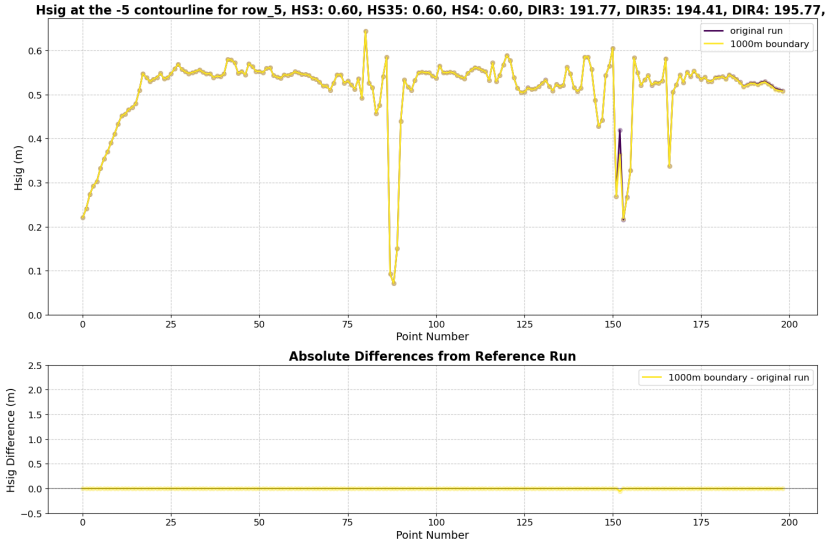

(b) Hsig at -5 m output locations for wave direction 190–200 (51.12%)

Figure 3.7: Top graph: Significant waveheight at the output points at the -5m contourline for different wave directions. The yellow line represents the 1000m boundary grid (grid figure: 3.6) and the purple line represents the original smaller grid (grid figure: 3.3). Lower graph: absolute difference between waveheights at the -5m contourline modeled in the 1000m boundary grid and the original grid

Depth ERA5

During the set-up of the SWAN model, the depth at the three locations for which the ERA5 hindcast data was extracted was assumed to be similar to the depth of the respective locations in the bathymetry. However, after further investigating the depths of the ERA5 hindcast dataset, it was found that the depths were not similar to the depths of the locations in the bathymetry. At the three locations the depth in the bathymetry used in the SWAN model was 1000 meter. However, the ERA5 hindcast data for location 6°N, 3°E was extracted at 79.00 meter, for location 6°N, 3.5°E was extracted at 138.01 meter and for location 6°N, 4°E was extracted at 166.99 meter. This mismatch could as well create a source of error in the model's wave predictions. At locations 5.5°N, 3°E, 5.5°N, 3.5°E and 5.5°N, 4°E in the ERA5 hindcast data the wave climate was extracted at approximately 1000 meter. A grid was constructed which is vertically extended in such a way that the forcing boundary is at the 5.5°N, this new grid can be seen in figure 3.8.

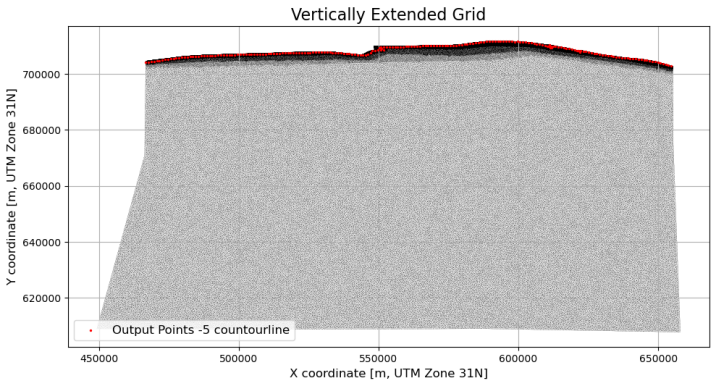

Figure 3.8: Input wave conditions at 1000 m depth grid with the output locations highlighted in red.

As can be seen from figure 3.9, which shows the significant wave height at the -5m contour line for a predominant wave direction of 190-200 degrees, the two model simulations demonstrate comparable outcomes. All the other representative wave directions can be seen in appendix A.

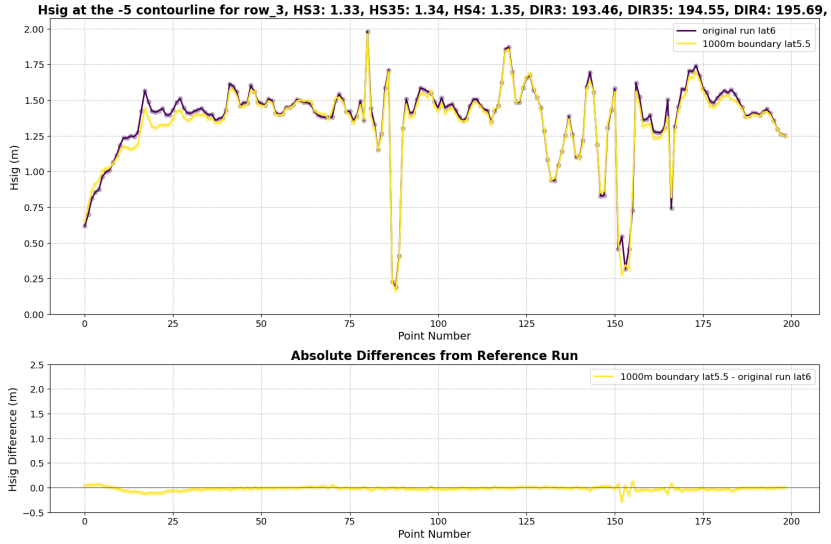

Figure 3.9: Significant wave height at the -5m contour line for wave direction 190–200 (51.12%). The yellow line represents the vertically extended grid up to latitude 5.5 (grid figure: 3.8), the purple line represents the grid adjusted to 1000m depth boundaries (grid figure: 3.6). The lower graph shows the absolute difference between wave heights at the -5m contour line modeled in the vertically extended grid and the 1000m boundary grid.

3.2.3. Maximum Dissimilarity Algorithm

Simulating the complete 3-hourly ERA5 hindcast wave climate from 1959 to 2021 for both wind and swell waves with SWAN to obtain the corresponding nearshore conditions would be too computational expensive. That is why a maximum dissimilarity algorithm was used to select a representative subset of the wave climate diversity of 400 time steps for both wind and swell waves. These 400 representative time steps are later used in a Gaussian Proces Model to convert the complete timeseries from offshore to nearshore conditions. This paragraph presents the main concepts of an MDA and outlines the methodology applied. The Python package mdapy, which was used in this master thesis, was developed by Pablo García Pérez [94], based on the MDA as proposed by Guanche et al. [95].

The steps in the MDA are as followed. First the algorithm is initialized by starting with an empty subset S and choosing the first data point arbitrarily. Secondly, the iteration starts in which for each data point in the subset S the minimum distance from that point to the points in the subset is calculated. The point with the greatest dissimilarity (maximum distance calculated) is included in the subset S.

In this project nine different parameters were used in the MDA to select 400 representative time steps in the wave conditions between 1959 and 2021. The parameters were significant wave height, peak wave period and wave direction for three offshore location. For the wind wave conditions not nine, but eleven parameters were used in the MDA, also including the u and v component of the wind velocity. The significant swell wave height is plotted against the swell peak wave period for location 6°N, 3°E in figure 3.10 to give an indication of the results of the MDA.

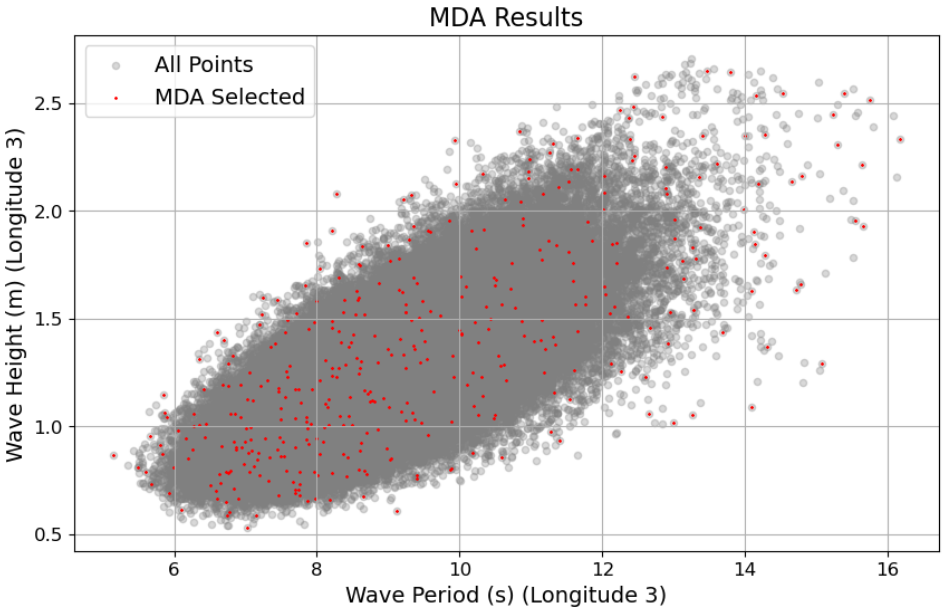

Figure 3.10: MDA results for 6°N, 3°E swell waves. The grey dots represent all the time steps in the ERA5 Hindcast dataset and the red dots indicate the points selected by the MDA algorithm.

3.2.4. Gaussian Process model

This paragraph provides the key aspects of the Gaussian Process model used. After the 400 SWAN runs have been completed for both wind and swell waves, a Gaussian Process model is used to convert all the 184.088 timesteps (3-hourly since 1959) offshore conditions into nearshore wave conditions at the approximately 200 nearshore output locations. Gaussian Process models offer a non-parametric probabilistic framework ideal for identifying nonlinear dynamic systems. In this thesis project a Gaussian Process model made by BJ van der Spek was used which has been used in previous projects for transferring offshore waves to nearshore waves conditions. Furthermore, Gaussian Process models have proven to be effective in deriving nearshore wave conditions from global wave model outputs [96, 97].

In the Gaussian process model, y represents the nearshore wave parameters and x represents the offshore wave parameters. Here, y is assumed to take the following form [98].

$$y = f(\mathbf{x}) + \epsilon \tag{3}$$

Where the noise term $\epsilon \sim \mathcal{N}(0, \sigma_n^2)$.. The function $f(\mathbf{x})$ is distributed as a Gaussian process [98].

$$f(\mathbf{x}) \sim \mathcal{GP}(m(\mathbf{x}), k(\mathbf{x}, \mathbf{x}')). \tag{3.1}$$

A Gaussian Process $\mathcal{GP}$ is defined by a mean ($m(\mathbf{x})$ and a covariance function $k(\mathbf{x}, \mathbf{x}')$). The mean function reflects the expected function value at input x. In this project a linear mean function was used [98].

$$m(\mathbf{x}) = \beta_0 + \beta_1 x_1 + \beta_2 x_2 + ... + \beta_n x_n \tag{3.2}$$

where β_i are coefficients that are learned during model training.

The covariance function $k(\mathbf{x}, \mathbf{x}')$ defines the similarity between function values at different input points. In our implementation, we selected the Matérn kernel (with v = 3), which is a type of radial basis function, as our covariance function [99]:

$$k_{\text{Matérn}}(\mathbf{x}, \mathbf{x}') = \sigma^2 \frac{2^{1-\nu}}{\Gamma(\nu)} \left(\sqrt{2\nu} \frac{|\mathbf{x} - \mathbf{x}'|}{l} \right)^{\nu} K_\nu \left(\sqrt{2\nu} \frac{|\mathbf{x} - \mathbf{x}'|}{l} \right) \tag{3.3}$$

where σ^2 is the signal variance, l is the characteristic length scale, Γ is the gamma function, and K_ν is the modified Bessel function of the second kind.

The Matérn kernel was chosen because it better captures the physical nature of ocean wave transformation processes, which typically exhibit some degree of smoothness but can also contain sharp transitions [99].

For making predictions with the trained GP model, we need to calculate the marginal probability distribution p(y). The joint probability distribution of observed targets conditioned on function values f(x) is defined as:

$$p(\mathbf{y}|f(\mathbf{x})) = \mathcal{N}(f(\mathbf{x}), \sigma^2 I) \tag{3.4}$$

where I is a diagonal matrix representing independent noise [100].

To predict the nearshore wave conditions at a new offshore point x*, we need to determine the marginal probability distribution $p(y*)$. This is obtained by marginalizing the conditional distribution $p(y* | f(x*))$ over the distribution $p(f(x*))$ [100]:

$$p(y^*) = \int p(y^*|f(\mathbf{x}^*))p(f(\mathbf{x}^*))df(\mathbf{x}^*) \tag{3.5}$$

$p(y* | f(x*))$ is Gaussian thus this integral yields another Gaussian distribution [100]:

$$p(\mathbf{y}) = \mathcal{N}(f(\mathbf{x})|m, K) \tag{3.6}$$

Gaussian Process model performance

In this section the performance of the Gaussian Process model will be analyzed. This was done by taking 20 random samples from the ERA5 Hindcast time series from 1959-2021 for both swell and wind waves. These 40 offshore wave conditions were converted to nearshore conditions both by SWAN and by the Gaussian Process Model. Figure 3.11 and 3.12 show the comparison between the SWAN and Gaussian Process Model for the signifcant wave height and the wave direction of the swell and wind waves. The perfect match is plotted in red and the colors indicate the density of the overlapping points, where brighter colors indicate a higher density.

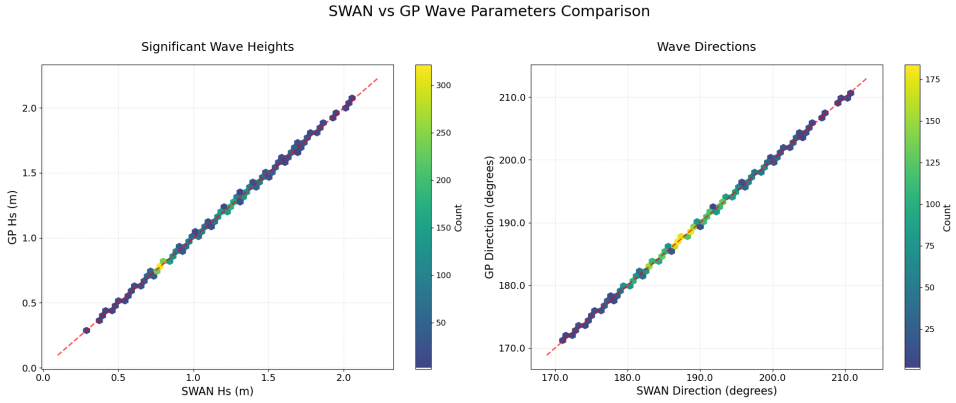

Figure 3.11: Comparison between SWAN and Gaussian Process model predictions for swell waves significant wave height (left) and wave direction (right) at the -10 m contour line for the 20 random samples at the approximately 200 nearshore output locations. Colors indicate the density of overlapping points, with brighter colors representing higher concentrations. The dashed red line shows the perfect match line.

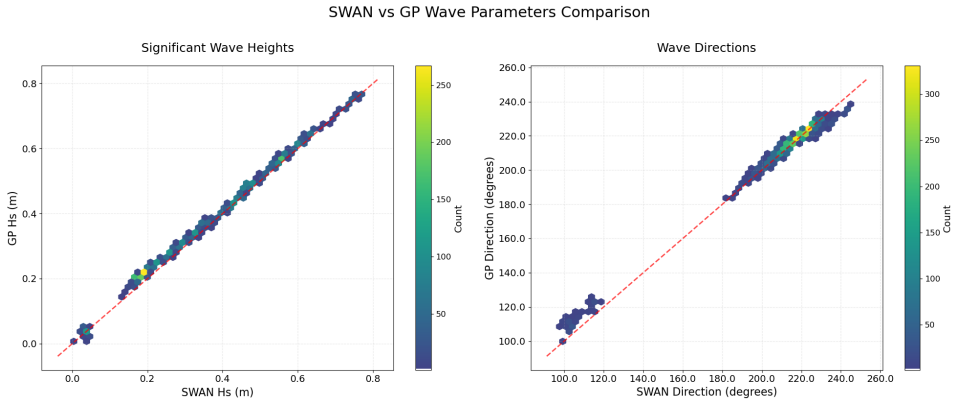

Figure 3.12: Comparison between SWAN and Gaussian Process model predictions for wind waves significant wave height (left) and wave direction (right) at the -10 m contour line for the 20 random samples at the approximately 200 nearshore output locations. Colors indicate the density of overlapping points, with brighter colors representing higher concentrations. The dashed red line shows the perfect match line.

The comparisons presented in Figure 3.11 and 3.12 demonstrate a high degree of concordance between the Gaussian Process model predictions and the SWAN simulation results. This validation confirms the capability of the Gaussian Process Model to accurately represent the nearshore wave climate with computational efficiency comparable to the physics-based SWAN model. The GP model shows stronger accordance for swell waves compared to wind waves, which can be attributed to the higher directional spreading typically exhibited by wind waves. The exceptional agreement observed for swell waves suggests that the substantial sample size of 400 may be larger than necessary, given the relatively consistent wave climate patterns observed across the three offshore locations. For wind waves, however, a larger sample size would have been beneficial to better capture the wider range of directional variability.

After converting both wind and swell waves from offshore to nearshore conditions, the two wave components are combined to create the total wave field at approximately 200 nearshore output locations.

3.2.5. Nearshore Wave Climate

Resulting from the previous explained steps, the nearshore wave climate is computed for the nearshore output locations. Figure 3.13 shows the mean significant wave height and the mean wave direction for the relevant nearshore output locations for the years 2010-2019. The locations of structures are included for comprehensibility. The significant wave height fluctuates between a mean value of 0.9 and 1.5 meters. At all locations, the mean wave direction exceeds 180°. Note that this is measured

clockwise from true (geographic) north, not relative to the shoreline.

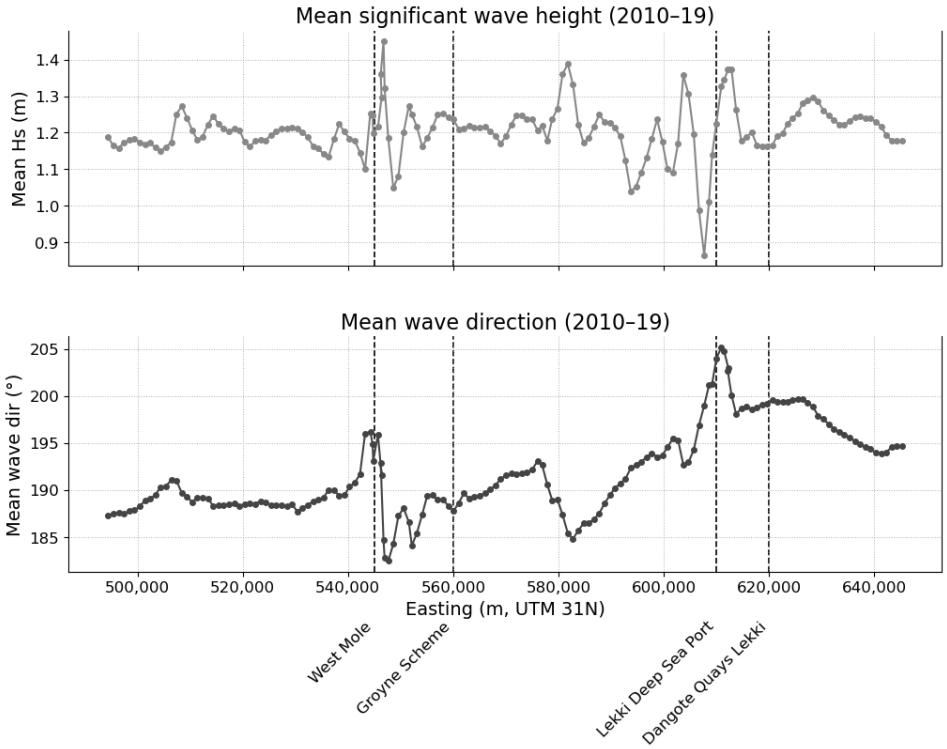

Figure 3.13: Mean significant wave height and mean wave direction for the relevant nearshore output locations at -10 m depth for the years 2010-2019. Locations of structures are included for comprehensibility.

3.2.6. Incorporating Climate Change

To account for climate change, the respective changes in significant wave height and wave direction are applied to the offshore wave conditions for both swell waves and wind waves, These waves are than transferred from offshore to nearshore conditions after which they are combined nearshore.

3.3. ShorelineS Model Setup and Calibration

ShorelineS, as described in chapter 2.3, is a 1D coastline model and is written in Matlab. This paragraph provides an overview of the model set-up and calibration.

3.3.1. Model Set-up

ShorelineS requires inputs that need to be defined: The initial coastline, the structures coordinates, the wave climate, boundary conditions and additional data.

Initial Conditions

Initial conditions for the model required establishing both the initial shoreline position and existing coastal structures.

Initial shoreline

The initial shoreline used for this study is based on the 2020 shoreline position derived from the spin-up and calibrated ShorelineS simulations covering the period from 2000 to 2020. This approach ensures that the initial shoreline has already partially adjusted to the model's internal dynamics and equilibrium state, reducing potential artificial behavior that might occur if starting from raw observational data. The resulting shoreline is subsequently converted into a .xy format, compatible with the ShorelineS model.

Structures

The structures present at the Lagos State coast include: revetments and groynes. These structure

locations have been allocated and converted to xy coordinates which can be used as ShorelineS input parameters. To develop a more efficient model, several simplifications were implemented. The ports are modeled as simple groynes rather than complex port structures. Similarly, Eko Atlantic and its associated groyne system have been consolidated into a single representative groyne. This simplification is appropriate given the regional scale of the study, where the cumulative effect of the entire protection system on the larger shoreline dynamics is of greater interest than the localized effects between individual structures. These simplifications significantly reduce computational demands while maintaining the ability to capture the essential large-scale coastal processes and interventions.

Transport Equation

As explained in chapter 2.3, there are multiple transport equations available in the ShorelineS model. In this thesis project the van Rijn 2014 equation was used as this is the latest transport equation which also incorporates the specification of the sediment.

Boundary Conditions

As explained in chapter 2.3 there are multiple ways to define the boundaries in ShorelineS. It has been chosen to set the transport at the boundary at the same rate as the adjacent transport point.

Wave Climate

The nearshore wave climate needs to be defined in the form of the nearshore H_{br} and θ_{br}. As explained in chapter 3.2 the nearshore conditions are derived from offshore ERA5 hindcast wavedata [23] and converted to nearshore conditions by SWAN. For the future wave climate (2020-2075), the wave conditions from 2010-2020 were cyclically repeated to represent subsequent decades. Climate change predictions for significant wave height and wave direction were also included which will be further explained in chapter 3.4.3.

Profile Parameters

The active profile is defined by inner depth of closure to the dune toe. The inner depth of closure is based on Hallermeier equation (equation 3.7). Where H_{12hy} is the waveheight exceeded 12 hours per year and T_{12hy} is the associated wave period. For location 6°N, 3°E the H_{12hy} is 2.58 m and the associated T_{12hy} is 15.95 s. The H_{in} is calculated to be 5.7 meters. The dune toe is assumed to be 4 meters, which is in line with previous projects by CDR Internation BV. The total active profile height comes down to approximately 10 meters. The beach slope $tan(\beta)$ has been set at 1:25. The D_{50} is set at 0.0004 m.

$$H_{in} = 2.28 \cdot H_{12hy} - 68.5 \cdot \frac{H_{12hy}^2}{g \cdot T_{12hy}^2} \tag{3.7}$$

Space and Time Step

The time step is set to variable with a maximum of 1 day. The space step is spatially varying with, utilizing 2000 meters for consistent transects and 300 meters in less consistent regions, such as those with coastal structures.

Calibration factor

A calibration factor q_{scal} is required in ShorelineS. Based on calibration, q_{scal} has been set at 0.45. In chapter 3.3.2 and 4.2 a more elaborate explanation of the calibration process is given.

Model parameter	Setting
Time step	1 day
Initial space step	spatial varying (300-2000) m
Transport formula	VR14
Active profile height	10 m
$tan(\beta)$	1:25
D_{50}	0.0004 m
Wave conditions	Conditions at -10 MSL contour line
Calibration coëfficient	0.45

Table 3.3: Summary of ShorelineS model setup

3.3.2. Calibration

This paragraph summarizes the key elements of the calibration process used to calibrate the ShorelineS model and thereby gives an answer to sub-question 3: *How can historical data be used to calibrate the engineering workflows?* The model will be calibrated based on the development of the coastline at multiple parts of the Lagos State Coastline based on two time periods. The first runs from 2000-2020 and the second from 2017-2021. From 2000-2020 the accretion at the west side of the west mole will be assessed. The second time period from 2017-2021 is interesting because just before this period the construction of the groyne scheme and Lekki Deep Sea Port was finished. These runs therefor simulate the influence of these coastal structures. During the calibration process the scaling parameter q_{scal} will be determined. A summary of the calibration periods can be seen in table 3.4.

Time period	Segments of interest	Note
2000-2020	2, 3 and 4	-
2017-2021	5 and 11	Groyne schema and Lekki Deep Sea Port implemented

Table 3.4: The two time periods for which ShorelineS calibration simulations will be performed including the segments of interest.

CoastSat

CoastSat is an open-source Python toolkit that can be used to obtain time-series of shoreline positions. It was created by Kilian Vos [101]. It is based on satellite images from Landsat 5-9. All the shorelines that were extracted were checked manually and where possible a yearly average shoreline was used in order to minimize errors in the analysis and provide more reliable results.

Because CoastSat cannot handle segments larger than $100km^2$, the coast was split up in segments. In total 11 segments of the Lagos State coast were analyzed with Coastsat. The segments can be seen in figure 3.14.

In the comparison between CoastSat and ShorelineS a reference line was used to calculate the average displacement compared to this reference line. This allows for an analysis where shoreline progression is visualized as displacement over time relative to this baseline. The shoreline displacement is corrected for tidal cycles to establish a baseline measurement.

Figure 3.14: The 11 different segments that were analysed in CoastSat

Calibration Model Set-Up

In this paragraph the model set-up for the calibration period will be elaborated. To a large extent it is similar to the model set-up explained in chapter 3.3.1, however it differs on some aspects. The

calibration period runs from 2000-2021 because in this timeperiod there is an abundance of shoreline position data. This makes it possible to take averages.

Initial Conditions
For the first time period the initial coastline is based on the average shoreline from 2000 based on CoastSat satelite images. In 2000 the coastal structures present were different from the ones present in 2020. The building of Eko Atlantic had not started yet and the two Lekki ports were also not constructed. There were groynes present at Commodore Channel.

For the second time period the initial coastline is based on the average shoreline from 2017 based on CoastSat satellite images. In 2017 Dangote deep see port, EKO Atlantic and the groyne scheme after eko atlantic were constructed. These coastal structures are all taken into consideration in this second calibration time period.

Boundary Conditions
Just as for the future runs, the transport at the boundary has been set to the same rate as the adjacent transport point. Chapter 2.3 provides more detailed information regarding the ShorelineS boundary condition implementation.

Wave Climate
The wave climate is based on the output of the Gaussian Process Model which is based on the ERA5 offshore hindscast data. The wave climate is spatial varying with output locations every 1000 m.

Other Parameters
In line with the future runs, the active profile height is set to 10 meters and the time step is set to variable with a maximum of 1 day. The space step is spatially varying with, using 2000 meters for uniform transects and 300 meters in less uniform areas, such as those with coastal structures.

Just as stated in chapter 3.3.1, the transport formula is the van Rijn 2014 transport formula.

Model parameter	**Setting**
Time step	1 day
Initial space step	spatial varying (300-2000) m
Transport formula	VR14
Active profile height (d)	10 m
ddeep	10 m
dnearshore	6 m
Wave conditions	Conditions at -10 MSL contour line
Calibration coëfficient	0.35; 0.45; 0.55

Table 3.5: Summary of ShorelineS model setup for calibration

3.4. Uncertainty

During the process of estimating the shoreline dynamics of the Lagos State coast, uncertainty plays an important role. In this project the uncertainty has been divided into three categories: Natural variability, Modeling uncertainty and Climate uncertainty.

3.4.1. Natural Variability

Natural variability refers to the fluctuations in the wave climate independent of long-term climate change trends or human interventions. In this project, natural variability has been incorporated by using a 10-year baseline period (2010-2020) for developing future wave climate projections. This approach has as advantages that it captures both the intra-annual variability and the inter-annual variability.

3.4.2. Modeling Uncertainty

The modeling uncertainty refers to the uncertainty in the ShorelineS model. The uncertainty of the SWAN model is not taken into account in this category as this is out of the scope of this project. The modeling uncertainty follows from the assumptions that have been made in setup of the model. As will be explained in chapter 3.3.2 optimal calibration coefficients q_{scal} vary between different segments of

the coastline and thus induce an uncertainty. The Van Rijn formula, which is the longshore sediment transport formula used in this project, is, next to the wave conditions, also dependent on the bed slope (β), sediment characteristics (d_{50} and ρ_s) and the percentage of swell waves present. All these factors function as scaling parameters, which means that variations in any of them will proportionally increase or decrease the total longshore sediment transport, similar to the effect of the q_{scal} parameter. That is why the modeling uncertainty in this project is included by assessing the possible ranges for q_{scal} following from the calibration.

3.4.3. Climate Uncertainty

Getting a grip on uncertainties in climate change predictions poses a challenge. To address this, in this project 20 different global wave climate simulations derived from six state-of-the-art CMIP5-based wave climate models are analyzed. The projected changes in significant wave height (as a percentage) and wave direction (in degrees) were measured for the period 2080-2099 for location 6°N, 3°E, under both the RCP4.5 and RCP8.5 scenarios. The global wave climate simulations were sourced from Morim et al. [25].

The mean of the future (2080-2099) significant wave heights and wave directions for the different scenarios were compared to the base period (1979-2004) and then adjusted to represent conditions for the year 2075. The resulting mean, median range for both scenarios can be seen in table 3.6.

Parameter	Scenario	Mean	Median	Range min	Range max
$H_{s,o}$	RCP4.5	+0.9%	+1.1%	-1.0%	+2.8%
	RCP8.5	+2.6%	+2.8%	-0.3%	+5.2%
θ_o	RCP4.5	+0.2°	+0.3°	-0.4°	+0.6°
	RCP8.5	+0.4°	+0.3°	-0.5°	+1.4°

Table 3.6: Mean, median and range for significant wave height and wave direction changes by the year 2075 based on 20 different wave climate models [25]

Sea Level Rise

Sea level rise under different emission scenarios for the whole world is modelled by the IPCC [26] and the values for the area offshore of the coast of Lagos State are summarized in table 2.1 in chapter 2.1.5. The values for 2080 are shown in table 3.7 and are the values that will be used in the ShorelineS model.

Climate scenario	SLR range
SSP1-2.6	0.16 m to 0.69 m
SSP2-4.5	0.22 m to 0.77 m
SSP3-7.0	0.28 m to 0.84 m
SSP5-8.5	0.322 m to 0.94 m

Table 3.7: Sea level rise at the Atlantic Barrier lagoon coast of Nigeria for the year 2080 [26], based on table 2.1.

3.5. Final Model Scenarios and Simulation Overview

Based on the climate uncertainties as outlined in chapter 3.4 different ShorelineS runs have been derived. First of all the different climate scenario's were applied in ShorelineS. These runs are summarized in table 3.8. The sea level rise median is calculated by taking the mean of the range per scenario. In addition, for both the low and high RCP4.5 and RCP8.5 scenarios, separate simulations were carried out in which sea level rise and wave climate changes (wave height and direction) were applied independently. These runs were specifically included to capture the potential counterbalancing effects of these drivers in accretive areas, where sea level rise tends to induce retreat while wave climate changes can enhance accretion. Secondly, to assess the individual contribution of the different climate change parameters, the runs as outlined in table 3.9 have been conducted.

Run	ΔH_s	$\Delta\theta_s$	SLR	note
1	0 %	0°	0 cm	base scenario
2	-1.0 %	-0.4°	22 cm	RCP4.5 low scenario
3	+1.1 %	+0.3°	45 cm	RCP4.5 median scenario
4	+2.8 %	+0.6°	77 cm	RCP4.5 high scenario
5	-0.3 %	-0.5°	32 cm	RCP8.5 low scenario
6	+2.8 %	+0.3°	56 cm	RCP8.5 median scenario
7	+5.2 %	+1.4°	94 cm	RCP8.5 high scenario

Table 3.8: The different ShorelineS runs and the change in parameters by the year 2075. The changes in significant wave height, wave direction and sea level rise increase or decrease at a constant rate until they reach their projected values for 2075.

Run	ΔH_s	$\Delta\theta_s$	SLR	note
8	+5.2 %	+0°	0 cm	Only ΔH_s (RCP8.5 high)
9	+0 %	+1.4°	0 cm	Only $\Delta\theta_s$ (RCP8.5 high)
10	+0 %	+0°	94 cm	Only SLR (RCP8.5 high)

Table 3.9: The different ShorelineS runs for assessing the individual contribution of the different climate change parameters and the change in parameters by the year 2075. The changes in significant wave height, wave direction and sea level rise increase or decrease at a constant rate until they reach their projected values for 2075.

3.5.1. Definition of Areas of Interest

To enable localized interpretation of the model results, five Areas of Interest were defined along the Lagos State coastline. These areas were selected based on the presence of major coastal infrastructure, known erosion hotspots, and observed variability in shoreline behavior.

These areas are later used in the results chapter to examine spatial differences in projected shoreline displacement. An overview of the Area of Interest locations and characteristics is provided in Figure 3.15.

Figure 3.15: The five areas of interest used to examine the projected shoreline displacement.

4

Results

4.1. Introduction

This chapter presents the findings from the analyses conducted in this research. First, the calibration results are discussed, focusing on shoreline displacement and longshore sediment transport. Secondly, the calibrated ShorelineS model is applied to simulate shoreline evolution and sediment transport under a range of future climate scenarios, providing insights into the potential impacts of sea level rise and wave climate change along the Lagos State coastline. This is followed by an assessment of the associated uncertainties, which highlight the variability in model outcomes.

4.2. Calibration

During the calibration, different segments along the Lagos State coast were assessed for two different time periods. This section first introduces the shoreline displacement analysis, followed by the longshore sediment transport rates for these periods.

4.2.1. Shoreline Displacement

As stated in chapter 3.3.2, the shoreline displacement analysis will be conducted by comparing historical satellite retrieved shorelines with the ShorelineS model. This is done by looking at different segments along the Lagos State Coastline. The segments can be seen in figure 3.14 and the segments of interest are stated in table 3.4.

In the analysis of the shoreline displacement, the average shoreline displacement across each segment was determined by first creating a reference line along the coast. From this line, 200 evenly spaced transects were generated perpendicular to the reference. For each transect, the distance between the reference line and the shoreline was measured along the transect direction, for both the modeled shorelines (from ShorelineS) and the observed shorelines (from CoastSat). The average of these distances was then used to quantify the mean shoreline displacement for each segment.

To account for uncertainty in the satellite-retrieved shorelines, multiple shoreline positions were used to compute a LOWESS (locally weighted scatterplot smoothing) trend of the average shoreline displacement. The LOWESS trend smooths short-term variability and outliers in the satellite data by fitting local regressions to subsets of the data, resulting in a clearer representation of the long-term shoreline movement, enabling a more robust comparison between ShorelineS and CoastSat. To quantify this comparison, yearly displacement rates were computed in meters per year for the LOWESS trend of the satellite retrieved shorelines and the modeled shorelines.

Time period 1 (2000-2020)

In the first time period, the ShorelineS model ran from 2000-2020. In these runs, the West and East Mole around the Commodore Channel were the coastal structures implemented making the segments around these (segments 2, 3 and 4) interesting to look at.

Segment 2

Segment 2 is located at a distance of approximately 12 km west of the commodore channel. The influence of the West Mole is visible in the results of both CoastSat and ShorelineS, both show a similar seaward trend as can be seen in figure 4.1a. When comparing the LOWESS trend and the modeled average displacement, a varying accretive rate of around 0.2 - 1.5 meters per year from 2000-2020 can be observed in the LOWESS trend. A q_{scal} of 0.35 renders an accretion rate of 1.4 meters per year, making it the best fit for segment 2. Figure 4.1b shows the yearly averaged satellite shorelines compared to ShorelineS shorelines.

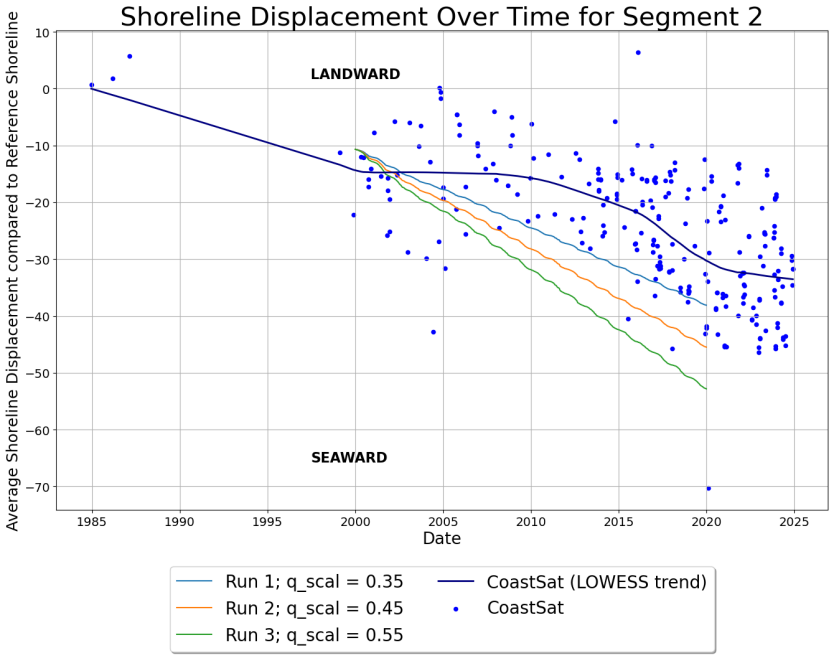

(a) Average distance from reference line. The blue dots indicate the individual CoastSat shorelineas and the dark blue line indicates the Lowess averag of these points. The green (q_{scal} = 0.55), orange (q_{scal} = 0.45) and light-blue (q_{scal} = 0.35) indicate ShorelineS runs from 2000-2020.

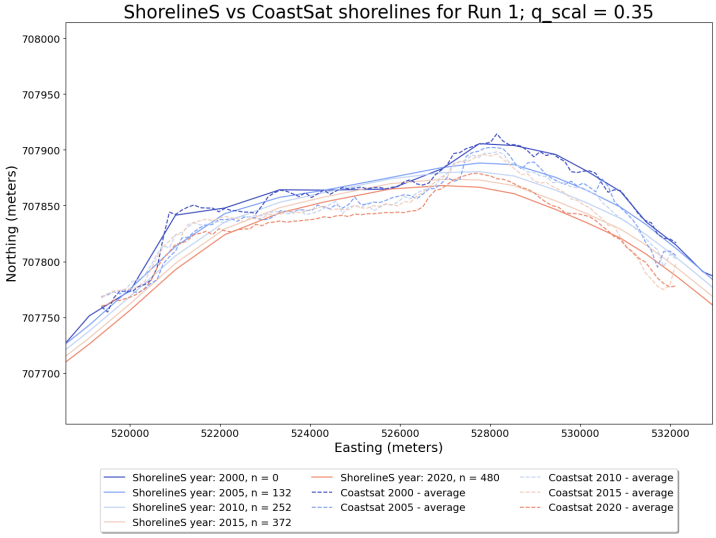

(b) CoastSat yearly averaged satellite shorelines compared to ShorelineS shorelines for the years 2000, 2005, 2010, 2015 and 2020 for $q_{scal} = 0.35$ (blue line in figure 4.1a

Figure 4.1: ShorelineS model runs compared to CoastSat satellite data for segment 2

Segment 3

Segment 3 is located just westward of the western Mole and is characterized by this west Mole that acts as a sediment trap. This results in an accumulation of sediment which is visible in both the CoastSat data and the ShorelineS model runs. As can be seen in figure 4.2 the ShorelineS runs have an accretive trend of 1.9, 2.6 and 3.4 meters per year approximately for q_{scal}=0.35, 0.45, 0,55 respectively. The CoastSat satellite based LOWESS trend shows an accretive trend of approximately 2.8 meters per year. This matches best with a value of q_{scal} of 0.45.

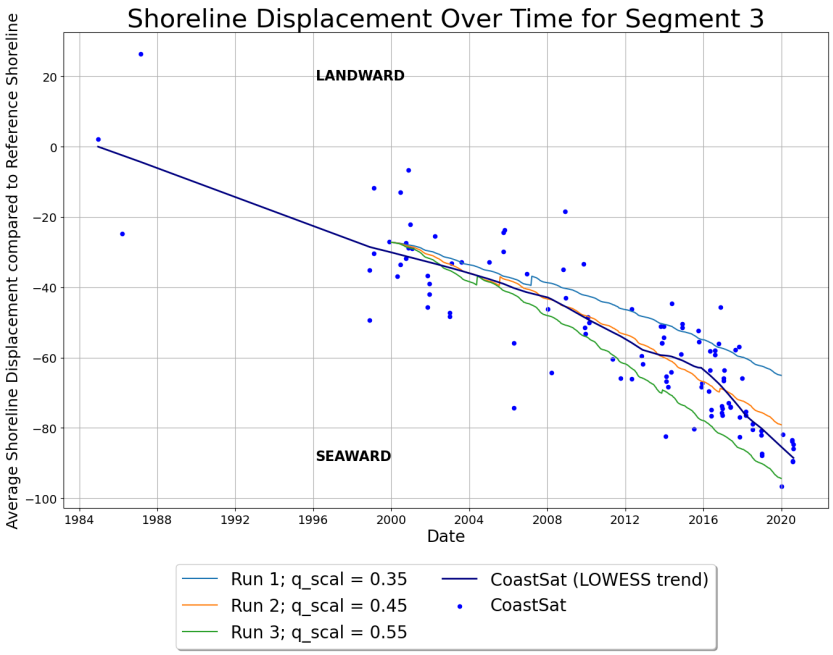

(a) Average distance from reference line. The blue dots indicate the individual CoastSat shorelineas and the dark blue line indicates the Lowess average of these points. The green (q_{scal} = 0.55), orange (q_{scal} = 0.45) and light-blue (q_{scal} = 0.35) indicate ShorelineS runs from 2000-2020.

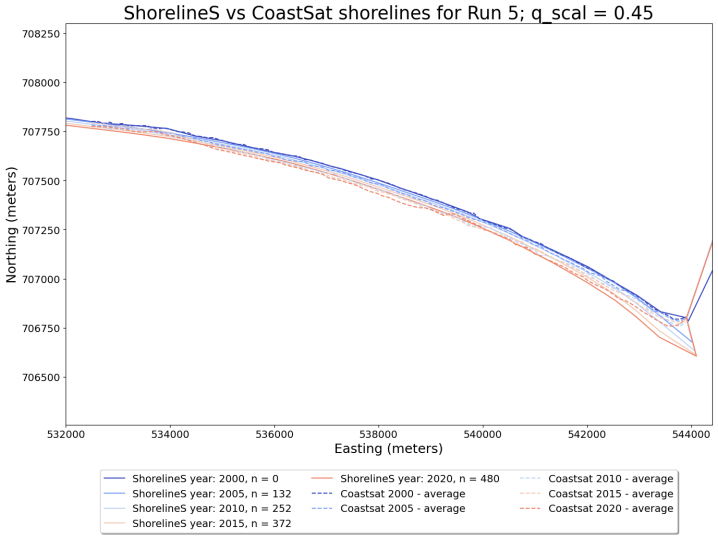

(b) CoastSat yearly averaged satellite shorelines compared to ShorelineS shorelines for the years 2000, 2005, 2010, 2015 and 2020 for $q_{scal} = 0.35$ (blue line in figure 4.1a

Figure 4.2: ShorelineS model runs compared to CoastSat satellite data for segment 3

Segment 4

Segment 4 is located east of the Commodore Channel and just east of EKO Atlantic. In this segment the groyne scheme was constructed around 2014. That is why the modeled shorelines and the satellite retrieved shoreline are only compared from 2000-2010. In this time period an erosive trend is visible in

figure 4.3 of 3.7, 4.5 and 5.3 meters per year for the modeled shorelines for values of q_{scal} of 0.35, 0.45 and 0.55 respectively during the time period 2000-2020. The LOWESS trend for the satellite-retrieved shorelines shows an erosion rate of approximately 5.2 meters per year, indicating that $q_{scal} = 0.55$ provides the best fit for this segment.

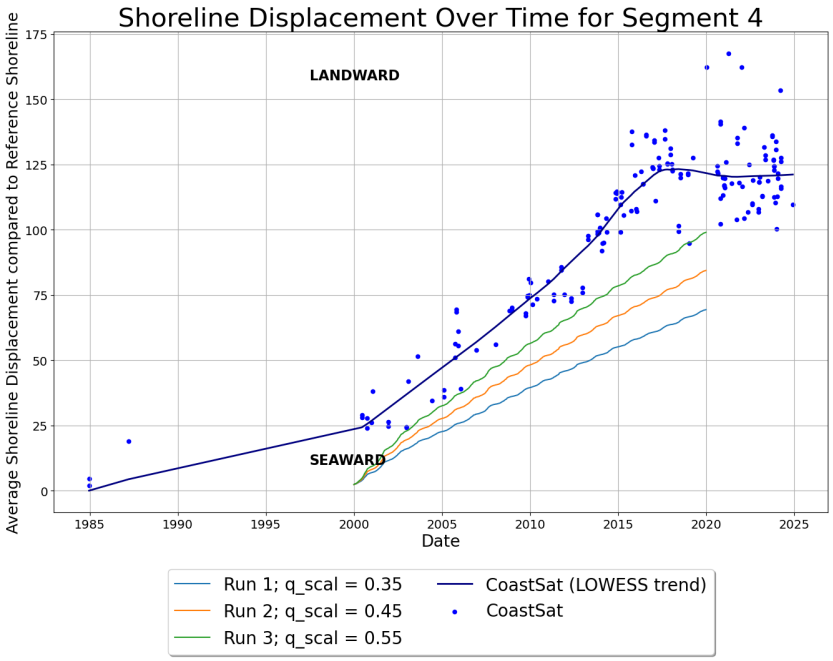

Figure 4.3: Average distance from reference line. The blue dots indicate the individual CoastSat shorelineas and the dark blue line indicates the Lowess averag of these points. The green (q_{scal} = 0.55), orange (q_{scal} = 0.45) and light-blue (q_{scal} = 0.35) indicate ShorelineS runs from 2000-2020.

Time period 2 (2017-2021)

For the second time period the ShorelineS model was run from 2017-2021. In this runs the coastal structures that were present in the first time period were present alongside the groyne scheme and the Lekki Deep Sea Port. That is why segment 5, next to the groyne scheme, and segment 11, next to Lekki Deep Sea Port are analysed in this section.

Segment 5

Segment 5 is situated just east of the groyne scheme which causes the shoreline to retreat in this area. This is also clearly visible in figure 4.4 where the model predicts an erosive rate of 13, 16.7 and 20.3 meters per year for q_{scal}=0.35, 0.45, 0,55 respectively. The LOWESS trend based on the satellite data renders an erosive trend of 19.3 meters per year and thus $q_{scal} = 0.55$ results in the best fit. Figure 4.4b also shows that directly after the groyne scheme, the ShorelineS model accurately describes the erosive landward trend.

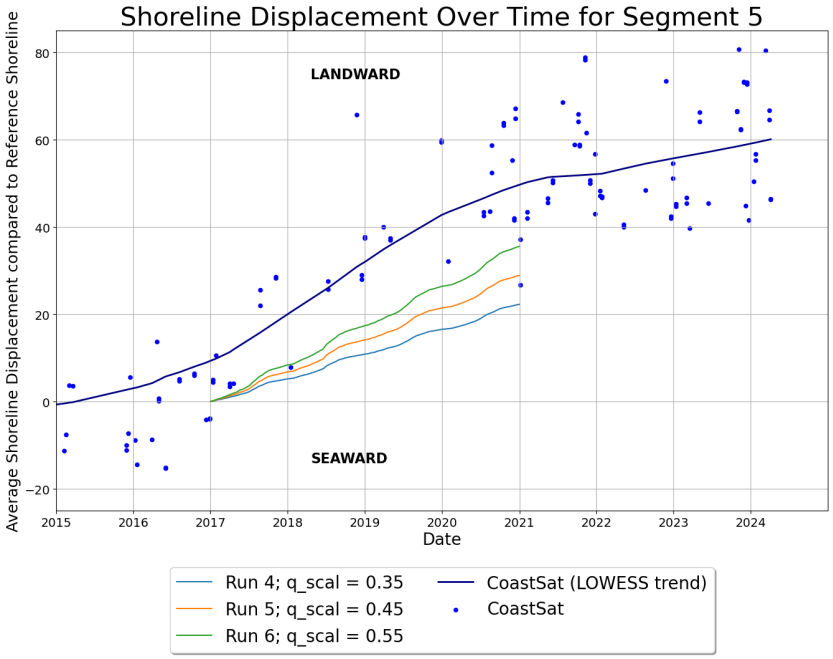

(a) Average distance from reference line. The blue dots indicate the individual CoastSat shorelineas and the dark blue line indicates the Lowess averag of these points. The green (q_{scal} = 0.55), orange (q_{scal} = 0.45) and light-blue (q_{scal} = 0.35) indicate ShorelineS runs from 2017-2021.

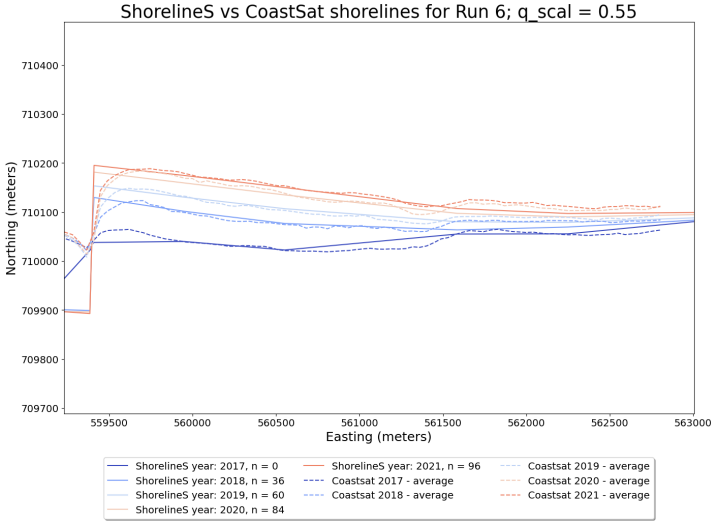

(b) CoastSat yearly averaged satellite shorelines compared to ShorelineS shorelines for the years 2017, 2018, 2019, 2020 and 2021 for $q_{scal} = 0.35$ (blue line in figure 4.4a

Figure 4.4: ShorelineS model runs compared to CoastSat satelite data for segment 5

Segment 11

Just west of Lekki Deep Sea Port segment 11 is situated. The accretion directly west of the port is captured by the ShorelineS model as can be seen in figure 4.5b. The accretive rates predicted by the ShorelineS model are approximately 4.8, 6.2 and 7.6 meters per year from 2017-2021 for q_{scal}=0.35, 0.45, 0,55 respectively and can be seen in figure 4.5a. The CoastSat based LOWESS trend has an erosive rate of 6.1 meters per year and thus a q_{scal} of 0.45 renders the best fitting results.

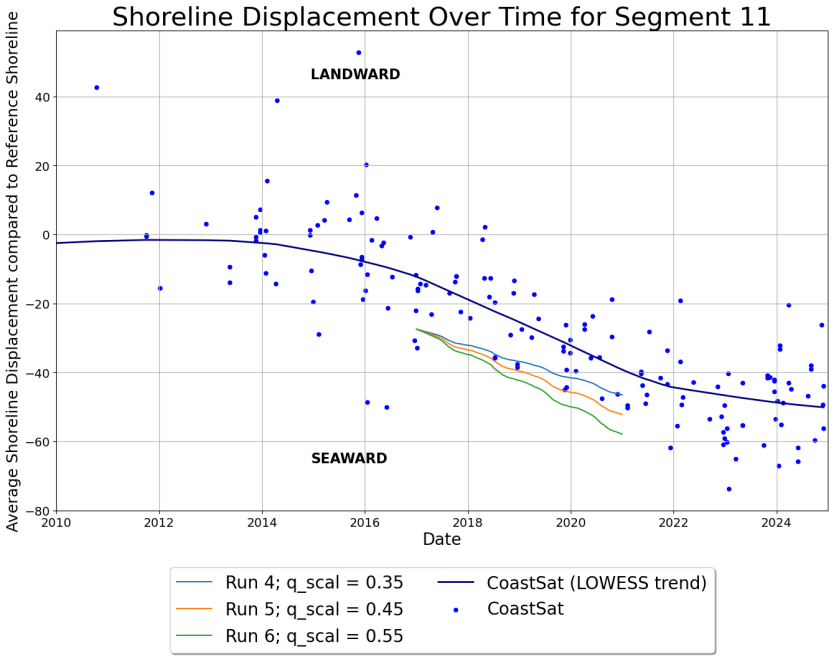

(a) Average distance from reference line. The blue dots indicate the individual CoastSat shorelineas and the dark blue line indicates the Lowess averag of these points. The green (q_{scal} = 0.55), orange (q_{scal} = 0.45) and light-blue (q_{scal} = 0.35) indicate ShorelineS runs from 2017-2021.

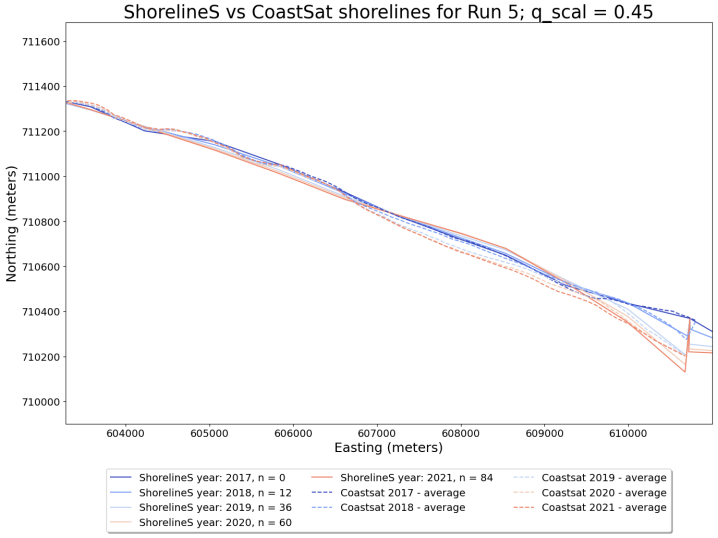

(b) CoastSat yearly averaged satellite shorelines compared to ShorelineS shorelines for the years 2017, 2018, 2019, 2020 and 2021 for $q_{scal} = 0.45$ (blue line in figure 4.5a

Figure 4.5: ShorelineS model runs compared to CoastSat satelite data for segment 11

4.2.2. Longshore Sediment Transport

Next to the shoreline displacement, the longshore sediment transport Q_s is also a valuable variable that provides additional insights into coastal processes. As stated in chapter 2.1.6, the longshore sediment transport was estimated to be around $600.000\ m^3/year$ to $1.000.000\ m^3/year$.

For analyzing the longshore sediment transport three locations have been selected at three different segments of the shoreline based on a couple of constraints:

- Sufficient distance from the boundary points.
- Sufficient distance from coastal structures.

- The local shoreline orientation is representative of the average orientation for that shoreline segment.

The three selected points are shown in figure 4.6. Building on the results of the CoastSat calibration results as stated in chapter 4.2, the total sediment transport is based on the results where $q_{scal} = 0.45$.

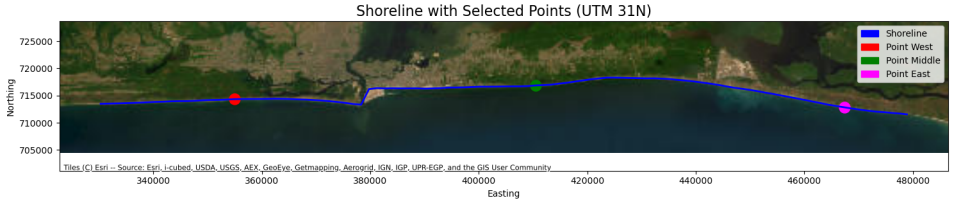

Figure 4.6: The three selected points for the western part, middle part and the eastern part.

Point West

Point West is located west of Eko Atlantic and is close to the study area of van Bentum [20], who researched the influence of Eko Atlantic and found a net longshore sediment transport of $600,000 - 700,000\ m^3/year$. As can be seen in figure 4.8, which shows the yearly mean sediment transport through Point West from 2010-2019, the sediment transport at this point is in line with these findings. The mean sediment transport for this time period is around $680,000\ m^3/year$ with yearly fluctuation being around +-10%.

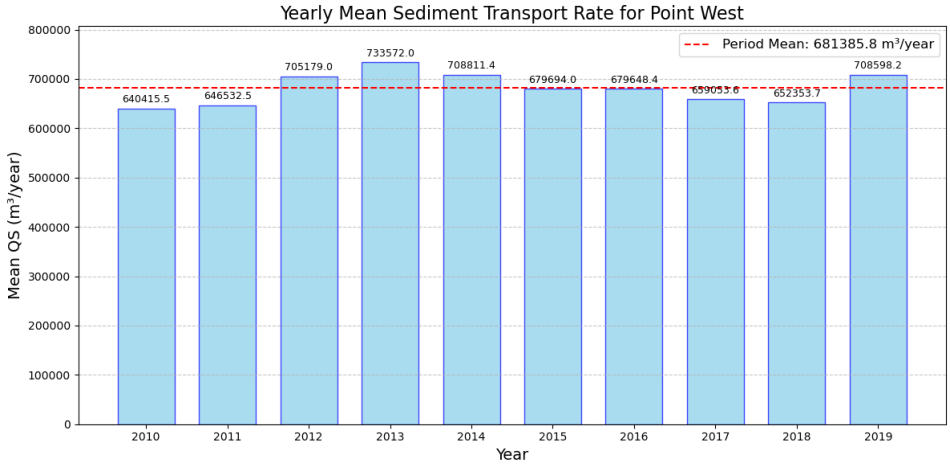

Figure 4.7: Yearly mean sediment transport through Point West for the period 2010-2019 with $q_{scal} = 0.45$.

Point Middle

Point Middle is located at the east of the groyne system and on the west of Lekki Deep Sea Port. However, the point is selected at a sufficient distance from these structures to ensure that it's longshore sediment transport is not influenced by the presence of these structures. Earlier research did not examine this exact location, however it is close to Lekki Deep Sea Port and Dangote Quays Lekki where Wang, Shen, and Zhao [4] found a longshore sediment transport of around $584,000\ m^3/year$ to $962,000\ m^3/year$ and van der Spek et al. [22] a longshore sediment transport of $650,000\ m^3/year$ to $1,000,000\ m^3/year$. Here a mean longshore sediment transport of around $1,070,000\ m^3/year$ is found for the period of 2010-2019, with yearly fluctuations of +- 5%. This is slightly larger than found in literature.

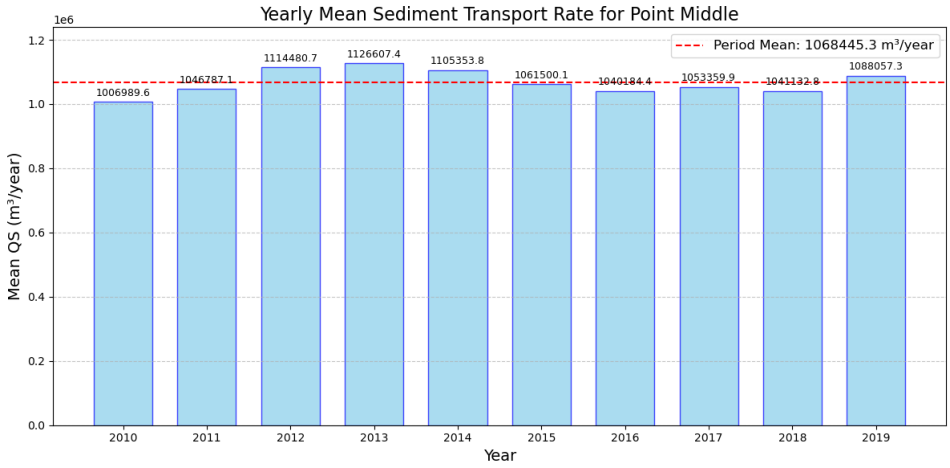

Figure 4.8: Yearly mean sediment transport through Point Middle for the period 2010-2019 with $q_{scal} = 0.45$.

Point East

Point East is located just east of where Dangote Quays Lekki located. It must be noted that in these calibration runs neither Lekki Deep Sea Port nor Dangote Quays Lekki were present. Here a mean longshore sediment transport of around $820,000\ m^3/year$ for the period of 2010-2019 is found which is in line with earlier findings in literature as presented in the paragraph above. The yearly mean sediment transport can be seen in figure 4.9.

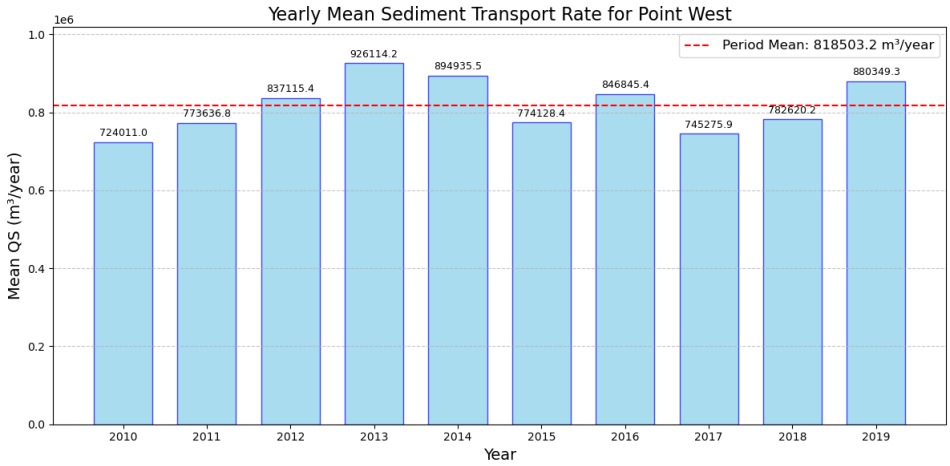

Figure 4.9: Yearly mean sediment transport through Point East for the period 2010-2019 with $q_{scal} = 0.45$.

4.2.3. Calibration Conclusions

This section will provide the conclusion of the calibration process. Based on the calibration results as shown in chapter 4.2, q_{scal} will be set at 0.45. For segments 3 and 11, the ShorelineS model followed the LOWESS-averaged CoastSat trends for this value of q_{scal}. Segments 2, 4, and 5 were more accurate at q_{scal} values of 0.35, 0.55, and 0.55 respectively. Therefore, a median value of $q_{scal} = 0.45$ was adopted as the optimal parameter for the entire study area, balancing model performance across all segments. A summary of all the displacement rates for both the ShorelineS based average displacements and the CoastSat based LOWESS trend can be seen in table 4.1.

The longshore sediment transport for this value aligns with the previous studies, providing increased validation for the selection of $q_{scal} = 0.45$.

Segment	CoastSat LOWESS (m/year)	$q_{scal} = 0.35$ (m/year)	$q_{scal} = 0.45$ (m/year)	$q_{scal} = 0.55$ (m/year)	Time Period
2	-0.2 to -1.5	**-1.4**	-1.7	-2.1	2000-2020
3	-2.8	-1.9	**-2.6**	-3.4	2000-2020
4	5.2	3.7	4.5	**5.3**	2000-2010
5	19.3	13.0	16.7	**20.3**	2017-2021
11	-6.1	-4.8	**-6.2**	-7.6	2017-2021

Table 4.1: Segment average shoreline displacement rates (m/year) for different segments comparing CoastSat observations and ShorelineS model with various values for q_{scal}. Erosion is defined positive. The timeperiod is the time period over which the rates were calculated. The optimal parameter values for each segment are highlighted in bold.

4.3. Nearshore Wave Climate Change Projections

This section introduces the influence of the different offshore wave climate change scenarios on the nearshore wave climate that is used as input for the ShorelineS runs assessing the future shoreline dynamics. The mean nearshore wave climate for 2010-2019, which is exactly the same wave climate as the base run, can be seen in figure 3.13. The specifications of the climate change scenarios can be seen in table 3.6.

Figure 4.10 shows the difference between the mean significant wave height for the base run (no climate change applied) and the different climate change scenarios in percentage of the base run for the period 2065-2074. It can be noticed that the increase or decrease is spatially uniform. The major fluctuations that are visible are mainly close to coastal structures, such as the fluctuation near Lekki Deep Sea Port. Interesting to notice is that for RCP4.5 High and RCP8.5 median, which have the same shift in offshore significant wave height, the nearshore significant wave height is approximately the same despite the difference in wave direction.

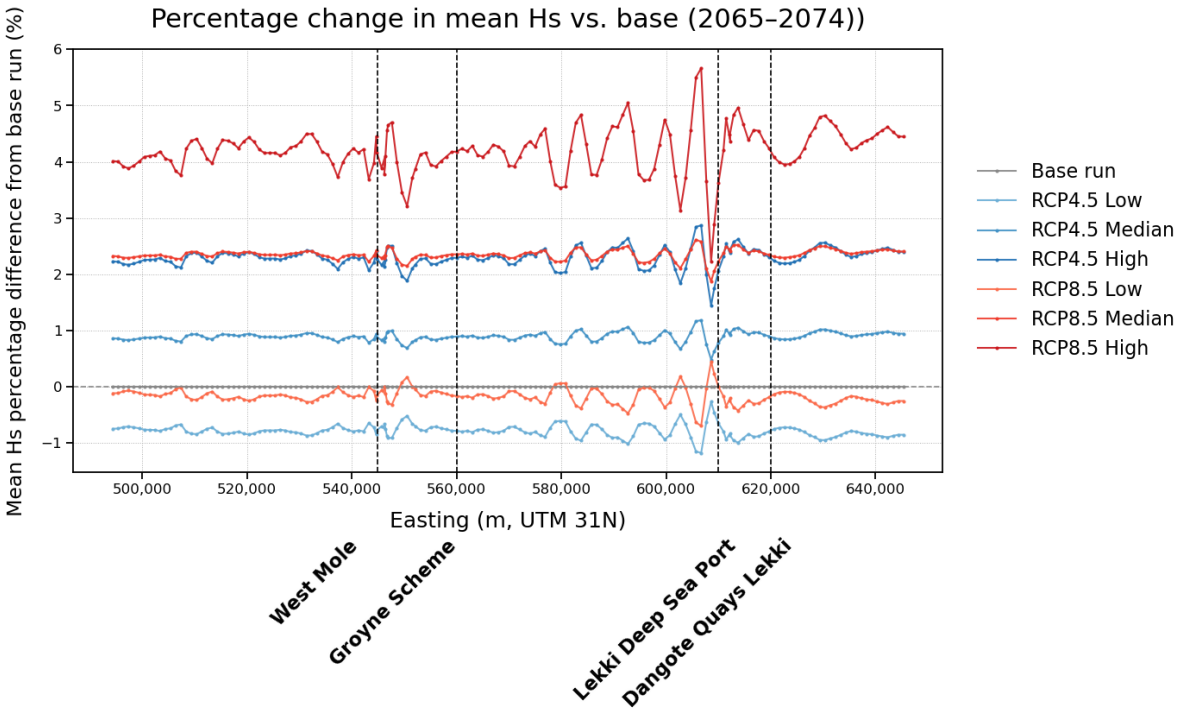

Figure 4.10: Difference in mean nearshore (-10 m depth) significant wave height between the base run (without climate change influence) and the different climate change scenarios for the period 2065-2074.

The same spatial uniformity is seen in the nearshore wave direction under the different climate change scenarios, as shown in Figure 4.11. This figure shows the difference in mean nearshore wave direction between the base run and the different climate change scenarios for the same period. Interestingly,

although both the RCP4.5 and RCP8.5 Median scenarios apply the same offshore directional shift, the resulting nearshore wave direction is slightly lower for the RCP8.5 Median scenario, which is characterized by a larger increase in offshore significant wave height.

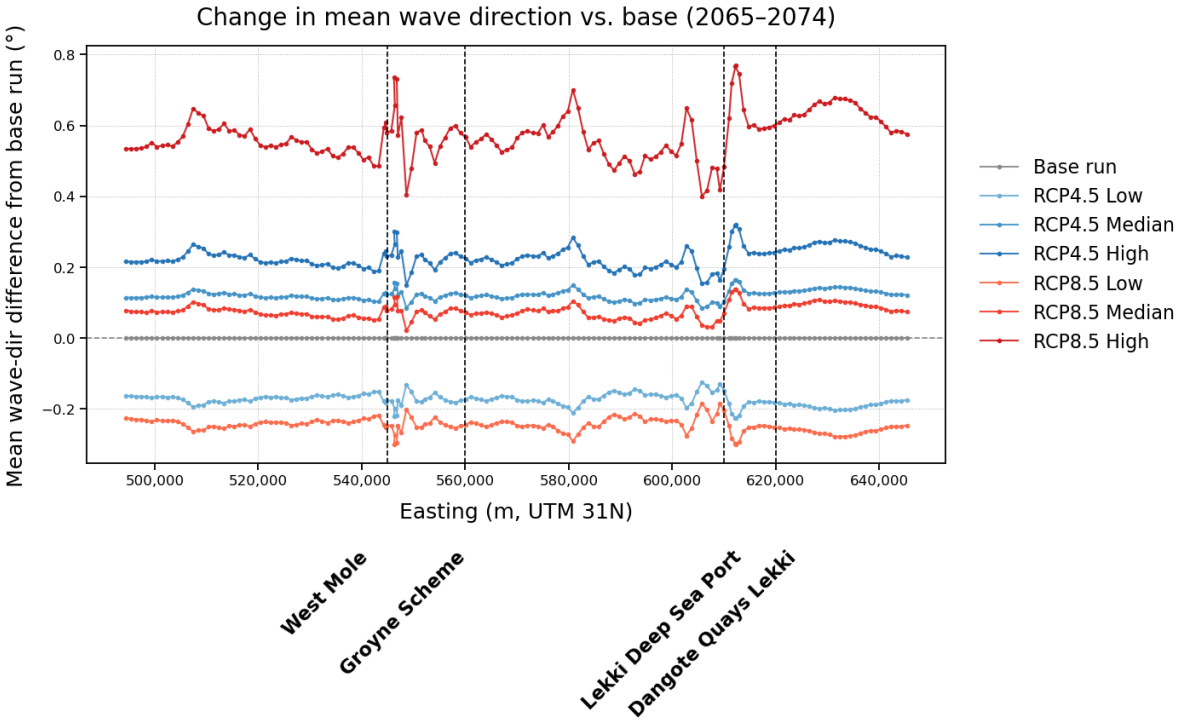

Figure 4.11: Difference in mean nearshore (-10 m depth) wave direction between the base run (without climate change influence) and the different climate change scenarios for the period 2065-2074.

4.4. Shoreline Displacement Assessment

This section presents an assessment of shoreline displacement patterns along five areas of interest along the Lagos coastline, analyzing the influence of coastal structures and climate change variables on projected erosion and accretion trends through 2075. the areas of interest can be seen in figure 4.6. For every area of interest, 3 transects have been allocated at 5 km distance from each other covering a total area of 10 km. At these transects the displacement relative to the initial shoreline position is calculated over time. This gives an indication of the erosion/accretion patterns at the areas of interest and illustrates the spatial extent of the coastal structure's influence on the surrounding shoreline morphology.

4.4.1. Area of Interest 1

This area is located west of the Commodore Channel and is characterized by the West Mole that acts as a sediment trap. In this model representation, the mole extends further seaward than its current real-world dimensions. The accretive trend is clearly visible in figure 4.13 and 4.14 where the relative shoreline displacement per transect is shown. The accretion is the highest directly next to the mole, reaching approximately 200 m of accretion by the year 2060 under all scenarios. The accretion declines further away from the Mole.

The influence of climate change is highest close to the Mole where, under RCP8.5, the range in displacement compared to the base run is between -26 m and +18 m being 10.6% more seaward or 7.4% more landward respectively and proportional to the base run as can be seen in figure 4.14. An increase in wave direction (becoming more westerly) and wave height will induce an increase in longshore sediment transport and thus enhance accretion rates. Sea level rise on the other hand will cause the land to retreat and thus weakens accretion rates. This counterbalancing effect is why the median line in figure 4.14 is very close to the base run. The visible range reflects scenarios in which the effects of

sea level rise and changes in wave climate were assessed independently.

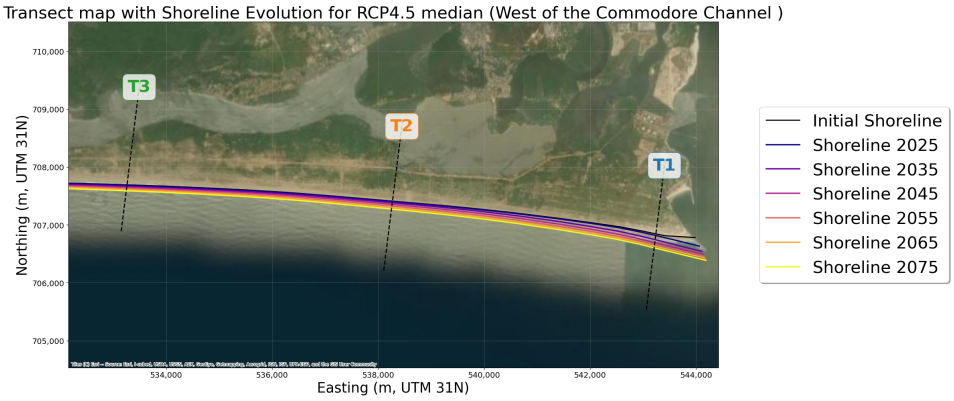

Figure 4.12: The shoreline positions over time at Area of Interest 1 for the median RCP4.5 scenario with the three transects indicated by the dotted lines. The satellite image is shown for reference only.

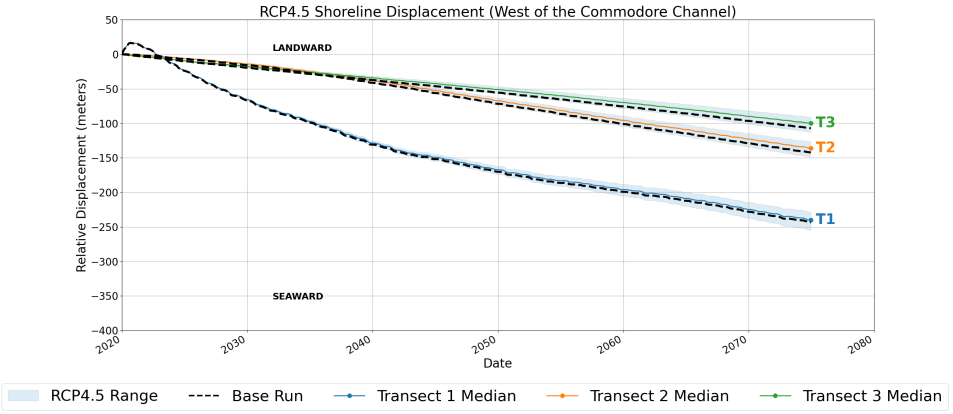

Figure 4.13: The displacement relative to the initial shoreline west of the Commodore Channel at the three transects as indicated in figure 4.12 under RCP4.5, the black dotted line indicates the base run where no changes are applied.

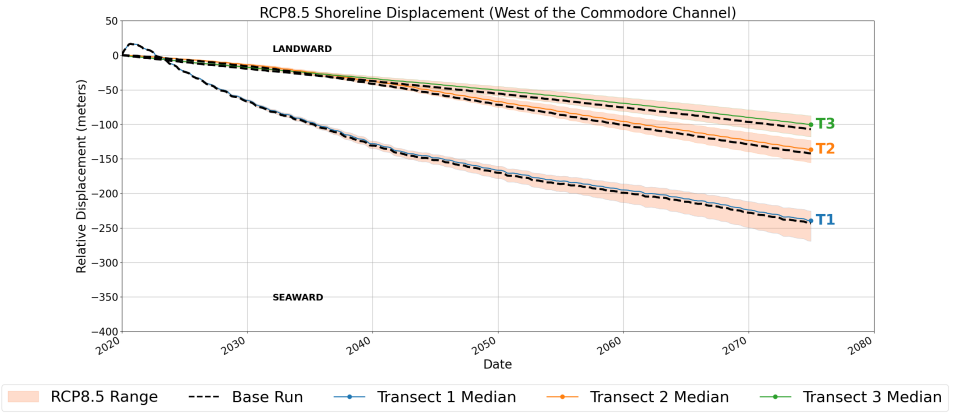

Figure 4.14: The displacement relative to the initial shoreline west of the Commodore Channel at the three transects as indicated in figure 4.12 under RCP8.5, the black dotted line indicates the base run where no changes are applied.

4.4.2. Area of Interest 2

Area of Interest 2 is located east of the groyne scheme. Based on the model simulations, the highest erosion rates by 2075 for the full area are projected to occur immediately adjacent to this groyne system

with shoreline retreat reaching 700 meters by this year as can be seen in figure 4.16 and 4.17. Further away from the groyne system, the influence of the coastal structure is still visible in the form of erosive trends with shoreline retreat reaching more than 140 meters at 10 km east of the groyne system.

Other than at Area of Interest 1, the climate change factors all enhance erosion at this location. The absolute influence of climate change on the erosion is largest at transect 1, closest to the groyne system. However, as can be noticed in table 4.2, further away from the coastal structure, the absolute difference between the RCP8.5 scenarios and the base run becomes smaller, while the relative difference becomes larger in the year 2075. The reason for this is that further away from the coastal structure, the erosive and accretive patterns are more guided by the wave climate rather than the presence of a coastal structure. A difference in wave climate induced by climate change will therefor have a relative larger impact further away from the coastal structure.

	Displacement T1		Displacement T2		Displacement T3	
Base	709 m		341 m		144 m	
Scenario	T1		T2		T3	
	Abs. (m)	Rel. (%)	Abs. (m)	Rel. (%)	Abs. (m)	Rel. (%)
RCP8.5 min	-11	-1.6	-3	-0.9	-1	-0.7
RCP8.5 median	+27	+3.8	+25	+7.4	+20	+13.6
RCP8.5 max	+65	+9.2	+48	+14.2	+35	+24.2

Table 4.2: Displacement by the year 2075 for the base run and the absolute (Abs.) and relative (Rel.) displacement differences from the base run for transects T1–T3 under RCP8.5 minimum, median, and maximum scenarios by 2075. Relative values are expressed as percentages of the total projected displacement at each transect for the base run.

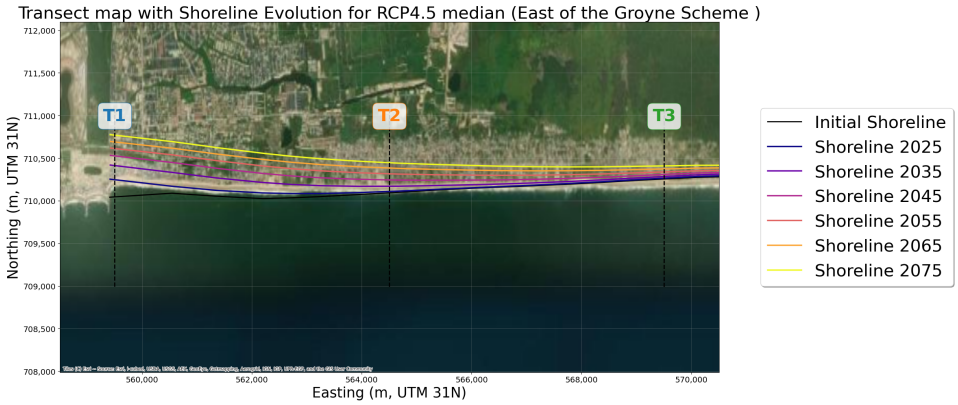

Figure 4.15: The shoreline positions over time at Area of Interest 2 for the median RCP4.5 scenario with the three transects indicated by the dotted lines. The satellite image is shown for reference only.

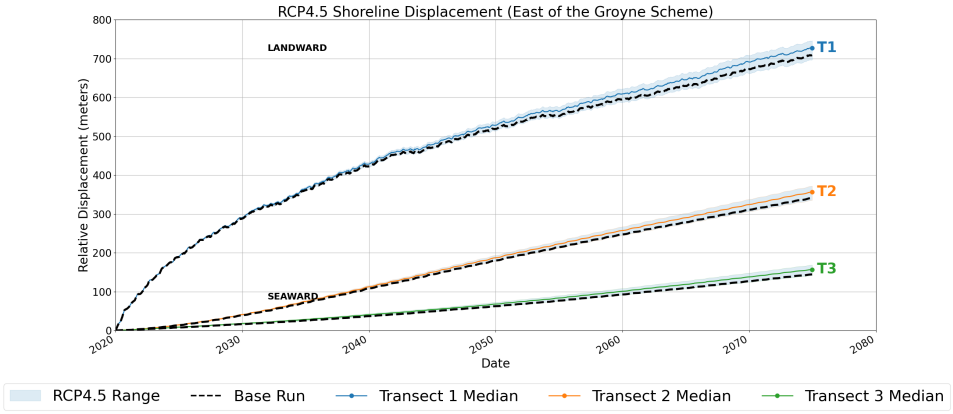

Figure 4.16: The displacement relative to the initial shoreline west of the Commodore Channel at the three transects as indicated in figure 4.15 under RCP4.5, the black dotted line indicates the base run where no changes are applied.

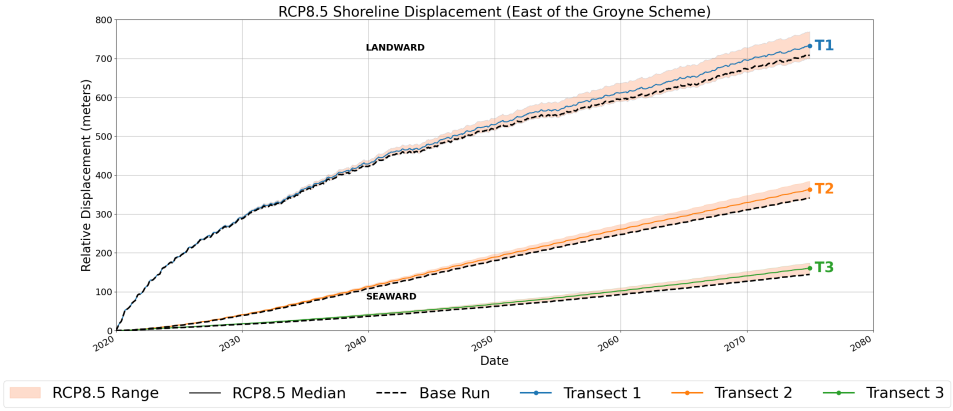

Figure 4.17: The displacement relative to the initial shoreline east of the groyne scheme at the three transects as indicated in figure 4.15 under RCP8.5, the black dotted line indicates the base run where no changes are applied.

4.4.3. Area of Interest 3

Area of Interest 3 is located west of Lekki Deep Sea Port. Just as Area of Interest 1, this area is characterized by an accretive trend due to the presence of Lekki Deep Sea Port as can be seen in figure 4.18. After 10 years the western tip of the port structure is reached after which the accretion rates slow down and bypassing of the groyne increases, this can be seen in both figure 4.19 and 4.20. Also further away from the port, at T3, the model predicts accretion of almost 100 m by the year 2075 for all climate scenarios.

Similarly to Area of Interest 1, the climate change factors are counterbalancing each other. Furthermore, the climate uncertainty range at T1 is noticeably smaller than at T2 and T3, suggesting that closer to the coastal structure, the influence of the presence of the coastal structure on shoreline displacement outweighs that of sea level rise or changes in wave climate.

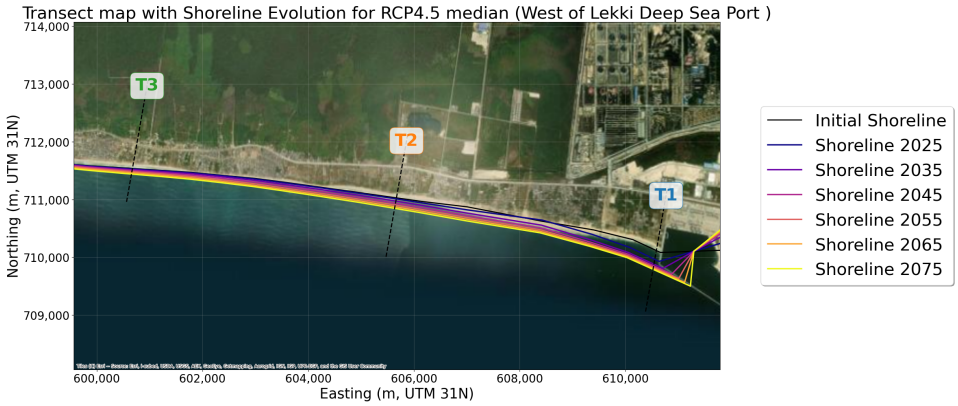

Figure 4.18: The shoreline positions over time at Area of Interest 3 for the median RCP4.5 scenario with the three transects indicated by the dotted lines. The satellite image is shown for reference only.

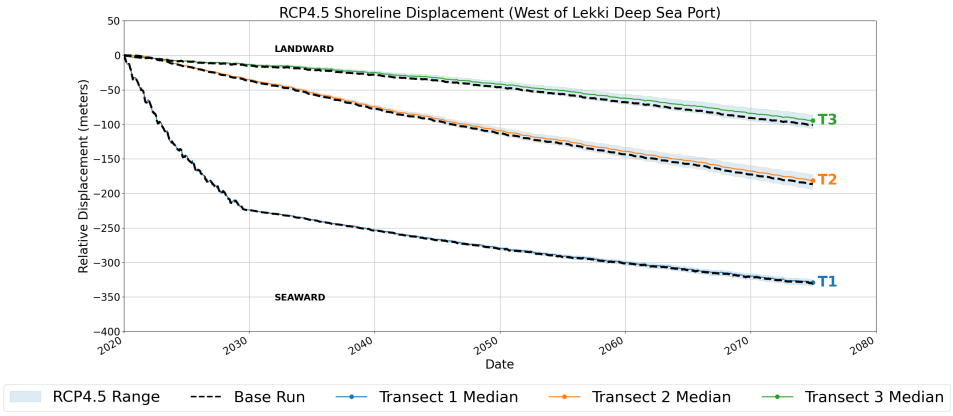

Figure 4.19: The displacement relative to the initial shoreline west of the Commodore Channel at the three transects as indicated in figure 4.18 under RCP4.5, the black dotted line indicates the base run where no changes are applied.

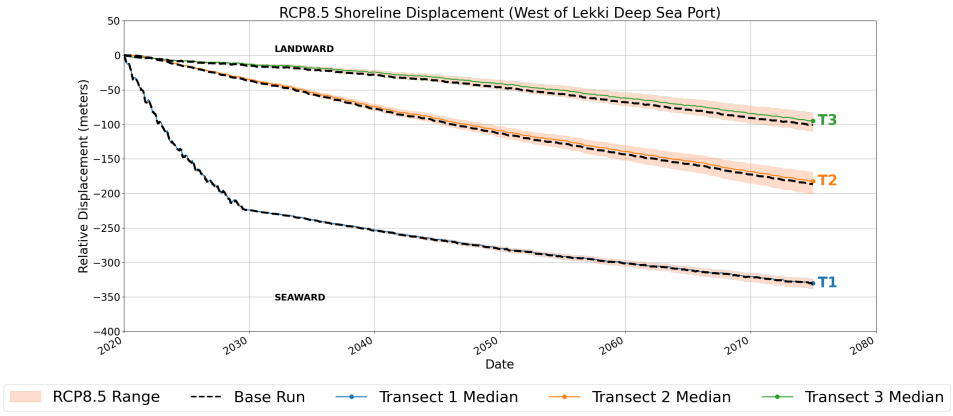

Figure 4.20: The displacement relative to the initial shoreline east of the groyne scheme at the three transects as indicated in figure 4.18 under RCP8.5, the black dotted line indicates the base run where no changes are applied.

4.4.4. Area of Interest 4

Area of Interest 4 is located between Lekki Deep Sea Port (on the west end) and Dangote Quays Lekki (on the east end) causing both erosive and accretive trends in this area. In the model representation, the tip of the groyne of Dangote Quays Lekki is at current real-word location. The erosion in transect T1 can reach 200 meters after 10 years in all scenarios. After this, the bypassing from the west side of

Lekki Deep Sea Port also increases as stated in chapter 4.4.3 and can be seen in figures 4.19 and 4.20. The accretion in transect T3 stabilizes after the year 2040, when the tip of the breakwater is reached and all the sediment bypasses the breakwater.

The influence of the climate change factors on the accretion rates is minimal. For the erosion in transect T1 a clear range is visible for both RCP4.5 and RCP8.5 in figures 4.22 and 4.23 respectively. In table 4.3 the absolute and relative changes between the base scenario and the different climate scenarios is shown where it can be noticed that in the most extreme RCP8.5 scenario, the erosion is modeled to increase by almost 10%.

	T1	
Base	474 m	
Scenario	T1	
	Abs. (m)	Rel. (%)
RCP4.5 min	-9	-1.8
RCP4.5 median	+14	+3.1
RCP4.5 max	+27	+5.6
RCP8.5 min	-10	-2.0
RCP8.5 median	+17	+3.6
RCP8.5 max	+47	+9.8

Table 4.3: Displacement by the year 2075 for the base run at transect T1 and the Absolute (Abs.) and relative (Rel.) difference in displacement between the base run and T1 transect for the minimum, median and maximum scenarios for RCP4.5 and RCP8.5 by 2075. Relative values are expressed as percentages of the total projected displacement at transect T1.

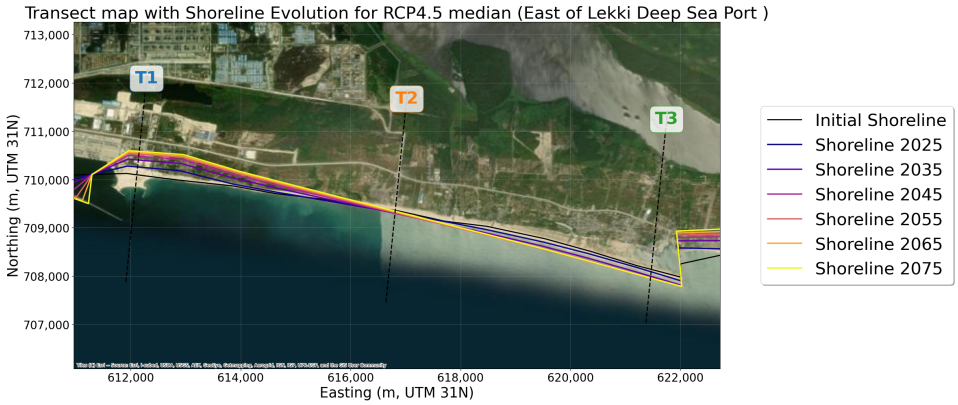

Figure 4.21: The shoreline positions over time at Area of Interest 4 for the median RCP4.5 scenario with the three transects indicated by the dotted lines. The satellite image is shown for reference only.

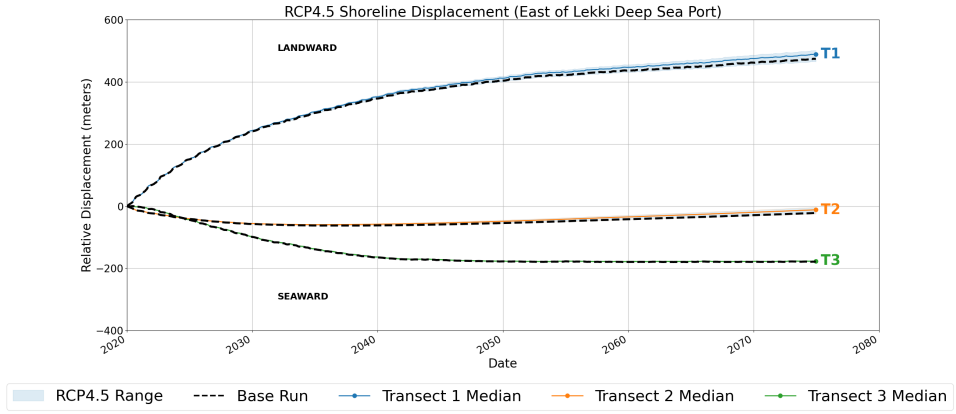

Figure 4.22: The displacement relative to the initial shoreline west of the Commodore Channel at the three transects as indicated in figure 4.21 under RCP4.5, the black dotted line indicates the base run where no changes are applied.

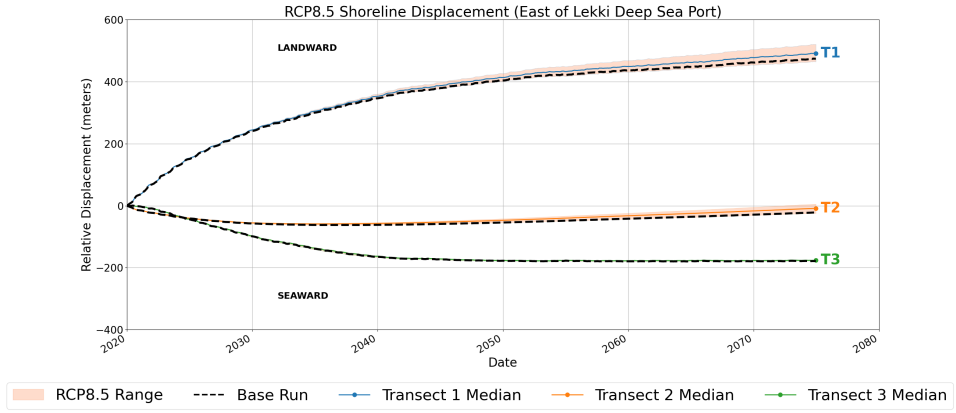

Figure 4.23: The displacement relative to the initial shoreline east of the groyne scheme at the three transects as indicated in figure 4.21 under RCP8.5, the black dotted line indicates the base run where no changes are applied.

4.4.5. Area of Interest 5

Area of Interest 5 is located just east of Dangote Quays Lekki and is characterized by erosion. By 2070, the model projects that the shoreline just next to the coastal structure will retreat more than 600 meters inland under all climate scenarios.

The same climate change impact pattern is visible as in Area of Interest 2. Erosion is most severe in absolute terms close to the structure, increasing by 64 meters or 10.1% at maximum under RCP8.5. As distance from the structure increases, the relative erosion becomes more pronounced, increasing by 28 meters or 35.1% at maximum under RCP8.5.

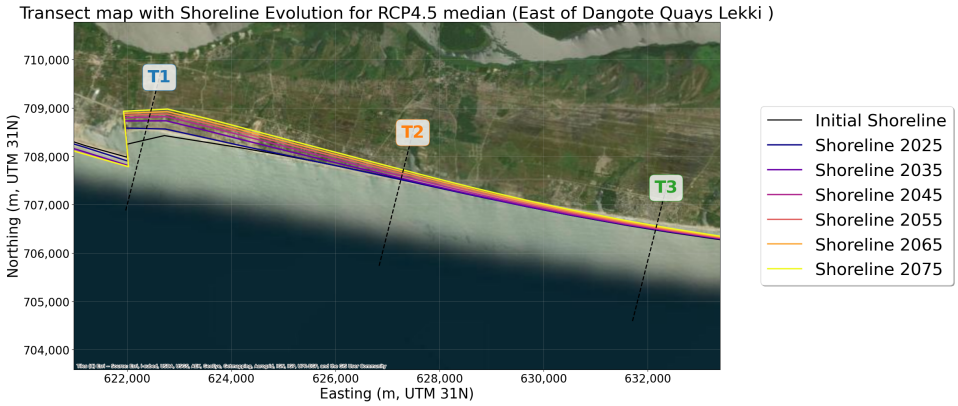

Figure 4.24: The shoreline positions over time at Area of Interest 5 for the median RCP4.5 scenario with the three transects indicated by the dotted lines. The satellite image is shown for reference only.

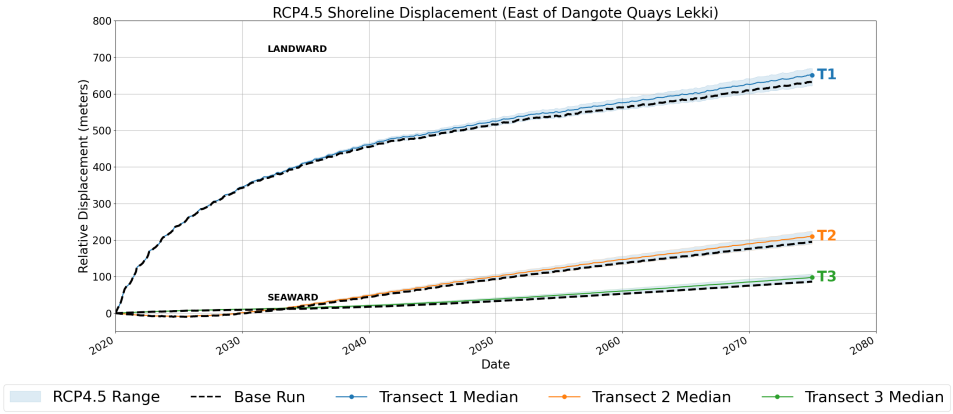

Figure 4.25: The displacement relative to the initial shoreline west of the Commodore Channel at the three transects as indicated in figure 4.24 under RCP4.5, the black dotted line indicates the base run where no changes are applied.

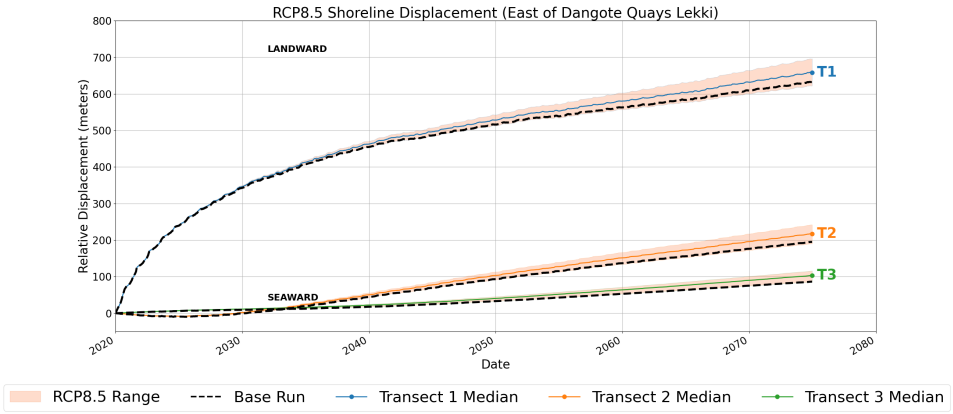

Figure 4.26: The displacement relative to the initial shoreline east of the groyne scheme at the three transects as indicated in figure 4.24 under RCP8.5, the black dotted line indicates the base run where no changes are applied.

4.4.6. Influence of Individual Climate Change Parameters

This paragraph introduces the assessment of the influence of the individual climate change parameters on the total displacement. Area of Interest 1, which displays a clear accretive pattern, and Area of Interest 2, which shows the most significant erosion, are selected for analysis. To clearly distinguish the influence of various climate change parameters, the analysis employs the most extreme climate

scenario for RCP8.5 projected for the year 2075. This scenario consists of an increase in significant wave height of 5.2%, an increase of wave direction of 1.4% (becoming more westerly) by 2075 and a sea level rise of 94 cm by 2075.

Area of Interest 1

Just west of the Western Mole, Area of Interest 1 is located, which is characterized by an accretive trend which is largest close to the Mole. As stated in chapter 4.4.1, the climate change parameters counter balance each other. This is also seen in table 4.4, which shows that sea level rise reduces shoreline accretion by 18 m, while both increased significant wave height and a more westerly wave direction enhance accretion by 5 m and 20 m respectively. The absolute change between the base run and the total scenario, where all the climate change parameters are present, is approximately the sum of all the individual contributions, meaning that the different climate change parameters do not interact synergistically to amplify their effects.

Scenario	Shoreline Position Change (2020 vs 2075)	Absolute Change from Base	Percentage Change from Base
Base	-243 m	-	-
only SLR	-225 m	+18 m	+7%
only ΔHS	-248 m	-5 m	-2%
only ΔDir	-263 m	-20 m	-8%
Total	-251 m	-8 m	-3%

Table 4.4: Impact of different climate change parameters on shoreline position just next to the Western Mole in Area of Interest 1 (transect T1 in figure 4.12) under the most extreme RCP8.5 scenario for 2075. Under the total scenario all the parameters are active and is the same as in the maximum RCP8.5 scenario in chapter 4.4.1. Accretion is defined as negative and erosion as positive.

Area of Interest 2

Area of Interest 2 is located just east of the groyne system and is characterized by an erosive trend which is largest close to the coastal structure. As stated in chapter 4.4.2, the climate change parameters all enhance the erosion in this area. This erosive trend also becomes visible in table 4.5, which shows that sea level rise, increase in wave direction and increase in significant wave height enhances shoreline retreat by approximately 19 m, 26 m and 17 m respectively. The absolute change between the base run and the total scenario, which incorporates all climate change parameters, approximates the sum of individual parameter contributions. This relationship indicates that the climate change parameters do not interact synergistically to amplify their effects, a finding consistent across both areas of interest.

Scenario	Shoreline Position Change (2020 vs 2075)	Absolute Change from Base	Percentage Change from Base
Base	709 m	-	-
only SLR	728 m	+19 m	+3%
only ΔHS	735 m	+26 m	+4%
only ΔDir	726 m	+17 m	+2%
Total	774 m	+65 m	+9%

Table 4.5: Impact of different climate change parameters on shoreline position in just next to the groyne scheme in Area of Interest 2 (transect T1 in figure 4.15) under the most extreme RCP8.5 scenario for 2075. Under the total scenario all the parameters are active and is the same as in the maximum RCP8.5 scenario in chapter 4.4.1. Accretion is defined as negative and erosion as positive.

Figure 4.27 shows the spatial variability of the influence of the individual climate change parameters along the three different transects as indicated in figure 4.15. This shows that further away from the groyne system, the influence of the change in direction diminishes. The influence of the change in significant wave height slightly fluctuates and the influence of sea level rise stays approximately the same.

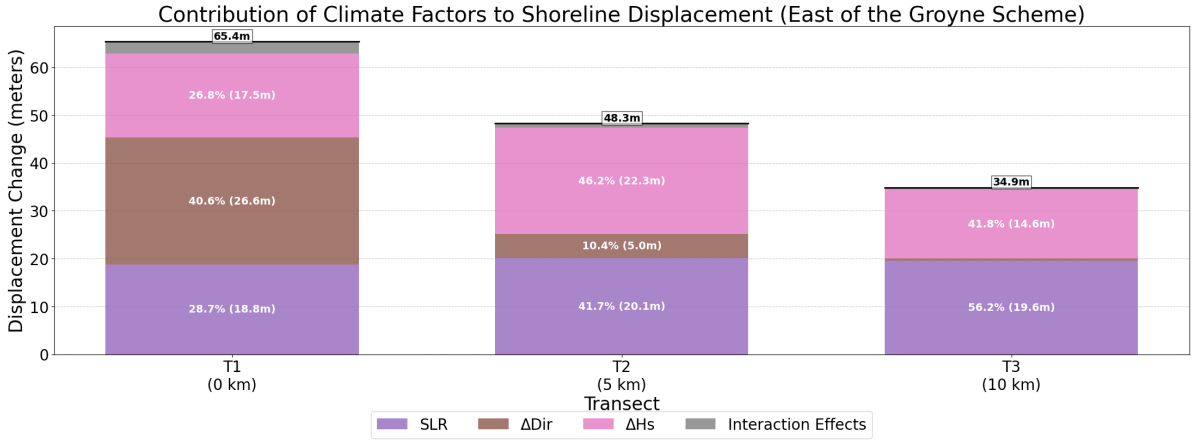

Figure 4.27: Influence of the different climate change parameters to the difference in displacement by the year 2075 compared to the base run at the three different transects as are indicated in figure 4.15.

These observations can be explained by examining how changes in wave direction and significant wave height affect the Van Rijn (2014) longshore sediment transport formula used in ShorelineS. A change in wave direction alters the angle of wave incidence in the transport calculation. Near coastal structures, the shoreline tends to adjust relatively quickly toward an equilibrium orientation at which the angle of incidence approaches zero and longshore sediment transport is minimized. A shift in wave direction changes this equilibrium orientation, thereby reintroducing a sediment flux gradient near the structure and triggering shoreline adjustment. Further from coastal structures, the longshore sediment flux increases or decreases uniformly, resulting in minimal changes to the sediment flux gradient and thus minimal contribution to the shoreline displacement. Chapter 4.5 provides more information about this.

The significant wave height affects the van Rijn 2014 formula differently. The longshore sediment transport Q_s is proportional to $H_s^{3.1}$, meaning that changes in H_s exponentially influence the sediment transport, amplifying flux gradients and consequently enhancing erosion rates.

In ShorelineS, the influence of SLR is calculated by applying the Bruun coastal retreat rule that accounts for the beach slope and the projected sea level rise to determine shoreline position changes. This means that the observed spatial uniformity of the influence of sea level rise is expected as the slope is assumed constant along the coast.

It is important to note that the influence of climate change parameters is also time-dependent. In the RCP8.5 scenario, wave direction and height change linearly over time, meaning the results for 2075 represent the cumulative effect of progressive changes. If the same analysis were conducted for an earlier time window (e.g. 2020–2030), the spatial patterns would be similar, but the magnitude of displacement would be smaller. Additionally, shoreline orientation itself evolves over time due to erosion and accretion, which alters the local angle of wave incidence and introduces further variation in the response to wave direction changes. These dynamic interactions are important to consider when interpreting long-term shoreline evolution.

4.4.7. Modeling Uncertainty

As discussed in chapter 3.4, modeling uncertainty is accounted for by evaluating shoreline displacement across a range of q_{scal} values derived from the calibration. As shown in chapter 3.3.2, the most suitable values for q_{scal} range between 0.35 and 0.55. In this section, shoreline displacement over time is plotted in a similar manner as for the climate change scenarios, including the same transects. To provide a concise overview, uncertainty envelopes are presented for two Areas of Interest: Area 1 and Area 2. The uncertainty envelopes for the other areas can be seen in appendix B.

In figure 4.28, the uncertainty ranges for Area of Interest 1 are shown. The accretive trend is visible for all ranges, only the rate of accretion varies between the different values of q_{scal}. Table 4.6 provides more insight into the magnitude of displacement uncertainty in the year 2075. The results show that

displacement at T1 can vary by approximately ±20% relative to the base run, while at T2 and T3, the variation is around ±25%. This highlights that although the overall trend remains consistent, the choice of q_{scal} has a significant influence on the absolute shoreline position, especially further away from the coastal structure.

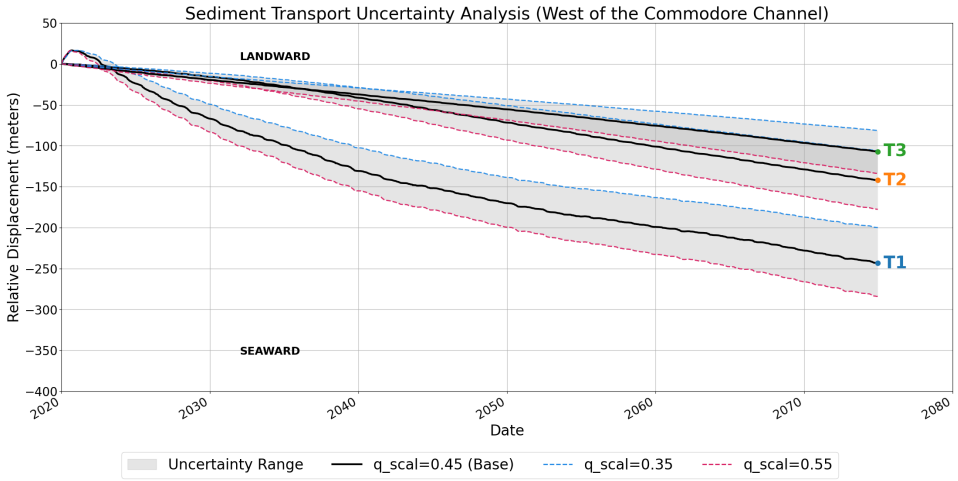

Figure 4.28: The displacement relative to the initial shoreline east of the west mole at the three transects as indicated in figure 4.12 for different values of q_{scal}. The black dotted line indicates the base run ($q_{scal} = 0.45$), the red dotted line indicates the upper limit ($q_{scal} = 0.55$) and the blue dotted line indicates the lower limit ($q_{scal} = 0.35$). The gray area indicates the uncertainty range.

	Displacement T1		Displacement T2		Displacement T3	
Base run ($q_{scal} = 0.45$)	-243 m		-142 m		-107 m	
Scenario	T1		T2		T3	
	Disp. (m)	Rel. (%)	Disp. (m)	Rel. (%)	Disp. (m)	Rel. (%)
Base run ($q_{scal} = 0.35$)	-200	-18	-106	-25	-81	-24
Base run ($q_{scal} = 0.55$)	-284	+17	-178	+25	-134	+25

Table 4.6: Displacement (Disp.) by the year 2075 for the base run and the relative (Rel.) displacement differences from the base run for transects T1–T3 for area 1 for the different values of q_{scal} by 2075. Relative values are expressed as percentages of the total projected displacement at each transect for the base run.

The same trend that is visible in Area of Interest 1, is visible in Area of Interest 2, where the overall shoreline retreat is consistently present for all q_{scal} values. As shown in figure 4.29, the magnitude of erosion increases with higher values of q_{scal}, while lower values reduce the rate of shoreline retreat. Table 4.7 quantifies these differences by 2075, revealing that the variability in projected displacement ranges from approximately ±15% near the structure (T1) to ±30% further downdrift (T3). This highlights that the choice of calibration coefficient q_{scal} has a considerable impact on the projected shoreline position, particularly further from the coastal intervention. It underlines the need for careful calibration when using the model for long-term shoreline predictions.

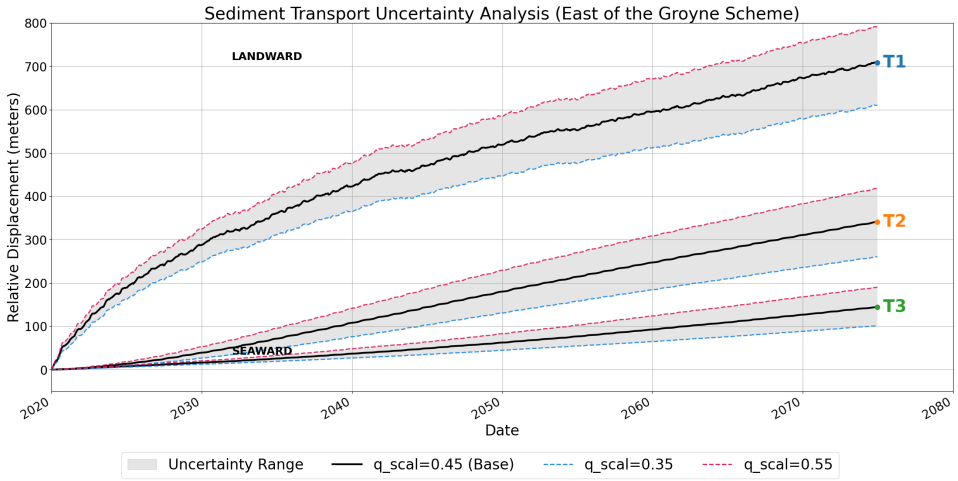

Figure 4.29: The displacement relative to the initial shoreline west of the groyne system at the three transects as indicated in figure 4.15 for different values of q_{scal}. The black dotted line indicates the base run ($q_{scal} = 0.45$), the red dotted line indicates the upper limit ($q_{scal} = 0.55$) and the blue dotted line indicates the lower limit ($q_{scal} = 0.35$). The gray area indicates the uncertainty range.

	Displacement T1		Displacement T2		Displacement T3	
Base run ($q_{scal} = 0.45$)	+709 m		+341 m		+144 m	
Scenario	T1		T2		T3	
	Disp. (m)	Rel. (%)	Disp. (m)	Rel. (%)	Disp. (m)	Rel. (%)
Base run ($q_{scal} = 0.35$)	+610	-14	+260	-24	+101	-30
Base run ($q_{scal} = 0.55$)	+792	+12	-418	+23	+190	+32

Table 4.7: Displacement (Disp.) by the year 2075 for the base run and the relative (Rel.) displacement differences from the base run for transects T1–T3 of area 2 for the different values of q_{scal} by 2075. Relative values are expressed as percentages of the total projected displacement at each transect for the base run.

4.5. Longshore Sediment Transport Assessment

To assess the influence of climate change on longshore sediment transport, Point West and Point Middle of the calibration points as introduced in chapter 3.3.2 are re-evaluated under climate change scenarios. Point East is left out of this analysis as this point is located close to Dangote Quays Lekki, which is incorporated in the future runs. These points can be seen in figure 4.6. Furthermore, the individual climate change parameters will be assessed by separating them to determine their relative influence and spatial variability along the coast.

In this analysis, the mean longshore sediment transport of the years 2065-2074 for the different climate scenarios will be compared to the base run.

4.5.1. Point West

Point west is located west of the Western Mole of the Commodore Channel. The longshore sediment transport at this location shows significant sensitivity to climate change scenarios, with projections ranging from a slight decrease under low emission scenarios (-4%) to substantial increases under higher emission scenarios. Notably, under the most severe climate change projection (RCP8.5 high), sediment transport could increase by up to 20% compared to the base run.

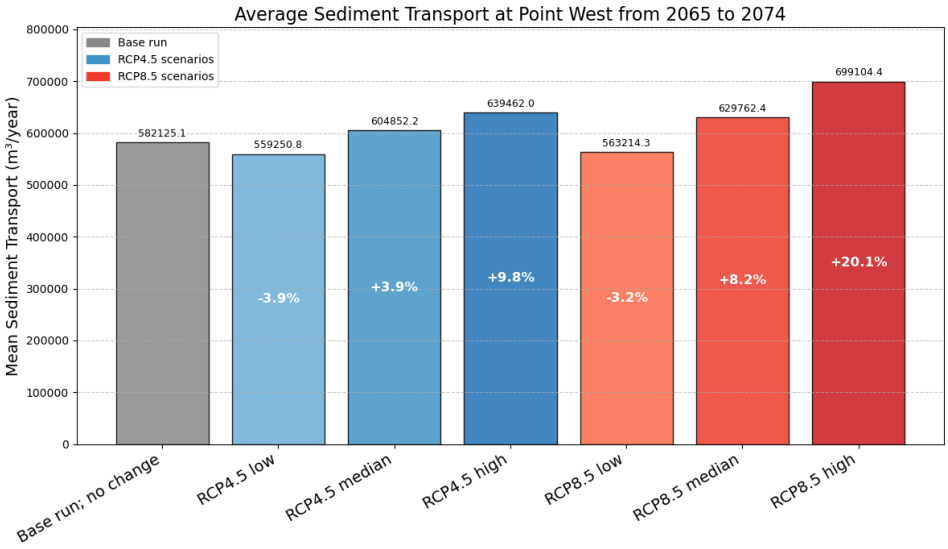

Figure 4.30: Mean longshore sediment transport for Point West during the years 2065-2074 for different climate scenarios. The difference from the base run is given in percentages.

4.5.2. Point Middle

Point middle is located east of the groyne system and west of Lekki Deep Sea Port. Point Middle exhibits a similar pattern of climate change impacts on longshore sediment transport. The projected transport rates for 2065-2074 show considerable variation across scenarios, with low emission scenarios indicating slight decreases (-3%) relative to the base run. However, there is a progressive increase in transport rates with higher emission scenarios, culminating in an 18% increase under the RCP8.5 high scenario.

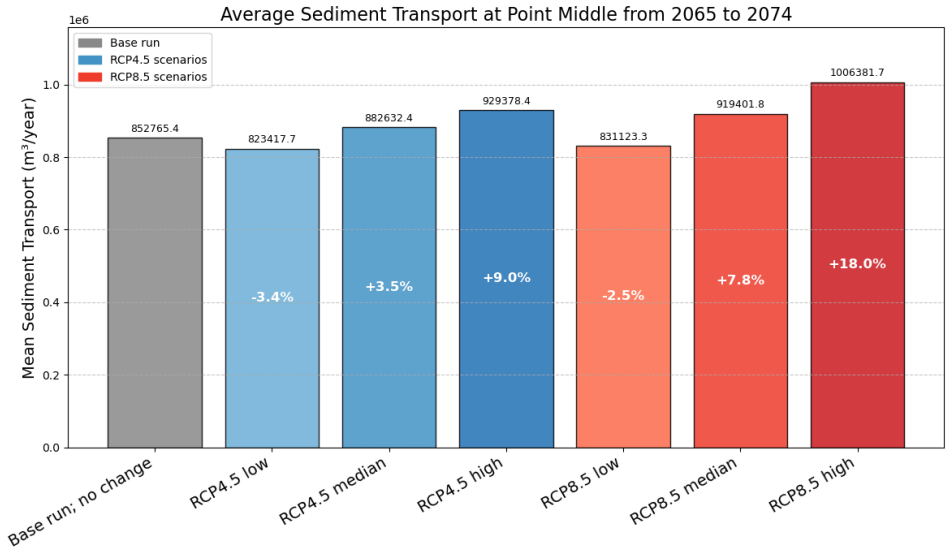

Figure 4.31: Mean longshore sediment transport for Point Middle during the years 2065-2074 for different climate scenarios. The difference from the base run is given in percentages.

4.5.3. Influence of Individual Climate Change Parameters

This section outlines the influence of the individual climate change parameters to the total longshore sediment transport along the Lagos State Coast. In this analyses the same runs as in chapter 4.4.6 are used which can be seen in table 3.9. To fully understand the influence of the individual parameters across the entire domain, the mean longshore sediment transport was calculated for each shoreline

location during the period 2065-2074. The results can be seen in figure 4.32. The upper graph represents the mean transport for different scenarios: the RCP8.5 high total scenario (grey), only wave direction change (brown), only significant wave height change (pink), only sea level rise (purple), and the base run where no changes were enforced. The lower graph shows the difference between each scenario and the base run, highlighting the isolated impact of each climate parameter.

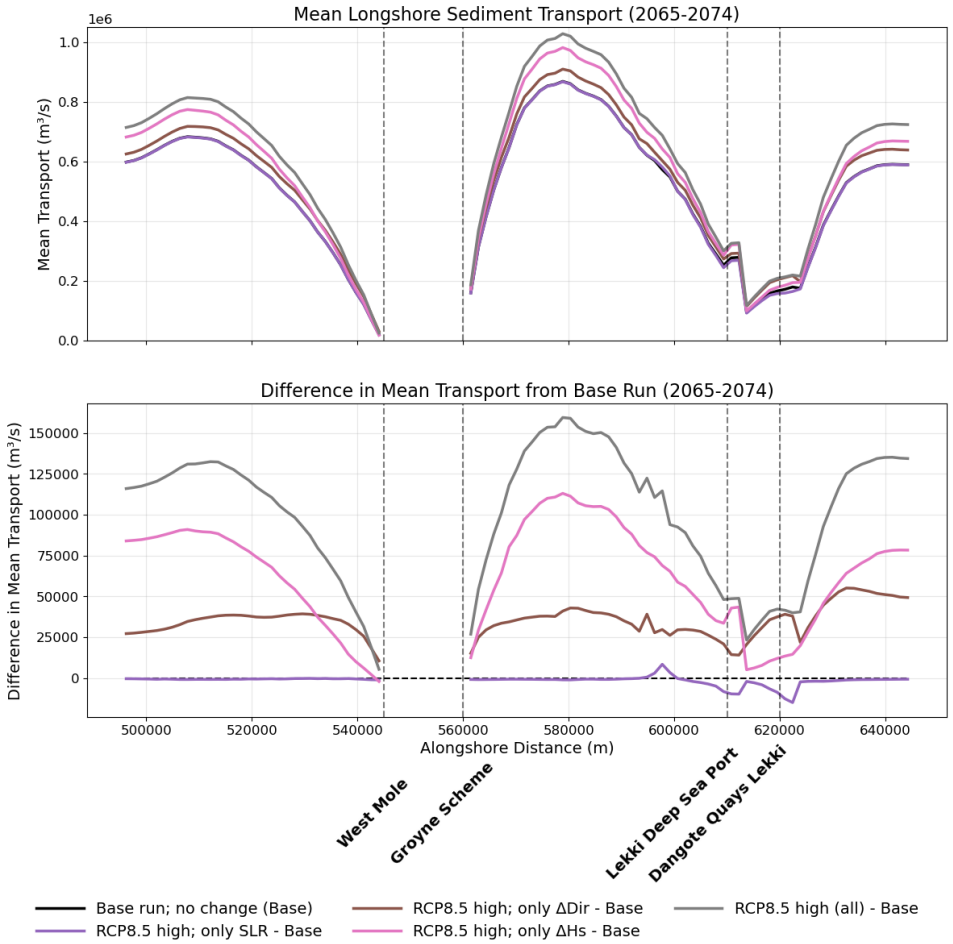

Figure 4.32: Mean longshore sediment transport analysis for 2065-2074. Top: Transport rates under various scenarios including RCP8.5 high (grey), isolated wave direction change (brown), wave height change (pink), sea level rise (purple), and baseline conditions (blue). Bottom: Difference between each climate change scenario and the baseline, illustrating the individual contribution of each parameter to the longshore sediment transport.

The influence of the change in significant wave height is the most dominant and is more profound further away from coastal structures and, due to the nonlinear relationship between the wave height and the longshore sediment transport, the influence of the changing wave height increases further away from coastal structures where the total longshore sediment transport is highest.

Another significant observation is that the change in wave direction has the strongest impact on sediment transport near coastal structures. This is because the local shoreline orientation in these areas quickly adjusts toward an equilibrium angle, where the wave incidence approaches perpendicular and longshore sediment transport is minimized. A slight shift in wave direction therefore reintroduces a transport gradient near the structure, triggering sediment movement and shoreline adjustment. This explains the dominant influence of directional change observed near structures and confirms the findings presented in chapter 4.4.6 regarding the spatial variability of climate parameter influence.

While the spatial pattern of influence remains largely consistent, the magnitude of the sediment transport change is time-dependent, as wave direction shifts occur linearly over the simulation period. The graphs (figure 4.32) shown represent a late-century snapshot (2065–2074), when the wave direction

has shifted most significantly. In earlier periods (e.g. 2020–2030), the same spatial distribution is visible but with smaller absolute changes.

Further away from coastal structures, the influence of wave direction becomes more uniform, showing consistent increases along the coast. This explains the low contribution of the wave direction to the total shoreline displacement, driven by a gradient in the longshore sediment transport, at transect T3 in figure 4.27. T3 is located at alongshore distance 570,000 approximately.

The influence of the sea level rise to the longshore sediment transport is zero along almost the whole shoreline. Only at the Lekki Deep Sea Port and Dangote Quays Lekki there is a fluctuation which is caused by sea level rise slowing down the accretion to the tip of the port structures and thereby influencing the by-passing at these locations.

5

Discussion

The aim of this thesis is to analyze the influence of climate change on the shoreline dynamics of the Lagos State coastline over a 50-year timespan. To achieve this, the 1D-shoreline model ShorelineS was used to simulate long-term coastline evolution under various climate scenarios. The general findings are discussed in chapter 5.1. Chapter 5.1.1 examines the specific mechanisms through which climate change affects shoreline dynamics, while subsequent sections address the research contributions, limitations, coastal management implications, and directions for future work.

5.1. General Findings

This section introduces the main findings of this thesis project. Due to the significant eastward directed longshore sediment transport, induced by the unidirectional south-south western wave direction, the Lagos State coast is prone to erosion. This erosion can become particularly severe near coastal structures, with projected retreat reaching up to 700 meters locally by 2075, even under baseline (no climate change) conditions. The impact of climate change, modeled through sea level rise and variations in wave height and direction, is more visible in erosion-prone areas, where sea level rise and changing wave conditions reinforce ongoing shoreline retreat. In accretive zones, sea level rise induces a shoreline retreat while a change in wave conditions enhance the accretive trend, effectively counterbalancing each other. At erosion-prone areas, climate change can increase erosion near structures by up to 10% in the year 2075 under extreme scenarios. This effect, however, is relatively limited when compared to the dominant role that coastal structures play in shaping local erosion and accretion patterns along the Lagos State coastline.

Longshore sediment transport is also sensitive to changes in wave climate, with increases of up to 20% observed by the year 2075 under the most severe RCP8.5 scenarios at the two locations analyzed in chapter 4.5. Analysis of individual climate change parameters revealed that wave height changes have the most significant overall impact, particularly further from coastal structures due to the nonlinear relationship between wave height and sediment transport. Wave direction changes produce stronger localized effects near coastal structures but have more uniform influence further along the shoreline. Sea level rise minimally affects longshore sediment transport patterns.

5.1.1. Climate Change Impact Mechanisms

An analysis of the individual climate parameters reveals that near coastal structures, the change in wave direction is the dominant driver of shoreline movement. However, its influence diminishes with increasing distance from these structures as can be seen in figure 4.27. This spatial pattern can be attributed to how wave direction affects the van Rijn 2014 longshore sediment transport formula. A shift to more westerly wave directions (which is seen in almost all climate scenario's) increases the total longshore sediment transport over the whole area, creating steeper transport gradients near structures where sediment transport approaches zero, resulting in steep gradients and enhanced erosion. Further from structures, directional changes produce more uniform shifts in sediment flux, resulting in minimal gradient alterations and reduced morphological impact.

Changes in wave height influence the shoreline differently. Since longshore sediment transport is proportional to $H_s^{2.1}$, even modest increases in significant wave height can substantially amplify sediment transport rates. This leads to enhanced sediment flux gradients and thus intensify erosion or accretion.

In contrast, sea level rise induces remarkably uniform shoreline retreat across the study area. This uniformity stems from ShorelineS' application of the Bruun rule, which calculates retreat based primarily on beach slope and projected sea level rise. With the model assuming a constant slope along the coast, the resulting shoreline displacement shows minimal spatial variation compared to the other climate parameters.

5.2. Research Contribution

This section introduces the main research contributions of this thesis project. This research contributes to the understanding of shoreline evolution in Nigeria by providing a quantitative assessment of climate change impacts on the Lagos State coastline over a 50-year time period. It partly extends the work of Giardino et al. [30], who conducted a large-scale sediment budget analysis from Côte d'Ivoire to Benin, west of Lagos State, incorporating both climate change and anthropogenic interventions. Their study concluded that man-made structures have played a dominant role in shaping shoreline dynamics along the West African coast, a finding confirmed and spatially refined in the present research.

A key advancement in this study is the separate evaluation of individual climate drivers, specifically significant wave height and wave direction, which were not assessed independently in the work by Giardino et al. [30]. By isolating these parameters, this research offers new insight into their respective contributions to future shoreline change, highlighting their spatially variable influence and interaction with local coastal structures.

Furthermore, this research confirms earlier estimates of longshore sediment transport along the Lagos State coastline, which ranged from approximately $500,000\ m^3/year$ to $1,000,000\ m^3/year$ [22, 20, 4, 28].

5.3. Research Limitations

Despite the valuable insights provided by this study, several limitations should be acknowledged regarding the modeling framework, input data, and assumptions made throughout the analysis. They are introduced in this section.

5.3.1. Wave Climate Forcing

The offshore wave climate used to drive the model was derived from ERA5 historical reanalysis data and transformed using SWAN. While these sources offer good regional coverage, they come with spatial and temporal limitations that may not fully capture local wave variability. The uncertainty in wave modeling was not addressed in this project and may represent a potential source of uncertainty in the results. The Gaussian Process model used to extend the offshore wave data into the nearshore performed well for swell waves, but was less accurate for wind-sea conditions. Moreover, only the wave climate from 2010–2020 was used to define future trends, which may not capture interdecadal variability. Climate change effects were incorporated as annually changing parameters, but the full uncertainty range in wave projections was not explored.

5.3.2. Bathymetry and Wave Transformation

A key limitation of this study is the absence of detailed nearshore bathymetric data. This introduces uncertainty in the nearshore wave climate generated by the SWAN model, as local wave patterns, particularly those influenced by small-scale bathymetric features, are not accurately captured. Furthermore, in the ShorelineS model, a single shoreline profile was assumed across the entire domain, and a representative median grain size (D_{50}) was applied uniformly. As a result, site-specific nearshore processes, such as wave refraction and local sediment transport pathways, are not fully resolved.

5.3.3. ShorelineS Model Framework

The ShorelineS model is a one-line (1D) shoreline evolution model, meaning that only longshore sediment transport is simulated. Cross-shore processes, including bar migration, profile steepening, and

storm-induced erosion (e.g., from extreme events such as tropical cyclones or surge events), are not included. Furthermore, due to computational efficiency, the grid resolution varied between 300 and 2000 meters, which may miss finer-scale shoreline variations. A single calibration factor was applied across the domain, resulting in a reasonable fit for most areas while producing deviations in others. This trade-off was deemed the most suitable given data constraints, but it adds uncertainty to the absolute displacement outcomes. A sensitivity analysis using different values of the sediment transport calibration parameter q_{scal} revealed that projected shoreline displacement can vary by up to ±30% depending on the chosen value. This highlights that while the model captures spatial patterns reliably, the absolute magnitudes of displacement should be interpreted with caution.

Additionally, sediment bypassing around coastal structures in ShorelineS is represented by a simplified calculation that does not consider cross-shore processes. For example, the model assumes immediate full sediment bypassing once the tip of a structure is reached, neglecting more complex nearshore dynamics.

5.3.4. Coastal Structures and Interventions

Other than the extension of the west mole, this study assumed no future coastal interventions, a simplification that is unlikely to hold, especially in a rapidly developing region such as Lagos State. Existing structures, such as the Dangote Quays in Lekki, were assumed to remain in place without further modification.

5.3.5. Interpretation and Scale of Results

It is important to emphasize that the results presented in this study should be considered indicative rather than predictive. The absolute values of shoreline displacement and sediment transport are intended to provide an order-of-magnitude estimate of the contribution of climate change to coastal evolution, rather than precise forecasts. As such, the results are best interpreted in terms of relative spatial trends and comparative impacts across the study area.

5.4. Implications for Coastal Management

The findings of this study highlight several important implications for coastal management in Lagos State. First, the analysis provides an overview of areas experiencing the highest rates of erosion and accretion along the Lagos State coastline, confirming that man-made structures, such as ports and groynes, currently exert a significant influence on shoreline dynamics.

Second, while climate change impacts do affect the overall sediment budget and shoreline position, their relative influence varies spatially. The isolated assessment of wave height and direction shows that wave climate changes can enhance erosion in some locations and promote accretion in others, depending on local orientation and boundary conditions. This underlines the need for site-specific adaptation measures and sediment management strategies.

Importantly, the study shows that even under high-emission climate scenarios (RCP 8.5), the effects of climate change on erosion patterns are in some areas still smaller than those of existing anthropogenic interventions. However, this balance may shift over time as climate change accelerates, emphasizing the urgency of developing proactive and adaptive planning frameworks.

Finally, these findings highlight the need for an integrated sediment management plan in Lagos State. While this study mainly addressed physical processes, future research should also include socioeconomic vulnerability, infrastructure exposure, and governance capabilities. Effective sediment management will require collaboration among local stakeholders such as port authorities, urban planners, and environmental agencies. Coordinated efforts are essential to ensure that management strategies are practical, sustainable, and fair to all affected communities.

5.5. Future Research

This section provides several directions that remain for future research.

- Future work could include the implementation of mitigation strategies such as beach nourishments, sediment bypassing, or additional groynes in the ShorelineS model. This would allow

for an assessment of their effectiveness under different climate scenarios and support the development of adaptive intervention plans. To address the inherent uncertainty associated with long-term climate change, future studies could apply the Dynamic Adaptive Policy Pathways (DAPP) framework. This approach would help identify tipping points and thresholds for intervention, enabling decision-makers to dynamically adjust coastal management strategies in response to observed shoreline changes and climate trends.

- Better input data could improve the reliability of the model results. As the model is primarily forced by the nearshore waves climate, more accurate nearshore bathymetry would help reduce uncertainty in how waves are transformed near the coast and how sediment is transported alongshore.
- The modeling approach could be expanded to include cross-shore processes, storm events, and seasonal variability, which are now left out. These processes are likely to become more important as extreme weather events increase in frequency and intensity due to climate change.
- Future research could include socioeconomic and ecological factors to allow for a more complete assessment of coastal vulnerability. This would make it possible to identify critical areas not just based on physical erosion risk, but also in terms of exposure of people, infrastructure, and natural habitats.

6

Conclusion

This study evaluated the impact of climate change on long-term shoreline dynamics along the Lagos State coastline, an area of growing economic, infrastructural, and demographic importance with the aim of answering the main research question *How will sea level rise and changing wave climate affect long-term shoreline dynamics along the Lagos State coastline?*. The presence of large-scale coastal structures, combined with a dominant wave climate from the south-southwest, has disrupted sediment transport along the coast. Climate change, through sea level rise and a changing wave climate, is expected to further affect these dynamics over the coming decades.

The ShorelineS model, calibrated with historical shoreline data, demonstrated reliable performance in simulating shoreline dynamics under various climate scenarios. The findings reveal that while climate change will impact erosion and accretion patterns, the presence of coastal structures remains the dominant factor shaping shoreline evolution. This research provides quantified projections of potential shoreline changes that can inform adaptive management approaches along this economically significant coastline.

Sub-question 1: What are the projected changes in wave climate and sea level over 50 years at the Lagos State coast?

The projections of future wave climate used in this study are based on outputs from global climate models, which simulate atmospheric conditions under different greenhouse gas emission scenarios. These projections indicate that climate change will gradually alter wind patterns and storm activity, leading to changes in wave energy and shifts in dominant wave directions—particularly under high-emission scenarios.

At the Lagos State coast, this results in a projected increase in significant wave height of up to 5.2% and a westward shift in wave direction of up to 1.4° by 2075 under the extreme RCP8.5 scenario. Simultaneously, sea level rise may reach up to 0.94 meters. Together, these changes are expected to increase longshore sediment transport and exert growing pressure on shoreline stability in the coming decades.

Sub-question 2: What engineering workflows are available to simulate long-term coastal morphological evolution in the context of climate change?

A review of coastal modeling approaches identified four main categories: data-driven, semi-empirical, process-based, and reduced-complexity models. This study employed the reduced-complexity 1D shoreline model ShorelineS, supported by wave transformation using SWAN and a Gaussian Process model to derive nearshore wave conditions from offshore ERA5 hindcast data. This workflow was selected for its ability to model large-scale, long-term morphological change under climate forcing.

Sub-question 3: How can historical data be used to calibrate the engineering workflows?

The ShorelineS model was calibrated using satellite-derived historical shoreline positions. A uniform calibration coefficient was applied across the domain to ensure consistency. Sensitivity analysis showed that shoreline displacement can vary by up to ±30% depending on the chosen calibration factor, indicating that model outcomes are sensitive to parameter selection but capable of reproducing general shoreline trends when appropriately tuned.

Sub-question 4: What are the expected patterns of erosion and accretion along the Lagos State coastline under future climate scenarios?

Shoreline changes are primarily driven by variations in longshore sediment transport, which depend largely on the wave climate and the presence of coastal structures. Under the extreme RCP8.5 scenario, sediment transport is projected to increase by up to 20% by 2075 compared to baseline conditions, where no climate change is enforced, amplifying erosion and accretion depending on local sediment flux gradients.

Model results reveal that erosion is most severe near coastal structures, where longshore sediment transport is disrupted. Even under baseline conditions, local retreat can reach up to 700 meters by 2075. Climate change intensifies these patterns, with an additional 10% increase in retreat projected in erosion-prone areas near structures under extreme RCP8.5 scenarios. In contrast, accretive zones show a more moderated response, where sea level rise tends to induce retreat but is counterbalanced by increased wave-driven accretion.

Sub-question 5: What are the relative contributions of different climate change variables (e.g. sea level rise, wave height, wave direction) to projected shoreline change?

The contribution of individual climate drivers on shoreline displacement varies spatially. Changes in wave direction have the most pronounced localized effect near these structures. In these areas, the shoreline often adjusts toward an equilibrium orientation where the angle of wave incidence, and therefore sediment transport, is minimized. Even small shifts in wave direction disturb this balance, reintroducing transport gradients that amplify erosion or accretion. This sensitivity is particularly pronounced near structures and evolves over time as both wave direction and shoreline orientation change.

Wave height increases have a nonlinear effect on transport due to the $H_s^{3.1}$ dependency, significantly increasing sediment flux. Sea level rise results in relatively uniform shoreline retreat across the coast, consistent with the Bruun rule implementation in ShorelineS.

Main Research Question: How will sea level rise and changing wave climate affect long-term shoreline dynamics along the Lagos State coastline?

Overall, this study shows that while climate change will increasingly affect coastal dynamics through rising sea levels and a changing wave climate, the primary driver of shoreline change along the Lagos State coastline remains the presence of large-scale coastal structures. Projected shifts in wave direction and increases in wave height are expected to intensify longshore sediment transport, contributing to greater erosion in already vulnerable areas. Nevertheless, these effects are spatially variable and interact strongly with existing human interventions. These findings emphasize the need for adaptive, site-specific coastal management strategies that address both climatic and anthropogenic influences on future shoreline evolution.

References

[1] United Nations Department of Economic and Social Affairs. *World Urbanization Prospects: The 2018 Revision*. New York: United Nations, 2018. URL: https://population.un.org/wup/.

[2] The World Bank Group. *Population Growth (Annual %) - Nigeria*. https://data.worldbank.org/indicator/SP.POP.GROW?locations=NG. Viewed 13 May 2020. 2019.

[3] World Bank. *The World Bank in Nigeria*. https://www.worldbank.org/en/country/nigeria/overview. Retrieved September 10, 2024. World Bank, 2024.

[4] Y. Wang, J. Shen, and S. Zhao. "Shoreline evolution and responses to port engineering at Lekki Coast, Nigeria". In: *Estuaries and Coastal Zones in Times of Global Change*. Springer, 2020, pp. 467–486.

[5] A. J. Osanyintuyi, Y. Wang, and N. A. H. Mokhtar. "Nearly five decades of changing shoreline mobility along the densely developed Lagos barrier-lagoon coast of Nigeria: A remote sensing approach". In: *Journal of African Earth Sciences* 194 (2022), p. 104628. DOI: 10.1016/j.jafrearsci.2022.104628.

[6] Lelia Croitoru et al. *THE COST OF COASTAL ZONE DEGRADATION IN NIGERIA: CROSS RIVER, DELTA AND LAGOS STATES*. en. Oct. 2020.

[7] Gregory T French, Larry F Awosika, and CE Ibe. "Sea-level rise and Nigeria: potential impacts and consequences". In: *Journal of Coastal Research* (1995), pp. 224–242.

[8] John A Church and Neil J White. "Sea-level rise from the late 19th to the early 21st century". In: *Surveys in geophysics* 32 (2011), pp. 585–602.

[9] Sönke Dangendorf et al. "Evidence for long-term memory in sea level". In: *Geophysical Research Letters* 41.15 (2014), pp. 5530–5537.

[10] Sönke Dangendorf et al. "Persistent acceleration in global sea-level rise since the 1960s". In: *Nature Climate Change* 9.9 (2019), pp. 705–710.

[11] Mary O. Oloyede, Akan B. Williams, and Nsikak U. Benson. "Simulated sea-level rise under future climate scenarios for the Atlantic Barrier Lagoon coast of Nigeria using simclim". In: *IOP Conference Series: Earth and Environmental Science* 665.1 (Mar. 2021), p. 012068. DOI: 10.1088/1755-1315/665/1/012068.

[12] Mark A. Hemer et al. "Projected changes in wave climate from a multi-model ensemble". en. In: *Nature Climate Change* 3.5 (May 2013), pp. 471–476. ISSN: 1758-6798. DOI: 10.1038/nclimate1791.

[13] pmnews pmnews pmnews. *Lagos tackles ocean surge with N36 billion*. May 1970. URL: https://pmnewsnigeria.com/2016/05/17/lagos-tackles-ocean-surge-with-n36-billion/.

[14] Olasunkanmi Akoni. *Lagos needs □1.2 trillion for 42km coastline protection – commissioner - politics - nigeria*. July 2024. URL: https://www.nairaland.com/8147924/lagos-needs-1.2-trillion-42km.

[15] C Mudde. "A CASE STUDY OF LOBITO, ANGOLA". MA thesis. Technical University of Delft, 2019.

[16] Dano Roelvink et al. "Efficient Modeling of Complex Sandy Coastal Evolution at Monthly to Century Time Scales". English. In: *Frontiers in Marine Science* 7 (July 2020). Publisher: Frontiers. ISSN: 2296-7745. DOI: 10.3389/fmars.2020.00535. URL: https://www.frontiersin.org/journals/marine-science/articles/10.3389/fmars.2020.00535/full (visited on 09/17/2024).

[17] Encyclopædia Britannica. *Gulf of Guinea*. Image. Accessed: March 6, 2025. URL: https://www.britannica.com/place/Gulf-of-Guinea#/media/1/248843/281947.

[18] Encyclopædia Britannica. *Bight of Benin*. Image. Accessed: March 6, 2025. URL: https://www.britannica.com/place/Bight-of-Benin#/media/1/60906/290834.

[19] Idowu Ajibade. “Can a future city enhance urban resilience and sustainability? A political ecology analysis of Eko Atlantic city, Nigeria”. In: *International Journal of Disaster Risk Reduction*. Africa’s Urban Risk and Resilience 26 (Dec. 2017), pp. 85–92. ISSN: 2212-4209. DOI: 10.1016/j.ijdrr.2017.09.029.

[20] van Bentum. “The Lagos coast – Investigation of the long-term morphological impact of the Eko Atlantic City project”. In: *NCK-days 2012: Crossing borders in coastal research: jubilee conference proceedings*. Enschede, the Netherlands: University of Twente, 2012.

[21] Copernicus Sentinel-2 Data European Union. *EKO Atlantic Sentinel-2 Image, True Color*. Copernicus Open Access Hub. Contains modified Copernicus Sentinel data 2024. Oct. 2024. URL: https://browser.dataspace.copernicus.eu/.

[22] Bart-Jan van der Spek et al. *Water | Free Full-Text | Sandbar Breakwater: An Innovative Nature-Based Port Solution*. Apr. 2020. URL: https://www.mdpi.com/2073-4441/12/5/1446.

[23] C3S. *ERA5 hourly data on single levels from 1940 to present*. 2018.

[24] Olusegun A. Dada et al. “Response of waves and coastline evolution to climate variability off the Niger Delta coast during the past 110 years”. In: *Journal of Marine Systems* 160 (Aug. 2016), pp. 64–80. ISSN: 0924-7963. DOI: 10.1016/j.jmarsys.2016.04.005.

[25] Joao Morim et al. “A global ensemble of ocean wave climate projections from CMIP5-driven models”. en. In: *Scientific Data* 7.1 (Mar. 2020), p. 105. ISSN: 2052-4463. DOI: 10.1038/s41597-020-0446-2.

[26] NASA Sea Level Change Team. *IPCC AR6 Sea Level Projection Tool*. 2021. URL: https://sealevel.nasa.gov/ipcc-ar6-sea-level-projection-tool (visited on 05/06/2025).

[27] Judith Bosboom and Marcel Stive. *Coastal Dynamics*. en. TU Delft OPEN Publishing, Jan. 2023.

[28] Egge Allersma and Wiel M. K. Tilmans. “Coastal conditions in West Africa—A review”. In: *Ocean & Coastal Management* 19.3 (Jan. 1993), pp. 199–240. ISSN: 0964-5691. DOI: 10.1016/0964-5691(93)90043-X.

[29] A. Giardino et al. “A quantitative assessment of human interventions and climate change on the West African sediment budget”. In: *Ocean & Coastal Management*. SI: MSforCEP 156 (Apr. 2018), pp. 249–265. ISSN: 0964-5691. DOI: 10.1016/j.ocecoaman.2017.11.008.

[30] A. Giardino et al. “A quantitative assessment of human interventions and climate change on the West African sediment budget”. In: *Ocean & Coastal Management*. SI: MSforCEP 156 (Apr. 2018), pp. 249–265. ISSN: 0964-5691. DOI: 10.1016/j.ocecoaman.2017.11.008.

[31] Grégoire Abessolo Ondoa et al. “Beach Response to Wave Forcing from Event to Inter-Annual Time Scales at Grand Popo, Benin (Gulf of Guinea)”. en. In: *Water* 9.66 (June 2017), p. 447. ISSN: 2073-4441. DOI: 10.3390/w9060447.

[32] Grégoire O. Abessolo et al. “Modeling the Bight of Benin (Gulf of Guinea, West Africa) coastline response to natural and anthropogenic forcing”. In: *Regional Studies in Marine Science* 48 (Nov. 2021), p. 101995. ISSN: 2352-4855. DOI: 10.1016/j.rsma.2021.101995.

[33] E. J. Anthony et al. “Response of the Bight of Benin (Gulf of Guinea, West Africa) coastline to anthropogenic and natural forcing, Part 2: Sources and patterns of sediment supply, sediment cells, and recent shoreline change”. In: *Continental Shelf Research* 173 (Feb. 2019), pp. 93–103. ISSN: 0278-4343. DOI: 10.1016/j.csr.2018.12.006.

[34] R. Almar et al. “Response of the Bight of Benin (Gulf of Guinea, West Africa) coastline to anthropogenic and natural forcing, Part1: Wave climate variability and impacts on the longshore sediment transport”. en. In: *Continental Shelf Research* 110 (Nov. 2015), pp. 48–59. ISSN: 02784343. DOI: 10.1016/j.csr.2015.09.020.

[35] Samuel Daramola et al. “Numerical assessment of potential sea level rise impacts on coastal retreat along the Nigerian Mahin mud coast”. en. In: *Journal of Coastal Conservation* 26.6 (Oct. 2022), p. 54. ISSN: 1874-7841. DOI: 10.1007/s11852-022-00894-z.

[36] Gbolahan S. Badru et al. “Numerical modelling of sediment transport in southwest coast of Nigeria: Implications for sustainable management of coastal erosion in the Bight of Benin”. In: *Journal of African Earth Sciences* 187 (Mar. 2022), p. 104466. ISSN: 1464-343X. DOI: 10.1016/j.jafrearsci.2022.104466.

[37] Jennifer Montaño et al. “Blind testing of shoreline evolution models”. en. In: *Scientific Reports* 10.1 (Feb. 2020), p. 2137. ISSN: 2045-2322. DOI: 10.1038/s41598-020-59018-y.

[38] Sheetal Mutagi, Arunkumar Yadav, and Chandrashekarayya G. Hiremath. “Shoreline Change Model: A Review”. en. In: *Sustainability Trends and Challenges in Civil Engineering*. Ed. by Lakshman Nandagiri et al. Singapore: Springer, 2022, pp. 1019–1031. ISBN: 9789811628269. DOI: 10.1007/978-981-16-2826-9_64.

[39] Steven W. H. Hoagland et al. “Advances in Morphodynamic Modeling of Coastal Barriers: A Review”. EN. In: *Journal of Waterway, Port, Coastal, and Ocean Engineering* 149.5 (Sept. 2023), p. 03123001. DOI: 10.1061/JWPED5.WWENG-1825.

[40] Emily Hunt et al. “Shoreline modelling on timescales of days to decades”. en. In: *Cambridge Prisms: Coastal Futures* 1 (Jan. 2023), e16. ISSN: 2754-7205. DOI: 10.1017/cft.2023.5.

[41] Evan B. Goldstein, Giovanni Coco, and Nathaniel G. Plant. “A review of machine learning applications to coastal sediment transport and morphodynamics”. In: *Earth-Science Reviews* 194 (July 2019), pp. 97–108. ISSN: 0012-8252. DOI: 10.1016/j.earscirev.2019.04.022.

[42] Clinton D Winant, Douglas L Inman, and Charles E Nordstrom. “Description of seasonal beach changes using empirical eigenfunctions”. In: *Journal of Geophysical Research* 80.15 (1975), pp. 1979–1986.

[43] Sasithorn Aranuvachapun and John A Johnson. “Beach profiles at Gorleston and Great Yarmouth”. In: *Coastal Engineering* 2 (1978), pp. 201–213.

[44] Kathelijne M Wijnberg and Joost HJ Terwindt. “Extracting decadal morphological behaviour from high-resolution, long-term bathymetric surveys along the Holland coast using eigenfunction analysis”. In: *Marine Geology* 126.1-4 (1995), pp. 301–330.

[45] Dominic Reeve, Bin Li, and Neil Thurston. “Eigenfunction analysis of decadal fluctuations in sandbank morphology at Gt Yarmouth”. In: *Journal of Coastal Research* (2001), pp. 371–382.

[46] Grzegorz Różyński. “Data-driven modeling of multiple longshore bars and their interactions”. In: *Coastal Engineering* 48.3 (2003), pp. 151–170.

[47] Magnus Larson, Michele Capobianco, and Hans Hanson. “Relationship between beach profiles and waves at Duck, North Carolina, determined by canonical correlation analysis”. In: *Marine geology* 163.1-4 (2000), pp. 275–288.

[48] José M Horrillo-Caraballo and Dominic E Reeve. “Morphodynamic behaviour of a nearshore sandbank system: The Great Yarmouth Sandbanks, UK”. In: *Marine Geology* 254.1-2 (2008), pp. 91–106.

[49] José M Horrillo-Caraballo and Dominic E Reeve. “An investigation of the performance of a data-driven model on sand and shingle beaches”. In: *Marine Geology* 274.1-4 (2010), pp. 120–134.

[50] Benjamin T Gutierrez, Nathaniel G Plant, and E Robert Thieler. “A Bayesian network to predict coastal vulnerability to sea level rise”. In: *Journal of Geophysical Research: Earth Surface* 116.F2 (2011).

[51] T Beuzen et al. “Physical model study of beach profile evolution by sea level rise in the presence of seawalls”. In: *Coastal Engineering* 136 (2018), pp. 172–182.

[52] Nathaniel G Plant and Hilary F Stockdon. “Probabilistic prediction of barrier-island response to hurricanes”. In: *Journal of Geophysical Research: Earth Surface* 117.F3 (2012).

[53] Christopher K Wikle and L Mark Berliner. “A Bayesian tutorial for data assimilation”. In: *Physica D: Nonlinear Phenomena* 230.1-2 (2007), pp. 1–16.

[54] MR Hashemi, Z Ghadampour, and SP Neill. “Using an artificial neural network to model seasonal changes in beach profiles”. In: *Ocean Engineering* 37.14-15 (2010), pp. 1345–1356.

[55] Rodrigo Mikosz Goncalves et al. “A comparison between three short-term shoreline prediction models”. In: *Ocean & Coastal Management* 69 (2012), pp. 102–110.

[56] BR Rajasree, MC Deo, and L Sheela Nair. “Effect of climate change on shoreline shifts at a straight and continuous coast”. In: *Estuarine, Coastal and Shelf Science* 183 (2016), pp. 221–234.

[57] Isabel López et al. “Artificial neural network modeling of cross-shore profile on sand beaches: The coast of the province of Valencia (Spain)”. In: *Marine Georesources & Geotechnology* 36.6 (2018), pp. 698–708.

[58] Saeed Zeinali, Maryam Dehghani, and Nasser Talebbeydokhti. “Artificial neural network for the prediction of shoreline changes in Narrabeen, Australia”. In: *Applied Ocean Research* 107 (2021), p. 102362.

[59] Jon K Miller and Robert G Dean. “A simple new shoreline change model”. en. In: *Coast. Eng.* 51.7 (Sept. 2004), pp. 531–556.

[60] MA Davidson and IL Turner. “A behavioral template beach profile model for predicting seasonal to interannual shoreline evolution”. In: *Journal of Geophysical Research: Earth Surface* 114.F1 (2009).

[61] MA Davidson, KD Splinter, and IL Turner. “A simple equilibrium model for predicting shoreline change”. In: *Coastal Engineering* 73 (2013), pp. 191–202.

[62] Lynn D Wright, Andrew D Short, and MO Green. “Short-term changes in the morphodynamic states of beaches and surf zones: an empirical predictive model”. In: *Marine geology* 62.3-4 (1985), pp. 339–364.

[63] Marissa L Yates, RT Guza, and WC O’reilly. “Equilibrium shoreline response: Observations and modeling”. In: *Journal of Geophysical Research: Oceans* 114.C9 (2009).

[64] Sean Vitousek et al. “A model integrating longshore and cross-shore processes for predicting long-term shoreline response to climate change”. In: *Journal of Geophysical Research: Earth Surface* 122.4 (2017), pp. 782–806.

[65] Olivier Burvingt et al. “Climate forcing of regionally-coherent extreme storm impact and recovery on embayed beaches”. In: *Marine Geology* 401 (2018), pp. 112–128.

[66] Tai-Wen Hsu, Shan-Hwei Ou, and Shun-Kung Wang. “On the prediction of beach changes by a new 2-D empirical eigenfunction model”. In: *Coastal Engineering* 23.3-4 (1994), pp. 255–270.

[67] J Tinker et al. “A cross-shore suspended sediment transport shape function parameterisation for natural beaches”. In: *Continental Shelf Research* 29.16 (2009), pp. 1948–1960.

[68] AJ Madsen and NG Plant. “Intertidal beach slope predictions compared to field data”. In: *Marine Geology* 173.1-4 (2001), pp. 121–139.

[69] Sam Prodger et al. “Understanding and predicting the temporal variability of sediment grain size characteristics on high-energy beaches”. In: *Marine Geology* 376 (2016), pp. 109–117.

[70] NG Plant et al. “A simple model for interannual sandbar behavior”. In: *Journal of Geophysical Research: Oceans* 104.C7 (1999), pp. 15755–15776.

[71] Giles R Lesser et al. “Development and validation of a three-dimensional morphological model”. In: *Coastal engineering* 51.8-9 (2004), pp. 883–915.

[72] Dano Roelvink et al. “Modelling storm impacts on beaches, dunes and barrier islands”. In: *Coastal engineering* 56.11-12 (2009), pp. 1133–1152.

[73] IR Warren and H_K_ Bach. “MIKE 21: a modelling system for estuaries, coastal waters and seas”. In: *Environmental software* 7.4 (1992), pp. 229–240.

[74] Catherine Villaret et al. “Morphodynamic modeling using the Telemac finite-element system”. In: *Computers & Geosciences* 53 (2013), pp. 105–113.

[75] Svasek Hydraulics. Oct. 2023. URL: `https://www.svasek.nl/model-onderzoek/finel/`.

[76] Barend Van Maanen et al. “Simulating mesoscale coastal evolution for decadal coastal management: A new framework integrating multiple, complementary modelling approaches”. In: *Geomorphology* 256 (2016), pp. 68–80.

[77] Magnus Larson and Nicholas C Kraus. *SBEACH: numerical model for simulating storm-induced beach change. Report 1, Emperical foundation and model development*. 1989.

[78] Mark Davidson. “Forecasting coastal evolution on time-scales of days to decades”. In: *Coastal Engineering* 168 (2021), p. 103928.

[79] Hans Hanson and Nicholas C Kraus. *Genesis: Generalized Model for Simulating Shoreline Change: Technical Reference. Report 1*. US Army Engineer Waterways Experiment Station, 1989.

[80] J William Kamphuis. *Introduction to coastal engineering and management*. Vol. 48. World Scientific, 2020.

[81] SE Kristensen et al. “Impact of groyne fields on the littoral drift: A hybrid morphological modelling study”. In: *Coastal Engineering* 111 (2016), pp. 13–22.

[82] RG Deltares. *UNIBEST-CL+ Manual: Manual for Version 7.1 of the Shoreline Model UNIBEST-CL*. 2011.

[83] Pieter Koen Tonnon et al. “Numerical modelling of erosion rates, life span and maintenance volumes of mega nourishments”. In: *Coastal Engineering* 131 (2018), pp. 51–69.

[84] Arthur Robinet et al. “A reduced-complexity shoreline change model combining longshore and cross-shore processes: The LX-Shore model”. In: *Environmental modelling & software* 109 (2018), pp. 1–16.

[85] José AA Antolínez et al. “Predicting climate-driven coastlines with a simple and efficient multiscale model”. In: *Journal of Geophysical Research: Earth Surface* 124.6 (2019), pp. 1596–1624.

[86] Andrew Ashton, A Brad Murray, and Olivier Arnoult. “Formation of coastline features by large-scale instabilities induced by high-angle waves”. In: *Nature* 414.6861 (2001), pp. 296–300.

[87] Andrew D Ashton and A Brad Murray. “High-angle wave instability and emergent shoreline shapes: 1. Modeling of sand waves, flying spits, and capes”. In: *Journal of Geophysical Research: Earth Surface* 111.F4 (2006).

[88] Chloe Leach et al. “The coastline evolution model 2D (CEM2D) V1. 1”. In: *Geoscientific Model Development* 14.9 (2021), pp. 5507–5523.

[89] Magnus Larson, Nicholas C. Kraus, and Hans Hanson. “SIMULATION OF REGIONAL LONGSHORE SEDIMENT TRANSPORT AND COASTAL EVOLUTION – THE “CASCADE” MODEL”. In: *Coastal Engineering 2002*. World Scientific Publishing Company, 2002, pp. 2612–2624. DOI: 10.1142/9789812791306_0218. eprint: https://www.worldscientific.com/doi/pdf/10.1142/9789812791306_0218. URL: https://www.worldscientific.com/doi/abs/10.1142/9789812791306_0218.

[90] A. E. Frey et al. *GenCade Version 1: Model Theory and User’s Guide*. Tech. rep. TR-12-25. Vicksburg, MS: Coastal and Hydraulics Laboratory - U.S. Army Corps of Engineers, 2012.

[91] Jaime Arriaga et al. “Modeling the long-term diffusion and feeding capability of a mega-nourishment”. In: *Coastal Engineering* 121 (Mar. 2017), pp. 1–13. ISSN: 0378-3839. DOI: 10.1016/j.coastaleng.2016.11.011.

[92] US Army Corps of Engineers (USACE). *Shore Protection Manual*. Vol. 1. Washington, DC: Coastal Engineering Research Center, US Army Corps of Engineers, 1984.

[93] N Booij, L H Holthuijsen, and R C Ris. “The “swan” wave model for Shallow Water”. In: *Coastal Engineering 1996*. Orlando, Florida, United States: American Society of Civil Engineers, Aug. 1997.

[94] Álvaro Rodríguez Luis Pablo García Pérez. *mdapy*. 2024. URL: https://github.com/IHCantabria/mdapy?tab=readme-ov-file#-instalation-note.

[95] Yanira Guanche et al. “A multivariate approach to estimate design loads for offshore wind turbines”. en. In: *Wind Energy, 16(7)* (2013). DOI: 10.1002/we.1542. URL: https://onlinelibrary.wiley.com/doi/10.1002/we.1542.

[96] Edward Roome, David Christie, and Simon Neill. “Predicting coastal wave conditions: A simple machine learning approach”. English. In: *Applied Ocean Research* 153 (Dec. 2024), p. 104282. ISSN: 0141-1187. DOI: 10.1016/j.apor.2024.104282.

[97] Sajni Malde et al. “Applying emulators for improved flood risk analysis”. In: *E3S Web Conf.* 7 (2016), p. 04002.

[98] Eric Schulz, Maarten Speekenbrink, and Andreas Krause. “A tutorial on Gaussian process regression: Modelling, exploring, and exploiting functions”. In: *Journal of Mathematical Psychology* 85 (Aug. 2018), pp. 1–16. ISSN: 0022-2496. DOI: 10.1016/j.jmp.2018.03.001.

[99] Andy Jones. *The Matérn class of covariance functions*. July 2021. URL: https://andrewcharlesjones.github.io/journal/matern-kernels.html.

[100] Natsnoyuki AI Lab. *Gaussian Process Models*. en. Dec. 2024. URL: https://medium.com/towards-data-science/gaussian-process-models-7ebce1feb83d.

[101] Kilian Vos et al. “CoastSat: A Google Earth Engine-enabled Python toolkit to extract shorelines from publicly available satellite imagery”. In: *Environmental Modelling & Software* 122 (Dec. 2019), p. 104528. ISSN: 1364-8152. DOI: 10.1016/j.envsoft.2019.104528.

A

Grid Assessment

A.1. Grid extent

All grid extent tests.

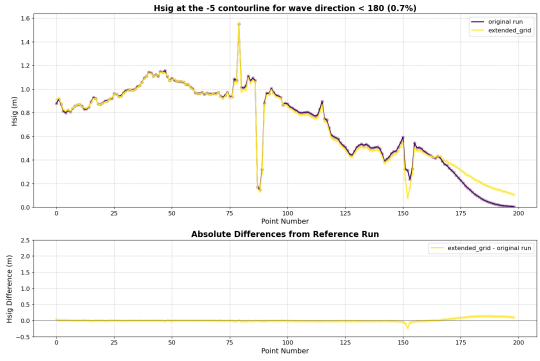

(a) Hsig for wave direction < 180 (0.7%)

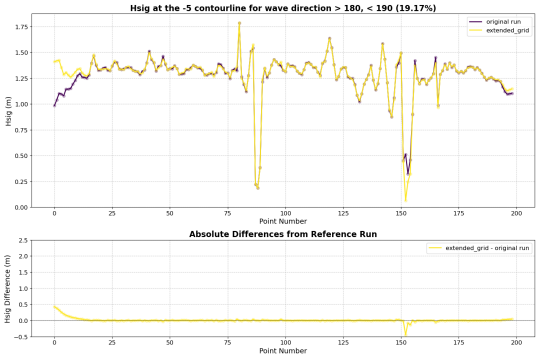

(b) Hsig for wave direction 180–190 (19.17%)

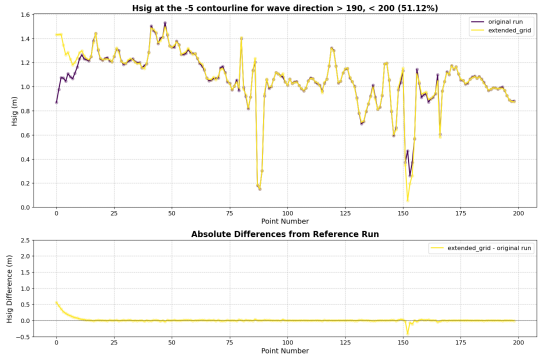

(c) Hsig for wave direction 190–200 (51.12%)

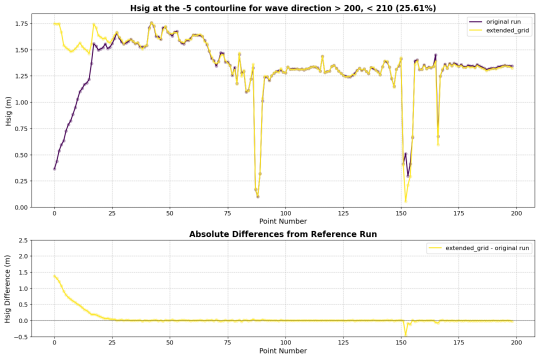

(d) Hsig for wave direction 200–210 (25.61%)

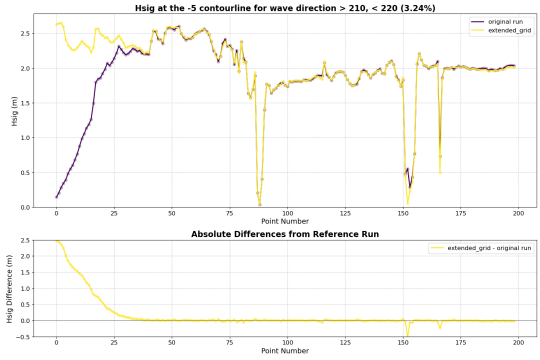

(e) Hsig for wave direction 210–220 (3.24%)

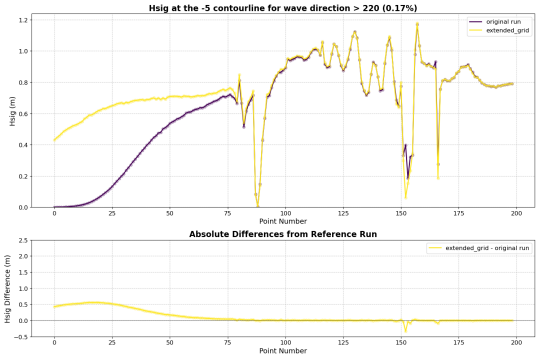

(f) Hsig for wave direction > 220 (0.17%)

Figure A.1: Top graph: Hsig at the output points at the -5m contourline for different wave directions. The yellow line represents the horizontally extended grid (grid figure: 3.4) and the purple line represents the original smaller grid (grid figure: 3.3). Lower graph: absolute difference between waveheights at the -5m contourline modeled in the horizontally extended grid and the original grid

A.2. Forcing boundary at 1000 m depth

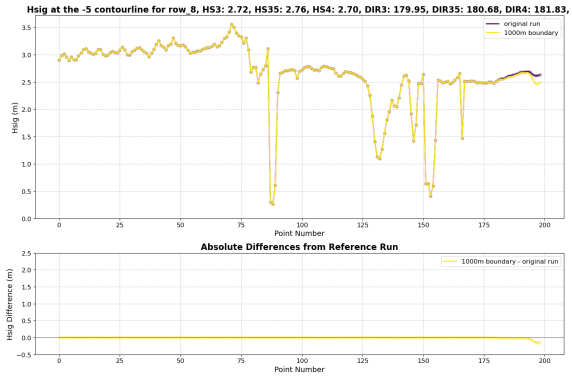

(a) Hsig at -5 m output locations for wave direction < 180 (0.7%)

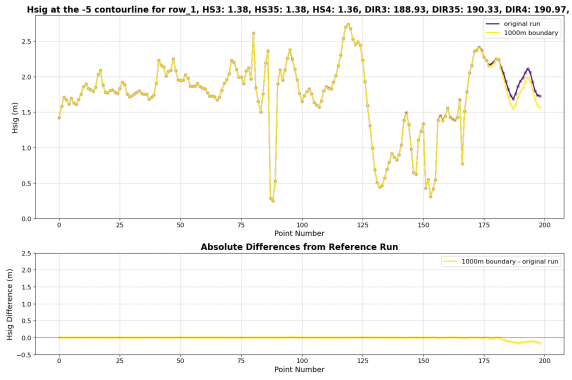

(b) Hsig at -5 m output locations for wave direction 180–190 (19.17%)

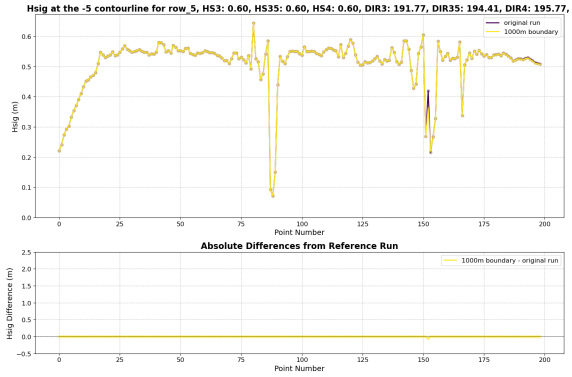

(c) Hsig at -5 m output locations for wave direction 190–200 (51.12%)

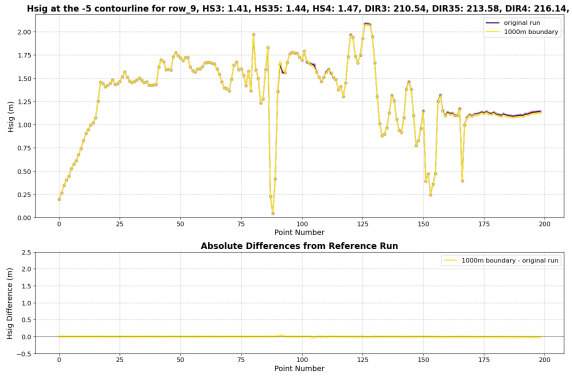

(d) Hsig at -5 m output locations for wave direction 200–210 (25.61%)

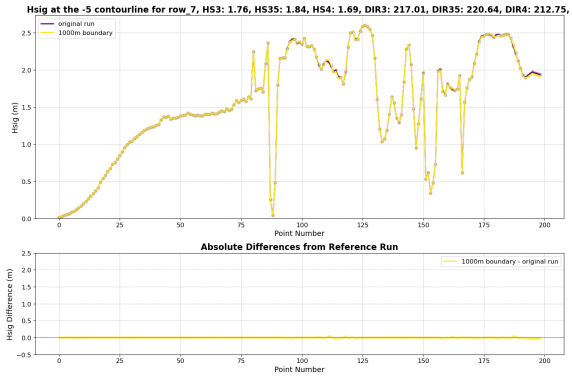

(e) Hsig at -5 m output locations for wave direction 210-220 (3.24%)

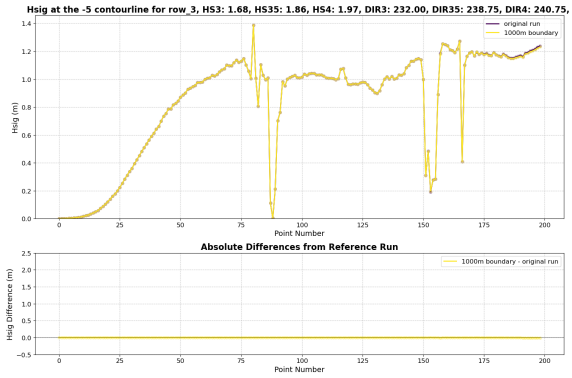

(f) Hsig at -5 m output locations for wave direction > 220 (0.17%)

Figure A.2: Top graph: Significant waveheight at the output points at the -5m contourline for different wave directions. The yellow line represents the 1000m boundary grid (grid figure: **??**) and the purple line represents the original smaller grid (grid figure: 3.3). Lower graph: absolute difference between waveheights at the -5m contourline modeled in the 1000m boundary grid and the original grid

A.3. Input wave condiation at 1000 m depth

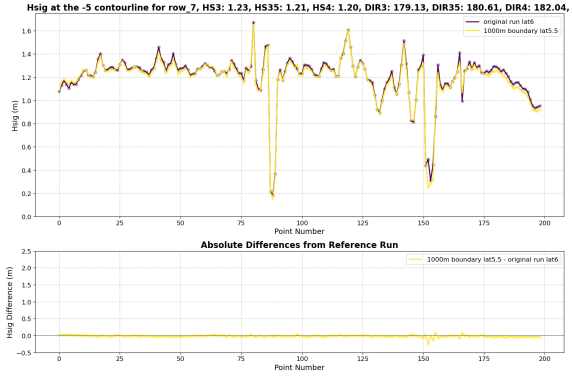

(a) Hsig at -5 m output locations for wave direction < 180 (0.7%)

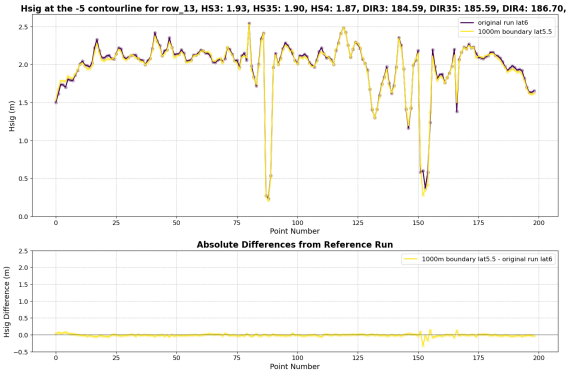

(b) Hsig at -5 m output locations for wave direction 180–190 (19.17%)

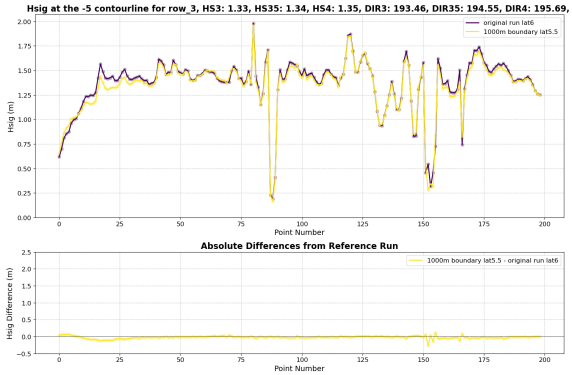

(c) Hsig at -5 m output locations for wave direction 190–200 (51.12%)

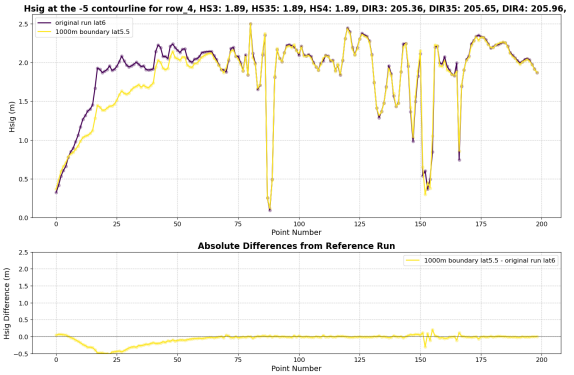

(d) Hsig at -5 m output locations for wave direction 200–210 (25.61%)

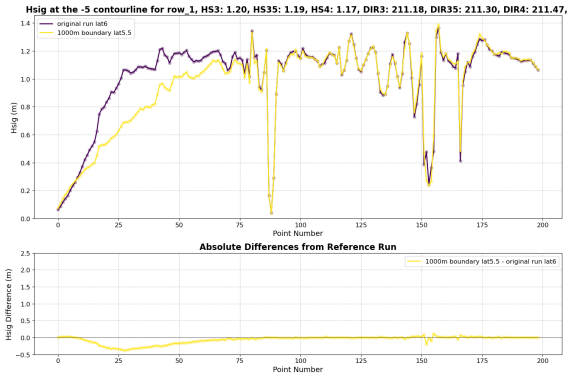

(e) Hsig at -5 m output locations for wave direction 210-220 (3.24%)

Figure A.3: Top graph: Significant wave height at the output points at the -5m contour line for different wave directions. The yellow line represents the vertically extended grid up to latitude 5.5 (grid figure: 3.9) the purple line represents the grid adjusted to 1000m depth boundaries (grid figure: 3.6) Lower graph: absolute difference between waveheights at the -5m contourline modeled in the vertically extended grid and the 1000m boundary grid

B

Modeling Uncertainty

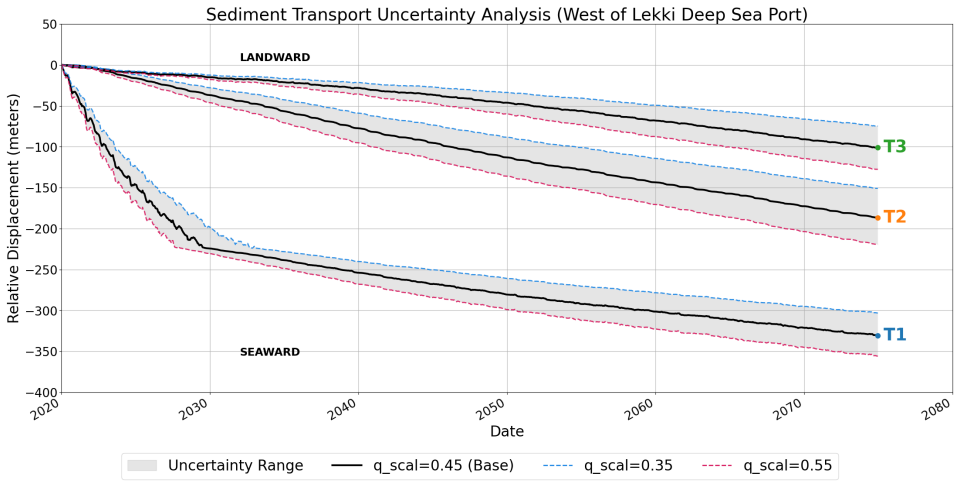

Figure B.1: The displacement relative to the initial shoreline east of the west mole at the three transects as indicated in figure 4.18 for different values of q_{scal}. The black dotted line indicates the base run ($q_{scal} = 0.45$), the red dotted line indicates the upper limit ($q_{scal} = 0.55$) and the blue dotted line indicates the lower limit ($q_{scal} = 0.35$). The gray area indicates the uncertainty range.

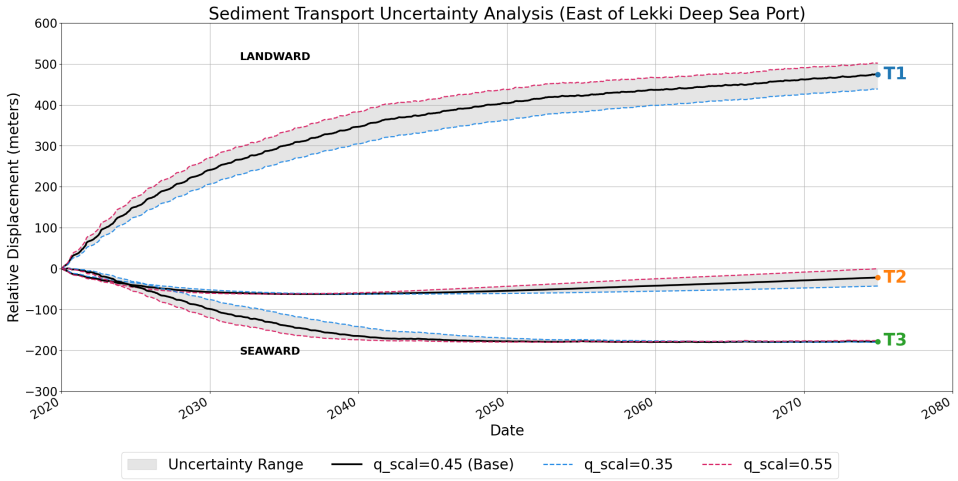

Figure B.2: The displacement relative to the initial shoreline east of the west mole at the three transects as indicated in figure 4.21 for different values of q_{scal}. The black dotted line indicates the base run ($q_{scal} = 0.45$), the red dotted line indicates the upper limit ($q_{scal} = 0.55$) and the blue dotted line indicates the lower limit ($q_{scal} = 0.35$). The gray area indicates the uncertainty range.

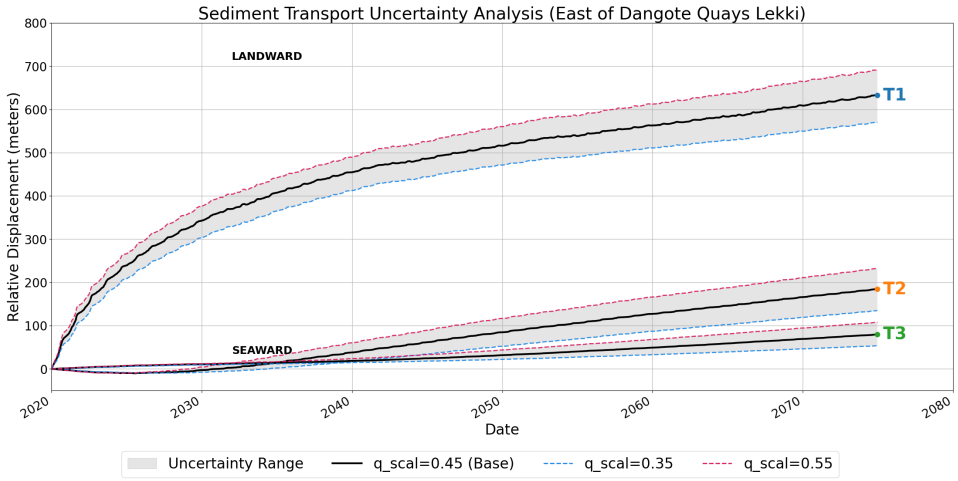

Figure B.3: The displacement relative to the initial shoreline east of the west mole at the three transects as indicated in figure 4.24 for different values of q_{scal}. The black dotted line indicates the base run ($q_{scal} = 0.45$), the red dotted line indicates the upper limit ($q_{scal} = 0.55$) and the blue dotted line indicates the lower limit ($q_{scal} = 0.35$). The gray area indicates the uncertainty range.